ADEQUACY ASSESSMENT OF ELECTRIC POWER SYSTEMS INCORPORATING WIND AND SOLAR ENERGY

A Thesis Submitted to the College of
Graduate Studies and Research
in Partial Fulfillment of the Requirements
for the Degree of Master of Science
in the Department of Electrical Engineering
University of Saskatchewan

by
Yi Gao

PERMISSION TO USE

I agree that the Library, University of Saskatchewan, may make this thesis freely available for inspection. I further agree that permission for copying of this thesis for scholarly purpose may be granted to the professor or professors who supervised the thesis work recorded herein or, in their absence, by the Head of the Department or the Dean of the College in which the thesis work was done. It is understood that due recognition will be given to me and to the University of Saskatchewan in any use of the material in this thesis. Copying or publication or any other use of this thesis for financial gain without approval by the University of Saskatchewan and my written permission is prohibited.

Request for permission to copy or to make any other use of the material in this thesis in whole or part should be addressed to:

Head of the Department of Electrical Engineering
57 Campus Drive
University of Saskatchewan
Saskatoon, Saskatchewan
Canada S7N 5A9

ACKNOWLEDGEMENTS

I would like to express my sincere gratitude to my supervisor Dr. Roy Billinton whose encouragement, support and guidance helped me all the time during my research and writing this thesis. His insights and knowledge were extremely valuable.

I also wish to express my appreciate to my graduate study teachers, Dr. Rajesh Karki, Dr. S.O. Faried and Dr. N.A. Chowdhury for strengthening my knowledge on electrical engineering. I would like to acknowledge Mr. Wijarn Wangdee for his assistance in providing some data for this thesis.

Financial support provided by the Natural Science and Engineering Research Council (NSERC) of Canada is gratefully acknowledged.

Last and certainly not least, I would also like to thank my family for their ongoing encouragement and support. To my husband, Yapeng Zhang, thank you so much for your love, patience and understanding. To my parents, Lingzhi Gao and Guilan Yang, thank you for loving me and encouraging me throughout my life. I would like to take upon this opportunity to present this thesis as a gift to my beloved daughter Xinbei.

ABSTRACT

Renewable energy applications in electric power systems have undergone rapid development and increased use due to global environmental concerns associated with conventional energy sources. Photovoltaics and wind energy sources are considered to be very promising alternatives for power generation because of their tremendous environmental, social and economic benefits, together with public support.

Electrical power generation from wind and solar energy behaves quite differently from that of conventional sources. The fundamentally different operating characteristics of these facilities therefore affect power system reliability in a different manner than those of conventional systems. The research work presented in this thesis is focused on the development of appropriate models and techniques for wind energy conversion and photovoltaic conversion systems to assess the adequacy of composite power systems containing wind or solar energy.

This research shows that a five-state wind energy conversion system or photovoltaic conversion system model can be used to provide a reasonable assessment in practical power system adequacy studies using an analytical method or a state sampling simulation approach. The reliability benefits of adding single or multiple wind/solar sites in a composite generation and transmission system are examined in this research. The models, methodologies, results and discussion presented in this thesis provide valuable information for system planners assessing the adequacy of composite electric power systems incorporating wind or solar energy conversion systems.

TABLE OF CONTENTS

LIST OF FIGURES

LIST OF TABLES

LIST OF ABBREVIATIONS

A	Availability
ARMA	Auto-Regressive and Moving Average
COPT	Capacity Outage Probability Table
DAFOR	Derating Adjusted Forced Outage Rate
DAFORW	Derating Adjusted Forced Outage Rate of WTG
DC	Direct Current
DPLVC	Daily Peak Load Variation Curve
EDLC	Expected Duration of Load Curtailment
EENS	Expected Energy Not Supplied
FOR	Forced Outage Rate
hrs	Hours
HL	Hierarchical Levels
HL-I	Hierarchical Level-I
HL-II	Hierarchical Level-II
HL-III	Hierarchical Level-III
IEEE-RTS	IEEE Reliability Test System
IEAR	Interrupted Energy Assessment Rate
I-V Curve	Current-Voltage Curve
kWh	Kilowatt-hours
LDC	Load Duration Curve
LOEE	Loss of Energy Expectation
LOLE	Loss of Load Expectation
LOLP	Loss of Load Probability
MCS	Monte Carlo Simulation

MDAFORW	Modified Darating Adjusted Forced Outage Rate of WECS
MECORE	Monte Carlo Simulation and Enumeration Composite System Reliability Evaluation Program
MTTF	Mean Time to Failure
MTTR	Mean Time to Repair
MPP	Maximum Power Point
MSCOPTW	Modified State Capacity Outage Probability Table of WECS
MW	Megawatt
MWh	Megawatt-hours
NID	Normally Independent Distributed
OPF	Optimal Power Flow
occ.	Occur
PLC	Probability of Load Curtailment
p.u.	Per unit
PV	Photovoltaic
PVCS	Photovoltaic Conversion System
RBTS	Roy Billinton Test System
SCOPT	State Capacity Outage Probability Table
SCOPTW	State Capacity Outage Probability Table of WTG
U	Unavailability
WECS	Wind Energy Conversion System
yr	Year

1. INTRODUCTION

1.1 Power System Reliability Evaluation

Modern electrical power systems have the responsibility of providing a reliable and economic supply of electrical energy to their customers. The economic and social effects of loss of electric service can have significant impacts on both the utility supplying electric energy and the end users of the service. Maintaining a reliable power supply is therefore a very important issue in power system design and operation.

The term “reliability” when associated with a power system is a measure of the ability of the system to meet the customer requirements for electrical energy. The general area of “reliability” is usually divided into the two aspects of system adequacy and system security [1, 2], as shown in Figure 1.1.

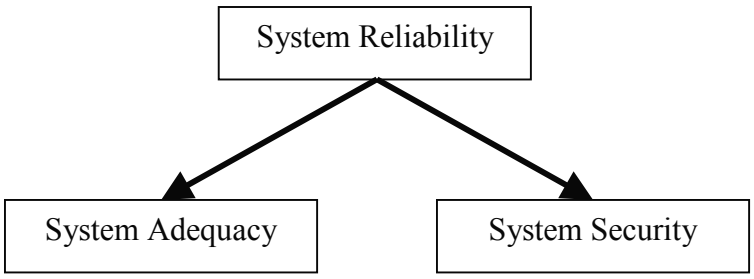

Figure 1.1: Subdivision of system reliability

System adequacy relates to the existence of sufficient facilities within the system to satisfy the customer demand. These include the facilities necessary to generate sufficient energy and the associated transmission and distribution facilities required to transport the energy to the actual customer load points. System security, on the other hand, is considered to relate to the ability of the system to respond to disturbances arising in the system, such as dynamic, transient, or voltage instability situations [1]. This thesis is restricted to adequacy assessment of power systems.

An overall power system can be divided into the three zones shown in Figure 1.2. The three segments are the functional zones of generation, transmission and distribution. Hierarchical levels are created by combining the functional zones.

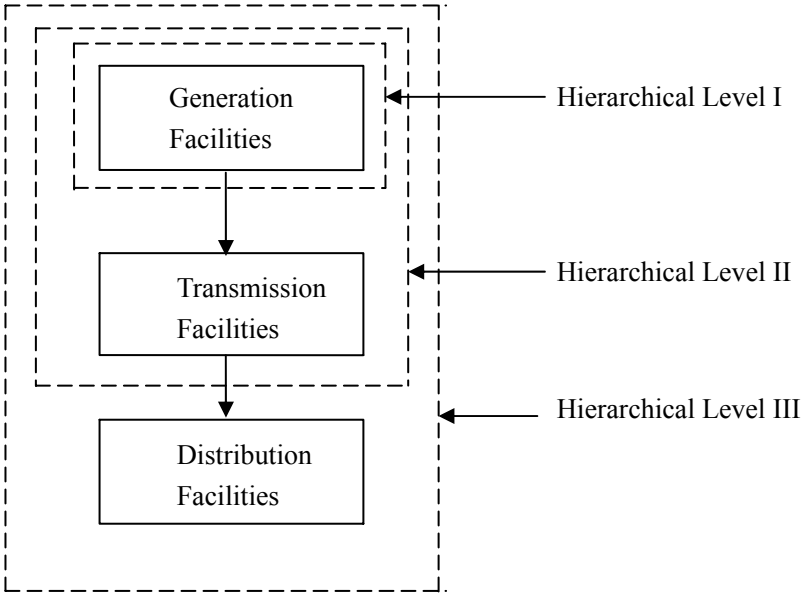

Figure 1.2: Hierarchical level structure

Reliability assessment at hierarchical level I (HL-I) is solely concerned with the generation facilities. At this level, the total system generation including interconnected assistance is examined to determine its ability to meet the total system load demand. Reliability assessment at HL-I is normally defined as generating capacity reliability

evaluation. The application of probability methods to HL-I analysis was first conducted well over 50 years ago and has been extensively investigated since that time [2-7]. Reliability evaluation at hierarchical level II (HL-II) includes both the generation and transmission in an assessment of the integrated ability of the composite system to deliver energy to the bulk supply points. This analysis is usually termed as composite system or bulk power system reliability evaluation. Adequacy evaluation at HL-II has received considerable attention and there are many publications in this area [2-8]. Overall assessment considering all three functional segments is known as HLIII analysis. The research described in this thesis is conducted at both HL-I and HL-II and is focused on adequacy analysis.

Reliability analysis of a power system can be conducted using either deterministic or probabilistic techniques. The early techniques used in practical application were deterministic and some of them are still in use today. The essential weakness of deterministic criteria is that they do not respond to the stochastic nature of system behavior, customer demands or component failures. System behavior is stochastic in nature, and therefore it is logical to consider probabilistic methods that are able to respond to the actual factors that influence the reliability of the system [1]. Limited computational resources, lack of data and evaluation techniques have limited the use of probability methods in the past. These factors are not valid today, and there has been a wealth of publications dealing with the development and application of probabilistic techniques in power system reliability evaluation [2-8]. The research described in this thesis extends the probabilistic evaluation of power systems incorporating renewable energy.

Power system reliability is usually expressed in the form of indices that reflect the system capability and the service provided to the customers. Two fundamental

methodologies are applied in power system reliability evaluation. These approaches can be categorized into the two general designations of analytical methods and simulation methods. Analytical methods represent the system by mathematical models and evaluate the reliability indices using direct numerical solutions. Simulation methods estimate the reliability indices by simulating the actual process and random behavior of the system.

1.2 Power Systems Including Renewable Energy

It is well known that there are many potential problems with the use of traditional energy sources such as coal and oil. Perhaps the most threatening of these problems is the greenhouse effect, where certain pollutants prevent the sun's radiation from escaping the Earth's atmosphere. This has the potential of creating dangerous climate changes and melting polar ice caps. Even small changes in average annual temperature such as two or three degrees can have devastating effects on certain species and ecosystems. Traditional fuels also have potential problems in regard to sustainability due to the limited reserves of coal, oil, and natural gas. Most governments now have programmes to support the exploitation of the so-called new renewable energy sources, which include wind power, micro-hydro, solar photovoltaics, landfill gas, energy from municipal waste and biomass generation [9].

In the past two decades, wind power has undergone rapid development and increased use in both small-sized isolated and grid connected applications. The global wind power industry installed 7,976 MW in 2004. This is an increase in total installed generating capacity of 20%, according to figures released by the Global Wind Energy Council. Global wind power capacity has grown to 47,317 MW. Table 1.1 shows the global data and Table 1.2 shows the wind power capacity in Canada tabulated by the Canada Wind Energy Association (CanWEA). The CanWEA’s goal is to achieve 10,000 MW of wind

energy by 2010 [10].

Table 1.1: Global wind power capacity data [10]

Country	MW Installed
Germany	16,629
Spain	8,263
U.S.A	6,740
Denmark	3,117
India	3,000
Italy	1,125
Netherlands	1,1078
UK	1,037

Table 1.2: Wind power in Canada [10]

Year	2000	2001	2002	2003	2004
MW Installed (at year end)	137	198	236	322	444

Photovoltaic (PV) power is a very promising renewable energy source throughout world and has the potential to provide enormous benefits. The most obvious benefit is that new capacity can be provided without adding to overall pollution production. In many systems, the greatest energy use tends to occur on days when the sun is the brightest, which enables PV energy to provide "peak shaving" capability. A further benefit of solar energy is that it can be used to reduce line losses. The placement of PV power systems at or near the point where the power is used avoids the need to transmit the power over the transmission and distribution network. Power that is transmitted is subject to resistive power losses. Those losses vary with the distance the power is transmitted and the voltage level at which the power is delivered [11].

The development of PV devices and systems has undergone continuous improvement over the last decade. Large photovoltaic generating systems with capacities of one megawatt or greater were installed in the U.S.A in the 1980s by private companies and

utilities. The Sacramento Municipal Utility District (SMUD) in the U.S.A installed 2 MW of PV modules next to the closed Rancho Seco nuclear power plant to provide power to 500 homes. Other megawatt scale grid-connected photovoltaic power plants are located in Japan and Norway. There are also a few experimental plants in Saudi Arabia and West Germany, and Italy has the world's largest PV power station with 3.3 MW.

In order to examine the future prospects for large-scale photovoltaic electricity generation, the Pacific Gas & Electric Company in the United States created a government industry partnership called the Photovoltaic for Utility Scale Applications (PVUSA) project [12]. The project was designed to bridge the gap between photovoltaic research and development and commercial implementation. Similar projects have been initiated around the world. For example, in Japan all the major utilities are involved in photovoltaic projects and the largest West German utility, Rheinisch Westfalisches Electrizitatswerk is evaluating several photovoltaic technologies [12].

1.3 Research Object and Overview of the Thesis

New technologies for electrical power generation from solar energy and wind energy have been developed and considerable research is being done to improve them. The fundamentally different operating characteristics of these new technologies will affect power system reliability in a different manner than conventional technology systems. As power generation plants using wind and solar energy are integrated into existing power systems, it becomes particularly important to evaluate the reliability of these plants and assess the effects that they will have on the overall system reliability.

Considerable research has been conducted to develop mathematical models and

techniques for reliability evaluation of power systems containing wind and/or solar energy. Many of the relevant publications are documented in five comprehensive bibliographies published since 1988 [3-7]. Some specific references considered in this research are presented in [13-23]. These references are focused on generating system reliability evaluation and most of them use the sequential Monte Carlo simulation technique. An analytical method for evaluating the reliability of generation system containing unconventional energy sources is presented in [14]. This approach does not incorporate the chronological nature of wind speed and solar radiation. Analytical methods are also presented in [15, 16] to evaluate the reliability performance of stand-alone renewable energy based systems. Considerably less work has been done on the reliability evaluation of composite power systems incorporating wind or solar energy.

The main object of the research described in this thesis is to develop appropriate models and techniques for wind energy conversion systems (WECS) and photovoltaic conversion systems (PVCS) that can be used to assess the adequacy of composite power systems containing wind or solar energy. The objectives of this research have been accomplished by focusing on the following tasks.

1. The development of appropriate multi-state WECS and PVCS models for adequacy evaluation.
2. The examination of appropriate multi-state WECS and PVCS models in generating system adequacy evaluation and the utilization of these models in the Monte Carlo state sampling approach to composite system evaluation.
3. An examination of the HL-I adequacy contribution of renewable energy sources by considering them as negative loads.
4. The adequacy benefit assessment associated with multiple independent wind or solar

energy facilities in a composite power system.

This thesis is organized into six chapters:

Chapter 1 introduces some of the basic concepts related to power system reliability evaluation and power systems including renewable energy. It also outlines the research objectives and the scope of the thesis.

Chapter 2 briefly describes relevant system reliability indices. Three techniques used in power system adequacy evaluation, i.e. the analytical technique, and the non-sequential and sequential Monte Carlo simulation techniques are illustrated in this chapter. A composite generation and transmission system reliability evaluation software known as MECORE [24] is introduced in this chapter. The two test systems designated as the Roy Billinton Test System (RBTS) [25] and the IEEE Reliability Test System (RTS) [26], which are used extensively in this thesis, are also briefly introduced. Base cases studies of the two test systems together with the corresponding assumptions are presented and the system adequacy indices obtained using the three evaluation techniques are presented and compared.

Chapter 3 presents the time series models utilized to simulate the hourly wind speeds and the basic models for wind turbine generator (WTG) units. Sample simulation results obtained using these models are also illustrated. The seasonal wind speeds of selected wind sites and wind power outputs are examined. An analytical procedure that incorporates the forced outage rate of the wind turbine units is applied to build a multi-state model of a wind energy conversion system (WECS). The apportioning method [27，28] is introduced and used to establish selected multi-state WECS models. The number of derated states in the WECS model required for an acceptable appraisal is analyzed in this chapter. The HL-I reliability indices for the RBTS including wind energy obtained by utilizing the three evaluation techniques are shown. The effect of

modifying the RBTS load model by considering WECS as negative load is presented.

Chapter 4 describes the basic solar energy models and how multi-state photovoltaic energy system (PVCS) models can be established. The program WATGEN and WATSUN [29, 30] are briefly introduced and used to generate hourly solar radiation data and hourly PV generating unit output power. This chapter illustrates the system reliability indices calculated using two-state and multi-state PVCS models. Attention is focused on how many PVCS derated states are required for an acceptable assessment in a MECORE or analytical method application. The effect of modifying the RBTS load model by considering PVCS as negative load is also studied.

Chapter 5 is focused on adequacy assessment in composite generation and transmission systems. The reliability indices of the RBTS incorporating WECS and PVCS are illustrated. The research described in this chapter examines the effects of various parameters, such as peak load variation, renewable energy installed capacity and wind or solar energy site locations for both the RBTS and RTS. The adequacy benefit assessment associated with single or multiple independent wind or solar energy facilities in composite power systems is analyzed and assessed.

Chapter 6 summarizes the research work described in the thesis and presents some general conclusions.

2. BASIC CONCEPTS IN POWER SYSTEM ADEQUACY ASSESSMENT

2.1 Introduction

As noted in Chapter 1, power system adequacy is usually expressed in the form of indices that reflect the system capability and the service provided to the system customers. Adequacy indices can be used to predict the performance of different system designs, reinforcements and expansion plans and the related cost/worth of the alternatives. Significant effort has been applied to develop techniques for predicting and assessing the adequacy performance of actual power systems [2-8]. The fundamental approaches used to calculate adequacy indices in a probabilistic evaluation can be generally described as being either analytical evaluation or Monte Carlo simulation. Analytical techniques represent the system by analytical models and evaluate the system adequacy indices from these models using mathematical solutions. Monte Carlo simulation techniques, on the other hand, estimate the adequacy indices by simulating the actual process and the random behavior of the system. Both approaches have advantages and disadvantages, and each of them can be very powerful with proper application.

Analytical methods are used in the research described in this thesis to conduct generating capacity adequacy evaluation. Monte Carlo methods [1, 31] are applied in both generating system and bulk power system studies. This chapter provides a brief description of some of the analytical methods for generating capacity adequacy evaluation. Non-sequential and sequential Monte Carlo simulation techniques are also described in this chapter.

This chapter introduces the reliability indices used in this research and an evaluation software known as MECORE [24]. The concepts are illustrated by application to the two composite test systems.

2.2 General Assessment Techniques

2.2.1 Analytical Techniques

Analytical techniques represent the system by analytical models and evaluate the system risk indices from these models using mathematical solutions. The analytical approach can in many cases provide accurate probabilistic indices in a relatively short calculation time. Analytical techniques have been extensively developed for HL-I and HL II studies [2-8]. Analytical techniques, however, usually require assumptions to simplify the solutions. This is particularly the case when complex systems and operating procedures have to be modeled. The resulting analysis can therefore lose some of its significance. Analytical techniques are applied in some of the HL-I studies described in this thesis.

The basic modeling approach in an HL-I analysis is shown in Figure 2.1. The generation model and the load model are combined to produce the risk model. The risk indices obtained are overall system adequacy indices and do not include transmission constraints and transmission reliabilities.

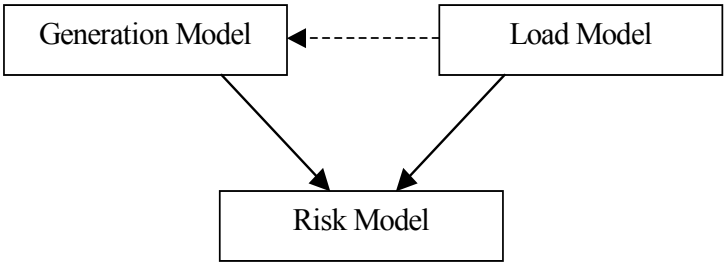

Figure 2.1: Conceptual tasks for HL- I evaluation

In most analytical techniques, the generation model is normally in the form of an array of capacity levels and their associated probabilities. This representation is known as a

capacity outage probability table (COPT) [1]. Each generating unit in the system is represented by either a two-state or a multi-state model. The COPT can be constructed using a recursive technique [1]. This technique is very powerful and can be used to add both two-state and multi-state generating units.

The load models used in the analytical methods depend on the reliability indices adopted, the availability of load data and the evaluation methods used. The load model is usually represented by either the daily peak load variation curve (DPLVC) or the load duration curve (LDC). The DPLVC is a cumulative load model formed by arranging the individual daily peak loads in descending order. The load duration curve is created by arranging the hourly load values in descending order. The DPLVC is used extensively, due to its simplicity. The LDC, however, is a more realistic representation of the system load.

Generating Unit Model

A COPT is usually used to represent the system generation model in most analytical techniques. Each individual generating unit in the system is represented by either a two-state or a multi-state model. In the two state model, the generating unit is considered to be either fully available (Up) or totally out of service (Down) as shown in Figure 2.2.

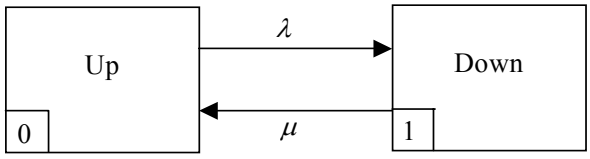

Figure 2.2: Two-state model for a generating unit

where λ = unit failure rate

μ = unit repair rate.

The availability (A) and the unavailability (U) of the generating unit are given by Equations (2.1) and (2.2) respectively. The unit unavailability is also known as the forced outage rate (FOR).

$$A = \frac{\mu}{\lambda + \mu} = \frac{m}{m + r} = \frac{\sum[UpTime]}{\sum[DownTime] + \sum[UpTime]} \tag{2.1}$$

$$U = \frac{\lambda}{\lambda + \mu} = \frac{r}{m + r} = \frac{\sum[DownTime]}{\sum[DownTime] + \sum[UpTime]} \tag{2.2}$$

where m = mean time to failure = MTTF = 1/ μ

r = mean time to repair = MTTR = 1/ λ

A multi-state generating unit is a unit that can exist in one or more derated or partial output states as well as in the fully up and fully down states [1]. The simplest model that incorporates derating is shown in Figure 2.3. This three-state model includes a single derated state in addition to the full capacity and failed states.

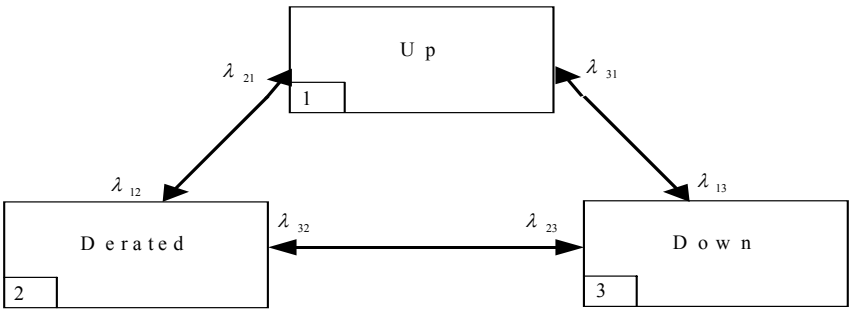

Figure 2.3: Three-state model for a generating unit

where λ_{ij} is the transition rate between state "*i*" and state "*j*".

Recursive Algorithm

A recursive algorithm [1] for adding two state generating units is given in Equation (2.3). This equation shows the cumulative probability of a certain capacity outage state of X MW calculated after a unit of capacity C MW, with a forced outage rate U, is added.

$$P(X) = (1 - U)P'(X) + (U)P'(X - C) \tag{2.3}$$

where $P'(X)$ and $P(X)$ are the cumulative probabilities of a capacity outage level of X MW before and after the unit of capacity C is added respectively. Equation (2.3) is initialized by setting $P'(X) = 1.0$ for X < 0 and $P'(X) = 0$ otherwise.

Equation (2.3) is modified as shown in Equation (2.4) for generating units with derated states.

$$P(X) = \sum_{i=1}^{n} p_i P'(X - C_i), \tag{2.4}$$

where n = the number of unit states,

C_i = capacity outage state i for the unit being added,

p_i = probability of existence of the unit state i.

The capacity outage probability table is complete after all the generating units are added.

Loss of Load Method and Indices

The generation model is convolved with the load model as shown in Figure 2.1. In the loss of load method [1], the generation system represented by the COPT and the load characteristic represented by either the DPLVC or the LDC are convolved to calculate the loss of load expectation (LOLE) index. The LOLE presents the expected number of days (or hours) in the specified period in which the daily peak load (or hourly load) exceeds the available capacity. Figure 2.4 shows a typical load-capacity relationship.

A capacity outage O_k, which exceeds the reserve, causes a load loss for a time t_k shown in Figure 2.4. Each such outage state contributes to the system LOLE by an amount equal to the product of the probability p_k and the corresponding time unit t_k. The summation of all such products gives the system LOLE in a specified period as expressed in Equation (2.5). A capacity outage less than the reserve does not contribute to the system LOLE.

$$LOLE = \sum_{k=1}^{n} p_k \times t_k = \sum_{k=1}^{n} P_k \times (t_k - t_{k-1}) \tag{2.5}$$

where n = the number of capacity outage state in excess of the reserve.

p_k = probability of the capacity outage O_k

t_k = the time for which load loss will occur.

P_k = the cumulative outage probability for capacity outage O_k.

If the time t_k is the per unit value of the total period considered, the index calculated by Equation (2.5) is called the loss of load probability (LOLP).

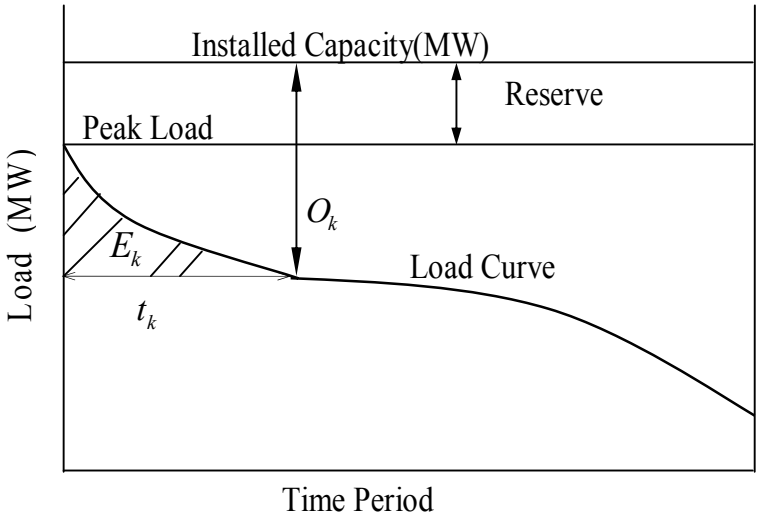

Figure 2.4: Relationship between capacity, load and reserve

When the load duration curve is used in Figure 2.4, the area under the LDC represents the total energy demand (E) of the system during the specific period considered. When an outage O_k with probability p_k occurs, it causes an energy curtailment of E_k, shown as the shaded area in Figure 2.4. The loss of energy expectation (LOEE) is given by Equation (2.6).

$$LOEE = \sum_{k=1}^{n} p_k \times E_k \tag{2.6}$$

The LOLE and LOEE methods are described in detail in [1], together with information on other techniques for HL-I evaluation.

2.2.2 Monte Carlo Simulation

As noted in Chapter 1, there are two general approaches for assessing power system reliability: the analytical method and the simulation method. Monte Carlo methods are more flexible when complex operating conditions and system considerations need to be incorporated. Considerable work has been done in the last two decades on the application of Monte Carlo simulation to power system reliability evaluation [1-8, 31]. These simulations utilize random number generators and probabilistic techniques to model the behavior of the power system. The two basic Monte Carlo methods used in power system reliability evaluation are generally known as the sequential and non-sequential techniques. Sequential evaluation involves a chronological analysis of the system and the component states. Non-sequential techniques are widely used for power system reliability evaluation and can be divided into the two categories of state sampling and state transition sampling. The following is a brief description of the basic techniques.

Non-Sequential Methods: State Sampling Approach

In this approach, the system state is obtained by sampling all the component states irrespective of the event chronologies. The basic sampling procedure is conducted by assuming that the behaviour of each component can be categorized by a uniform distribution under [0, 1]. The component can be represented by a two-state or multi-state model. In the case of a two-state component, each component has the two states of failure and success and component failures are independent events. The state of the system containing n components including generating units, transmission lines, transformers, etc., can be expressed by the vector S, where $S = (S_1, \ldots, S_i, \ldots, S_n)$, S_i is the state of the i_{th} component. When S equals zero, the system is in the normal state. When S is not equal to zero, the system is in a contingency state due to component outage(s). The following steps describe the process of this method.

Step 1. Generate a uniform random number U_i for the i_{th} component.

Step 2. Determine the state of component i using the following expression:

$$S_i = \begin{cases} 0 & (success \quad state) \quad if \quad U_i \geq FOR_i \\ 1 & (failure \quad state) \quad if \quad 0 \leq U_i < FOR_i \end{cases} \tag{2.7}$$

where FOR_i is the i_{th} component's forced outage rate.

Step 3. The system state S is obtained by applying Step 2 to all the components.

Step 4. Determine the system state. If S equals zero, the system is in the normal state. If S is not equal to zero, the system is in a contingency state.

Step 5. A linear programming optimization model is usually used to reschedule generation, alleviate line overloads and to avoid load curtailment if possible or to minimize the total load curtailment if unavoidable.

Step 6. Reliability indices for each load point and the system are accumulated and Steps 1 to 5 are repeated until the stopping criterion is reached.

One of the advantages of the system state sampling method is that multi-state components can be incorporated in the analysis without a significant increase in computing time. The probabilities of the i_{th} component including a single derated state for Step 2 are expressed in Equation (2.8), where PDR_i is the probability of the single derated state of the i_{th} component.

$$S_i = \begin{cases} 0 & (up \quad state) \quad if \quad U_i \geq PDR_i + FOR_i \\ 1 & (down \quad state) \quad if \quad PDR_i \leq U_i < PDR_i + FOR_i \\ 2 & (derated \quad state) \quad if \quad 0 \leq U_i < PDR_i \end{cases} \tag{2.8}$$

Additional derated states can be simulated in a similar manner.

The basic state sampling technique is relatively simple. It only involves the generation of uniformly distributed random numbers in the range of 0 to 1 instead of sampling a distribution function, and only basic reliability data in the form of component-state probabilities are required. The state sampling technique estimates the frequency of load curtailments as the sum of the occurrences of load curtailment states. This is actually an upper boundary of the actual frequency index.

Non-Sequential Methods: State Transition Sampling Approach

The state transition sampling technique focuses on system state transitions, instead of component states or component state processes. In this method, the state transition of any component leads to a system state transition and all the state residence times are assumed to be exponential distributed. The following steps briefly describe the procedure for this method.

Step 1. The simulation process starts from the normal system state in which all the system components are in the up state, which means every component in the system is available.

Step 2. If the present system state is a contingency state in which at least one component is in the outage state, the minimization model of load curtailment is used to evaluate the adequacy of this system state. Otherwise, proceed to the next step without utilizing the minimization model.

Step 3. Uniform distributed random numbers are generated to determine the next system state using the state transition sampling procedure. In this procedure, a system state transition sequence is directly created. It can therefore be used to calculate the actual frequency indices of the load points and for the total system.

Step 4. The process is repeated from Step 2 until the selected convergence criterion is satisfied.

The state transition sampling method can be used to calculate an exact frequency index without sampling the distribution function and storing chronological information as in the sequential technique. The main restriction in this technique is that it only applies to exponentially distributed component state durations. This technique is usually computationally slower than the state sampling simulation approach.

Sequential Method

The sequential or state duration approach is based on sampling the probability distributions of the component state durations. This technique can be used to model all the contingencies and operating characteristics inherent in the system. Chronological

load models can also be easily incorporated. The sequential approach is summed up in the following steps [32]:

Step 1. Specify the initial state of each component. Generally, it is assumed that all components are in the up state.

Step 2. Sample the duration of each component residing in its present state using the inverse transform method [31] and the distribution functions of the component failure and repair rates. For example, given an exponential distribution function, i.e. $f(t) = \lambda e^{-\lambda t}$, the sampling value of the state duration (T) is

$$T_i = -\frac{1}{\lambda_i} \ln U_i \tag{2.9}$$

where U_i is a uniformly distributed random number between [0, 1] corresponding to the i_{th} component. λ_i is a failure rate or repair rate depending on the current state of the i_{th} component.

Step 3. Repeat Step 2 in a given time span, usually one year (8760 hours). A chronological up and down state for each component is then constructed in a given time span. Reliability indices can be calculated by incorporating the load models.

Step 4. The simulated operation is assessed for each hour during a given time span. If constraints occur, corrective actions may be required to alleviate the constraints and load curtailed if necessary.

Step 5. At the end of each simulated year, the reliability indices are calculated and updated. Steps 2-4 are repeated until the coefficient of variation is less than the specified tolerance error.

The sequential method can be used to calculate the actual frequency index as well as related indices and can incorporate different state duration distributions. The statistical probability distributions of the adequacy indices can also be assessed in addition to their expected values. This method, however, requires more computation time and storage than the state sampling approach since it is necessary to generate and store information on the chronological state transition processes of all the system components in a long time span.

The state sampling technique and the sequential technique are used to conduct some of the reliability studies described in this thesis.

2.3 Adequacy Indices for the HL-I and the HL-II Studies

There are many possible indices that can be used to measure the adequacy of a power system and different countries and utilities use different indices. Most adequacy indices are expected values of random variables. It should be noted that an expected value is not a deterministic parameter, it is the long-run average of the value under study.

The basic indices in generating system adequacy are the LOLP, LOLE and LOEE as noted in the previous section. These indices can be calculated using either the analytical methods or the Monte Carlo simulation techniques.

The adequacy index concepts used in HL-I studies can be extended to composite system assessments. Additional indices are, however, required to reflect the composite system characteristics. Both load point and system indices are necessary to provide a complete assessment of composite system adequacy. The indices can be categorized as annualized and annual values. Annualized adequacy indices are determined using a single load level in a one-year period and the system peak load is normally used. Annual adequacy indices, however, are calculated based on the actual time-varying load throughout the year. These indices include the expected customer unsupplied energy and can be used to determine the expected damage costs for the system. The basic adequacy indices used in composite system studies are presented in the following section with reference to the MECORE program.

2.4 The MECORE Software

The MECORE software is a Monte Carlo based composite generation and transmission system reliability evaluation tool designed to perform reliability and reliability worth assessment of bulk electric power systems. MECORE was initially developed at the University of Saskatchewan and subsequently enhanced at BC Hydro [24].

It can be used to assess composite generation and transmission reliability, generation reliability in a composite system and transmission reliability in a composite system, and provides a wide range of reliability indices for the system and for the individual load points. It also provides unreliability cost indices, which reflect reliability worth. The indices produced by the program can be used to aid in comparing different planning alternatives from a reliability point of view. MECORE is based on a combination of Monte Carlo simulation (state sampling technique) and enumeration techniques. The state sampling technique is used to simulate system component states and to calculate annualized indices at the system peak load level. A hybrid method utilizing an enumeration approach for aggregated load states is used to calculate annual indices using an annual load curve [24]. MECORE is designed to handle up to 1000 buses and 2000 branches.

In MECORE, the generating unit states are modeled using multi-state random variables. This program was initially designed to model generating units with up to two derated states. In order to examine appropriate multi-state renewable energy models, the MECORE program was modified to recognize ten derated states. Transmission lines are represented by two-state models. The MECORE program uses DC load flow and a linear programming Optimal Power Flow (OPF) model is utilized to reschedule generation (change generation patterns), alleviate line overloads and avoid load curtailments if possible or minimize total load curtailments if unavoidable.

A brief description is presented in the following. The capabilities of MECORE are further described in [24].

I. Failure modes:
   - Independent failures of generators, lines and transformers
   - Common cause outages of transmission lines
   - Generating unit derating states
II. Failure criteria:
   - Capacity deficiency

- Line overload
- System separation-load loss
- Bus isolation-load loss

III. Load model:

- Annual, seasonal, and monthly load curve
- Multi-step models
- Bus load proportional scaling and flat level model

IV. Probability indices:

- System and bus indices
- Annualized and monthly/seasonal/annual indices
- Basic and IEEE-proposed indices [1, 24]:

Basic Indices

(1) Probability of load curtailment (PLC)

$$\text{PLC} = \sum_{i \in S} P_i \tag{2.10}$$

where P_i is the probability of system state i and S is the set of all system states associated with load curtailments.

(2) Expected number of load curtailment (ENLC)

$$\text{ENLC} = \sum_{i \in S} F_i \text{ occ./yr} \tag{2.11}$$

The ENLC is the sum of the occurrences of the load curtailment states and is therefore an upper boundary of the actual frequency index. The system state frequency F_i can be calculated by the following relationship between the frequency and the system state probability P_i:

$$\text{F}_\text{i} = P_i \sum_{K \in N} \lambda_K \text{ occ./yr} \tag{2.12}$$

where λ_k is the departure rate of component k and N is the set of all components of the system.

(3) Expected duration of load curtailment (EDLC)

$$\text{EDLC} = \text{PLC} \times 8760 \text{ hrs/yr} \tag{2.13}$$

(4) Average duration of load curtailment (ADLC)

$$\text{ADLC} = \text{EDLC/EFLC} \quad \text{hrs/disturbance} \tag{2.14}$$

(5) Expected load curtailment (ELC)

$$\text{ELC} = \sum_{i \in S} C_i F_i \quad \text{MW/yr} \tag{2.15}$$

where C_i is the load curtailment of system state i.

(6) Expected demand not supplied (EDNS)

$$\text{EDNS} = \sum_{i \in S} C_i P_i \quad \text{MW} \tag{2.16}$$

(7) Expected energy not supplied (EENS)

$$\text{EENS} = \sum_{i \in S} C_i F_i D_i = \sum_{i \in S} 8760 C_i P_i \quad \text{MWh/yr} \tag{2.17}$$

where D_i is the duration of system state i.

(8) Expected damage cost (EDC)

$$\text{EDC} = \sum_{i \in S} C_i F_i D_i W \quad \text{k\$/yr} \tag{2.18}$$

where C_i is the load curtailment of system state i; F_i and D_i are the frequency and the duration of system state i; W is the unit damage cost in \$/kWh.

IEEE Proposed Indices

(9) Bulk power interruption index (BPII)

$$\text{BPII} = \frac{\sum_{i \in S} C_i F_i}{L} \quad \text{MW/MW-yr} \tag{2.19}$$

where L is the annual system peak load in MW.

(10) Bulk power/energy curtailment index (BPECI)

$$\text{BPECI} = \frac{EENS}{L} \quad \text{MWh/MW-yr} \tag{2.20}$$

(11) Bulk Power-supply average MW curtailment index (BPACI)

$$\text{BPACI} = \frac{ELC}{EFLC} \quad \text{MW/disturbance} \tag{2.21}$$

where EFLC is expected frequency of load curtailment:

$$\text{EFLC} = \sum_{i \in S} (F_i - f_i) \quad \text{occ./yr} \tag{2.22}$$

F_i is the frequency of departing system state i and f_i is the portion of F_i which corresponds to not going through the boundary wall between the loss-of-load state set and the no-loss-of-load state set.

(12) Modified bulk energy curtailment index (MBECI)

$$\text{MBECI} = \frac{EDNS}{L} \text{ MW/MW} \tag{2.23}$$

(13) Severity index (SI)

$$\text{SI} = BPECI \times 60 \text{ system min/yr} \tag{2.24}$$

The basic indices can be applied to an overall system or to a single load point, while the IEEE proposed indices apply to the overall system. The advantage of the IEEE proposed indices is that they can be used to compare the adequacy of systems having different sizes. When the MECORE program is used in HL-I studies, the transmission elements in the test system are assumed to be 100% reliable. The basic indices of LOLP, LOLE and LOEE used in HL-I analyses are the same as the PLC, EDLC and EENS respectively used in MECORE.

The rate of convergence in a Monte Carlo simulation of a composite system is different for the various load bus and system indices. A larger number of samples leads to higher accuracy but involves more computing time. The coefficient of variation of a particular index can be used as the convergence criterion. The coefficient of variation for the EDNS index is most often used and is outputted with the calculated results.

2.5 Two Composite Test Systems

The two test systems used in this thesis are the Roy Billinton Test System (RBTS) [25] and the IEEE Reliability Test System (IEEE-RTS) [26]. The single line diagrams of the RBTS and the IEEE-RTS are shown in Figures 2.5 and 2.6 respectively.

The RBTS is a small composite system developed for educational and research purposes at the University of Saskatchewan. It is a six-bus test system with five load buses. It has

eleven generators, nine transmission lines and seven branches. The total installed capacity is 240 MW and the system peak load is 185 MW. The system voltage level is 230 KV.

The IEEE-RTS is a relatively large system compared with the RBTS. It was developed by an IEEE Task Force to provide a practical representative bulk power system for research and comparative study purposes. The generating system contains 32 generators with capacities from 12 to 400 MW. The transmission system has 24 buses, which include 10 generator buses, 10 load buses, and 4 connection buses, connected by 33 lines and 5 autotransformers at two voltages levels: 138KV and 230 KV. The total installed capacity of the IEEE-RTS is 3405 MW and the system peak load is 2850 MW.

Both the RBTS and the RTS use the same per-unit load model, designated as the IEEE-RTS load model. This load model can be used to create 8760 hourly chronological loads on a per unit basis. The basic data for the two test systems are given in Appendix A.

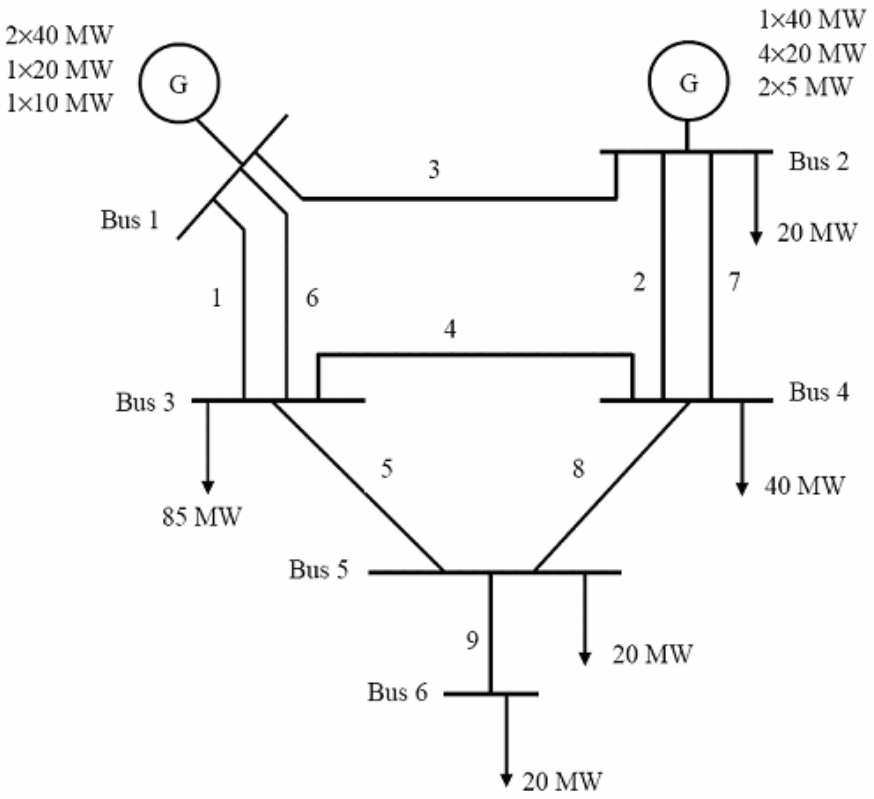

Figure 2.5: Single line diagram of the RBTS

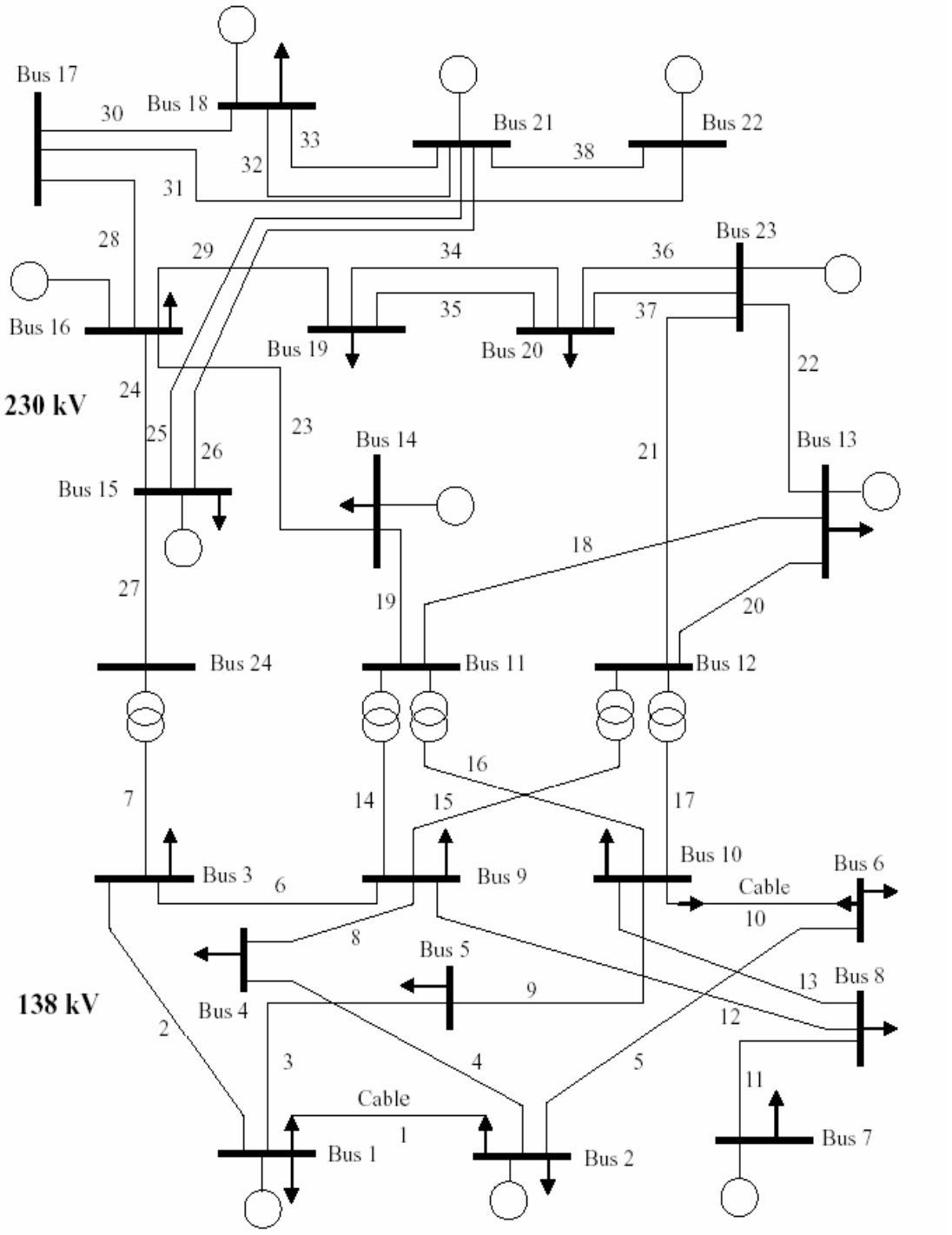

Figure 2.6: Single line diagram of the IEEE-RTS

2.6 Initial Studies on the RBTS and IEEE-RTS

Base case studies provide a reference framework for system modification and data sensitivity analyses. Many factors can be included in a composite system assessment, such as derated states of generating units, common mode failures of transmission lines, station originated failures and so on. In order to clearly understand the base case results, it is important to appreciate which factors are included and which factors are not considered. The following conditions were used in the base case analyses of the RBTS and IEEE-RTS in the research described in this thesis.

- The economic priority order for load curtailment is utilized.
- The step-down transformers at transformer stations are assumed to be customer owned and the reliability indices are calculated at the high voltage bus bars.
- Station configurations are not incorporated in the evaluation process.
- Transmission line common mode failures are not considered.

As noted earlier, both load point and system indices can be used to assess composite system adequacy. Load point indices indicate the reliability at the individual load buses, and system indices provide an overall evaluation of total system reliability and reliability worth. Individual load point indices are highly dependent on the system load curtailment philosophy. Each load bus has a different priority in an actual power system. One common method to determine the priority order is based on economic factors which recognize the customer cost associated with failure of supply. The most convenient index for this purpose is the Interrupted Energy Assessment Rate (IEAR), as it measures the customer monetary loss as a function of the energy not supplied [1]. The higher the IEAR, the more disruptive is the loss of supply and a higher priority code is applied.

The IEAR values for each load point [28, 33] and the corresponding priority order for the RBTS load points are given in Table 2.1. The values for each load point [28, 33] of the IEEE-RTS and the corresponding priority order are shown in Table 2.2.

Table 2.1: Bus IEAR values and priority order in the RBTS

Bus No.	IEAR ($/kWh)	Priority Order
2	7.41	1
3	2.69	5
4	6.78	2
5	4.82	3
6	3.63	4

Table 2.2: Bus IEAR values and priority order in the IEEE-RTS

Bus No.	IEAR ($/kWh)	Priority Order
1	6.20	1
2	4.89	9
3	5.30	8
4	5.62	3
5	6.11	2
6	5.50	4
7	5.41	5
8	5.40	6
9	2.30	16
10	4.14	10
13	5.39	7
14	3.41	14
15	3.01	15
16	3.54	13
18	3.75	11
19	2.29	17
20	3.64	12

The Expected Damage Cost (EDC) is an important index that can be used to perform economic analysis in composite system adequacy assessment. MECORE calculates this index by multiplying the EENS of the overall system by the system IEAR calculated using the following equation [1].

$$Average\ system \quad IEAR = \sum_{k=1}^{NB} IEAR_k q_k \tag{2.25}$$

where NB is the total number of load buses in the system, $IEAR_k$ is the Interrupted

Energy Assessment Rate (IEAR) at load bus *k,* and q_k is the fraction of the system load utilized by the customers at load bus *k*. The representative system IEAR of the RBTS can be calculated using the data in Table 2.1 and Table A.1, and is 4.42 $/kWh in this case. The representative system IEAR of the IEEE-RTS can be calculated using the data in Table 2.2 and Table A.4, and is 4.22 $/kWh.

The number of simulation samples should be carefully selected in order to obtain meaningful reliability results. Studies conducted earlier [28, 33] show that acceptable accuracy at HL-II can be achieved when the numbers of samples for the RBTS and the IEEE-RTS are 2,000,000 and 500,000 respectively. These sample sizes are used in the HL-II adequacy analyses described in this thesis.

The annualized system and bus indices are calculated at the annual system peak load level and expressed on a base of one year. The initial annual indices were calculated using 15-step load model. The annualized and annual load point indices of the RBTS under these conditions are shown in Tables 2.3 and 2.4 respectively. The annualized and annual system indices are given in Table 2.5.

Table 2.3: Annualized load point indices for the RBTS

Bus No.	PLC	ENLC (1/ yr)	ELC (MW/yr)	EDNS (MW)	EENS (MWh/yr)
2	0.00000	0.00150	0.004	0.00000	0.044
3	0.00869	4.08024	48.162	0.09699	849.637
4	0.00003	0.02135	0.142	0.00013	1.113
5	0.00003	0.03020	0.300	0.00033	2.888
6	0.00139	1.30199	24.081	0.02471	216.460

Table 2.4: Annual load point indices for the RBTS

Bus No.	PLC	ENLC (1/ yr)	ELC (MW/yr)	EDNS (MW)	EENS (MWh/yr)
2	0.00000	0.00000	0.000	0.00000	0.000
3	0.00018	0.10162	1.171	0.00201	17.564
4	0.00000	0.00109	0.008	0.00000	0.038
5	0.00000	0.00554	0.059	0.00003	0.296
6	0.00120	1.18265	15.095	0.01535	134.452

Table 2.5: Annualized and annual system indices for the RBTS

Indices	Annualized	Annual
ENLC (1/yr)	5.25586	1.27965
ADLC (hrs/disturbance)	16.48	9.45
EDLC (hrs/yr)	86.61	12.09
PLC	0.00989	0.00138
EDNS (MW)	0.122	0.017
EENS (MWh/yr)	1070.141	152.3497
EDC (K$/yr)	N/A	673.386
BPII (MW/MW- yr)	0.39292	0.08829
BPECI (MWh/MW- yr)	5.785	0.824
BPACI (MW/disturbance)	13.830	12.764
MBECI (MW/MW)	0.00066	0.00009
SI (system minutes/yr)	347.07	49.41

It can be seen from Table 2.3 and 2.4 that the EENS values at load buses 3 and 6 are much larger than those at the other load buses. It shows that Bus 3 and 6 are the least reliable load points in the RBTS, as Bus 3 has the lowest priority and Bus 6 has the second lowest priority among all the load buses in Table 2.1. Bus 6 has the highest annual EENS because Bus 6 is connected to the rest of the system by a single radial line and is relatively far from the generating units, as shown in Figure 2.1.

The annualized and annual load point indices of the IEEE-RTS are shown in Tables 2.6 and 2.7 respectively. The annualized and annual system indices are given in Table 2.8. Table 2.6 and 2.7 illustrate that the EENS at load buses 9, 14, 15 and 19 are larger than those at the other buses in the IEEE-RTS. These four buses have the four lowest priorities, as shown in Table 2.2.

Table 2.6: Annualized load point indices for the IEEE-RTS

Bus No.	PLC	ENLC (1/yr)	ELC (MW/yr)	EDNS (MW)	EENS (MWh/yr)
1	0.00000	0.00000	0.000	0.00000	0.000
2	0.00022	0.21533	7.517	0.00743	65.052
3	0.00012	0.12469	5.997	0.00579	50.685
4	0.00000	0.00000	0.000	0.00000	0.000
5	0.00000	0.00000	0.000	0.00000	0.000
6	0.00000	0.00000	0.000	0.00000	0.000
7	0.00000	0.00327	0.082	0.00005	0.438
8	0.00000	0.00294	0.062	0.00004	0.368
9	0.05080	35.32409	2612.315	3.86918	33894.023
10	0.00056	0.50498	35.025	0.03860	338.171
13	0.00003	0.03218	1.463	0.00126	11.073
14	0.01217	9.29683	639.791	0.81732	7159.724
15	0.03938	25.78817	2481.552	3.48197	30502.036
16	0.00552	4.43487	178.765	0.21584	1890.757
18	0.00237	1.90038	174.843	0.20937	1834.097
19	0.08419	58.09929	4160.457	5.99921	52553.046
20	0.00351	2.93097	153.836	0.18786	1645.678

Table 2.7: Annual load point indices for the IEEE-RTS

Bus No.	PLC	ENLC (1/yr)	ELC (MW/yr)	EDNS (MW)	EENS (MWh/yr)
1	0.00000	0.00000	0.000	0.00000	0.000
2	0.00000	0.00140	0.049	0.00005	0.397
3	0.00000	0.00082	0.027	0.00002	0.215
4	0.00000	0.00000	0.000	0.00000	0.000
5	0.00000	0.00000	0.000	0.00000	0.000
6	0.00000	0.00075	0.052	0.00003	0.293
7	0.00000	0.00041	0.004	0.00000	0.021
8	0.00000	0.00004	0.000	0.00000	0.002
9	0.00113	0.87165	53.880	0.06935	607.472
10	0.00001	0.00535	0.295	0.00029	2.541
13	0.00000	0.00013	0.004	0.00000	0.031
14	0.00021	0.17742	10.795	0.01266	110.899
15	0.00067	0.52376	45.318	0.05604	490.941
16	0.00010	0.08251	3.165	0.00362	31.750
18	0.00003	0.03086	2.402	0.00255	22.367
19	0.00201	1.51929	96.376	0.12820	1123.034
20	0.00006	0.05564	2.484	0.00273	23.956

Table 2.8: Annualized and annual system indices for the IEEE-RTS

Indices	Annualized	Annual
ENLC (1/yr)	58.10550	1.52049
ADLC (hrs/disturbance)	12.691	11.564
EDLC (hrs/year)	737.504	17.584
PLC	0.08419	0.00201
EDNS (MW)	14.833	0.276
EENS (MWh/yr)	129932.7	2413.923
EDC (K$/yr)	N/A	10186.755
BPII (MW/MW- yr)	3.66724	0.07539
BECI (MWh/MW- yr)	45.590	0.847
BPACI (MW/disturbance)	179.873	141.305
MBECI (MW/MW)	0.00520	0.00010
SI (system minutes/yr)	2735.426	50.819

It can be seen from Tables 2.3 to 2.8 that the annual indices are much lower than the annualized indices. The annual indices are obtained using the annual load model in which the load resides at the peak level for only a short period of time during a year. It can be also seen from Tables 2.3, 2.4, 2.6 and 2.7 that the indices of the load points with low priority order are higher than at other load points, which indicates that the individual load point indices are highly dependent on the load curtailment priority order.

2.7 Comparison of the Different Adequacy Evaluation Techniques

The analytical technique, MECORE and the sequential Monte Carlo simulation (MCS) approach are introduced in the previous sections. A brief comparison of the three methods was conducted at HL-I using the RBTS. The system peak load is 185 MW and the total generation is 240 MW. The annual system LOLE and LOEE are used in the comparison. The output indices EDLC and EENS of MECORE in an HL-I assessment are the same as the LOLE and LOEE in the analytical method and the sequential MCS techniques respectively. As noted earlier, when the MECORE program is used for an HL-I study, the transmission elements of the system are considered to be 100% reliable. This is accomplished by inputting zero values for the transmission element

unavailabilities. The adequacy indices obtained using the sequential MCS technique [32] were provided by Mr. Wijarn Wangdee using a software developed in his research program.

2.7.1 The Annualized System Indices

The annualized system indices for the RBTS using MECORE are shown in Table 2.9 as a function of the number of samples in the simulation.

Table 2.9: The HL-I annualized system indices for the RBTS using MECORE

Number of Sample	PLC (/yr)	EDLC (hrs/yr)	EENS (MWh/yr)	SI (sys.mins/yr)	Variance coefficient of EDNS
5,000,000	0.00840	73.56	831.59	269.70	0.0066331
2,000,000	0.00839	73.53	828.96	268.85	0.0105102
1,000,000	0.00839	73.52	838.24	271.86	0.0148031
600,000	0.00828	72.49	817.23	265.05	0.0192989
500,000	0.00834	73.04	827.73	268.45	0.0210267

The annualized system LOEE values for the analytical method and sequential MCS simulation approach are 823.26 MWh/yr and 812.82 MWh/yr respectively. These values are shown in Figure 2.7 together with the MECORE EENS results as a function of the number of samples.

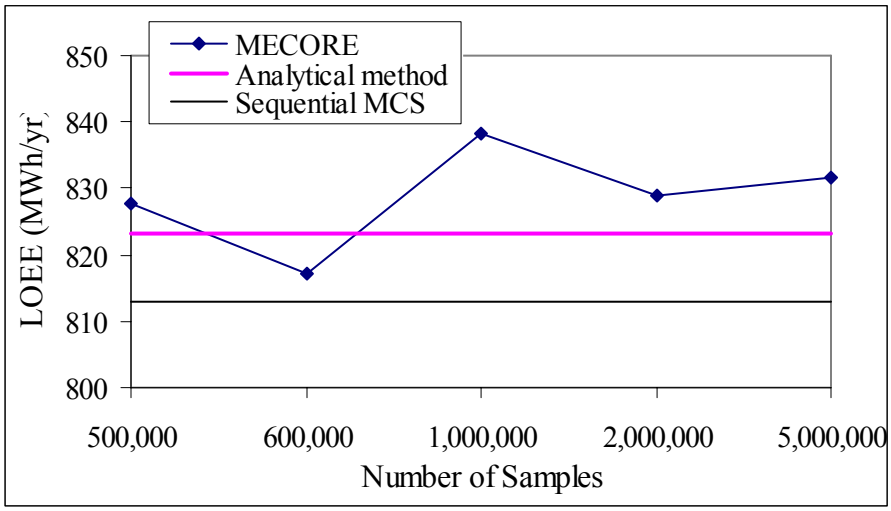

Figure 2.7: The annualized system LOEE for the three evaluation techniques

It can be seen from Figure 2.7 that the annualized system LOEE obtained using 600,000 iterations using MECORE is close to the values obtained using the analytical and sequential MCS techniques and Table 2.9 shows that it has a coefficient of variation of less than 2%. The 600,000 sample values are used in Table 2.10. This table presents the results from the three methods and illustrates that the three techniques provide similar estimates for the annualized system LOLE and LOEE.

Table 2.10: The HL-I annualized system indices for the RBTS

Indices	Analytical method	MECORE	Sequential MCS method
LOLE (hrs/yr)	73.07	72.49	70.51
LOEE (MWh/yr)	823.26	817.23	812.82

2.7.2 The Annual System Indices

Annual indices are normally calculated using a chronological load model or a load duration curve (LDC) on an annual basis (8760 hours). In this research, the IEEE-RTS annual load duration curve is divided into 15, 20 and 40 non-uniform load steps respectively as shown in Figure 2.8. The annual reliability indices are obtained by weighting the annualized indices for each load level by the load step probability [31]. This procedure is used in the MECORE software. Appendix B shows the results obtained using the MECORE program and the detailed data of the three multi-step load duration curves.

The number of steps in the load duration curve has considerable influence on the calculated annual indices. This effect is shown in Table 2.11. If the load curve is divided into only a few steps, the calculated annual indices will provide an inaccurate adequacy assessment. The maximum number of steps in the load model in MECORE is 40 and the original load model [24, 31] applied earlier in this thesis is a 15-step model. Table 2.11 shows the HL-I system indices obtained using 15, 20 and 40-step load models.

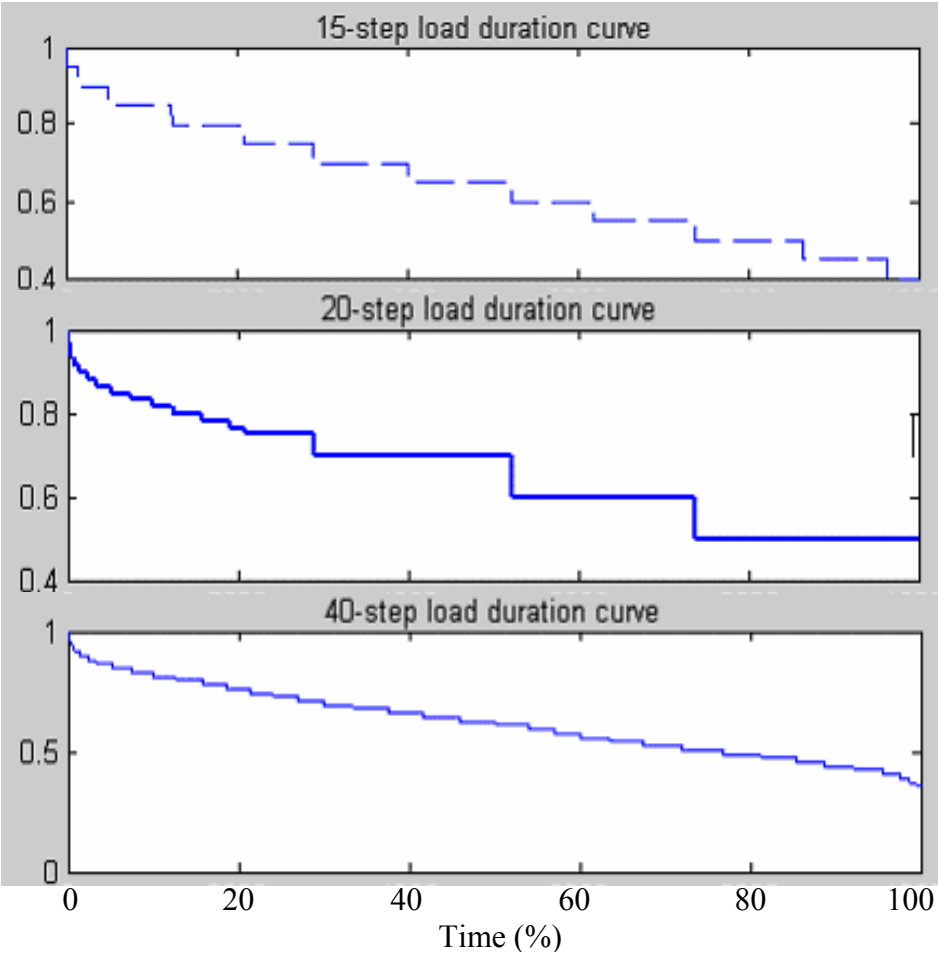

Figure 2.8: The multi-step load duration curves

Table 2.11: The HL-I annual system indices for the RBTS using MECORE

Multi-step LDC	EDLC (hrs/yr)	EENS (MWh/yr)	Calculation Time (seconds)
15-step	1.49	16.74	24.71
20-step	1.15	11.78	38.28
40-step	1.14	11.38	60.75

The annual system LOLE and LOEE for the RBTS were obtained by applying the analytical method using two load profiles. The first profile is a 20-step LDC and the second is an exact annual load model (8760 hours). A chronological load model was used in the sequential MCS simulation method to obtain the annual indices. The HL-I results for the three techniques are shown in Table 2.12.

Table 2.12: The RBTS HL-I annual system indices for the three techniques

Indices	Analytical Method		MECORE	Sequential MCS method
	20-step LDC	Exact Load Model (8760 points)		
LOLE (hrs/yr)	1.16	1.09	1.15	1.07
LOEE (MWh/yr)	12.00	9.86	11.78	9.65

The annual indices shown in Table 2.12 indicate that the differences between the indices for MECORE and the analytical method (20-step LDC) are relatively small when they use the same load model. The results obtained using the sequential technique are very similar to those obtained using the analytical method and the exact load model (8760 hours). The conclusion can be drawn that the load model is the main reason for the variability in the system reliability indices between the three methods.

Table 2.11 shows that the differences in the reliability indices for the 20 and 40 step load models are very small. The required calculation time for the 40-step load model is considerably higher. Both discrete step load models provide reliability indices that are slightly higher than those calculated using the detailed load data. The 20-step load model is utilized in the subsequent HL-I and HL-II studies described in this thesis.

2.8 Summary

This chapter briefly describes some basic concepts and evaluation techniques utilized in HL-I and HL-II analyses. Adequacy at these two hierarchical levels can be assessed either by analytical techniques or by Monte Carlo simulation methods. Three basic Monte Carlo simulation techniques designated as state sampling, state transition sampling and sequential analysis are introduced in this chapter. Each approach has its own advantages and disadvantages. The MECORE program is based on the state sampling approach and is designed to conduct reliability and reliability worth assessments of composite systems. Its capabilities are briefly presented in this chapter.

The MECORE program has been utilized in the research described in this thesis to conduct bulk system adequacy studies. It has been used to conduct generating system adequacy assessments by assuming that the transmission elements in the test systems are completely reliable.

The basic indices used in generating system reliability evaluation are briefly introduced in this chapter, followed by the basic indices used in bulk power systems. The basic indices can be used to measure the reliability at an individual load bus or for the entire system. The two sets of indices complement each other in providing an overall assessment of bulk system reliability.

Two composite test systems known as the RBTS and the IEEE-RTS are used in this research. The RBTS is a small system designed for education and research purposes. The IEEE-RTS is relatively large compared to the RBTS. The annualized and annual indices for the original RBTS and IEEE-RTS are given in this chapter. These results provide a base case reference for the system conditions covered in subsequent chapters.

This chapter briefly illustrates the utilization of the three different techniques to determine annualized and annual reliability indices at HL-I. The results are quite similar in the case of annualized analysis. The MECORE program using a discrete step load model is used as the basic tool for HL-II analysis in all research described in this thesis. The studies presented in this chapter illustrate that the HL-I results obtained using a 20-step load model are very similar to those produced using an analytical method with this load model and are slightly higher than those obtained using an analytical method or by sequential Monte Carlo simulation and a detailed load model. The 20-step load model is used in the subsequent HL-I and HL-II studies described in this thesis.

3. DEVELOPMENT OF MULTI-STATE WECS MODELS FOR ADEQUACY ASSESSMENT

3.1 Introduction

The development and utilization of wind energy to satisfy electrical demand has received considerable attention in recent years due to concerns regarding dwindling energy resources and enhanced public awareness of the potential impact of conventional energy systems on the environment. Improvements in wind generation technologies will continue to encourage the use of wind energy in both grid-connected and stand-alone systems. Wind generators behave quite differently than conventional generators due to the random nature of the wind and therefore it is important for power system planners and engineers to carefully consider the reliability issues associated with wind energy sources.

A wind energy conversion system converts the natural energy available due to the atmospheric condition at the system location into electric energy. The usable energy that can be converted at a point in time depends on the amount of available energy contained in the weather related site resource at that time. Developing an adequacy model for a wind turbine generator (WTG) requires the consideration of three factors which directly affect the generator output. The first factor is the random nature of the site resource. This randomness must be included in an appropriate model to reflect the chronological characteristics of the wind at the particular site. The second factor is the relationship between the power output and the site resource. This relationship can be determined using the WTG operational parameters and specifications. The third factor is the unavailability of the WTG expressed by the forced outage rate (FOR), noted in Chapter 2.

This chapter describes the time series models utilized to simulate hourly wind speeds. The power output of a WTG unit is then obtained using the relationship between the power output and the wind speed. An apportioning method [27, 28] is introduced and used to create multi-state models for a WTG unit and for a wind energy conversion system (WECS) containing multiple WTG. An analytical procedure that incorporates the WTG FOR is used to build a multi-state WECS model.

Attention is focused on examining the number of capacity states required in a WECS model in order to provide a reasonably accurate adequacy appraisal. The analyses described in this chapter are conducted at HL-I using the RBTS and the RTS. The adequacy impacts of system peak load variation and the WTG FOR are investigated.

3.2 Wind Turbine Generator Unit Models

Wind is caused by uneven heating of the earth's surface by the sun. The heat absorbed by the ground or water is transferred to the air, where it causes differences in air temperature, density and pressure. These differences, in turn, create forces that push the air around. Wind is, therefore, highly variable, site-specific and terrain specific. It has instantaneous, hourly, diurnal and seasonal variations.

One of the first steps for a utility company to consider when developing wind as an energy source is to survey the available wind resource. Unfortunately, reliable wind speed data suitable for wind resource assessment are difficult to obtain, and many records that have been collected are not available to the general public. Many utilities and private organizations, however, are now engaged in collecting comprehensive wind speed data. These data can be used to create site specific wind speed models.

3.2.1 Modeling and Simulating Wind Speeds

A time series model has been developed [13] to incorporate the chronological nature of the actual wind speed. Historical wind speeds are obtained for a specific site, based on

which, future hourly data are predicted using the time series model. This model has been utilized to perform reliability studies in both grid-connected and stand-alone power systems containing wind energy [17, 19-22]. This time series model is also used in the research described in this thesis to generate synthetic wind speeds based on measured wind data at a specific location.

In the time series model [13], the simulated wind speed SW_t can be obtained from the mean wind speed μ_t and its standard deviation σ_t at time t as follows:

$$SW_t = \mu_t + \sigma_t \times y_t \tag{3.1}$$

The original data series set y_t can be used to create a wind speed time series referred to as an ARMA (n, m) series model (Auto-Regressive and Moving Average Model). This is shown in Equation (3.2).

$$y_t = \phi_1 y_{t-1} + \phi_2 y_{t-2} + \ldots + \phi_n y_{t-n} + \alpha_t - \theta_1 \alpha_{t-1} - \theta_2 \alpha_{t-2} - \ldots - \theta_m \alpha_{t-m} \tag{3.2}$$

where ϕ_i (i=1,2,…,n) and θ_j (j=1,2,…,m) are the auto-regressive and moving average parameters of the model respectively, $\{\alpha_t\}$ is a normal white noise process with zero mean and variance of σ_a^2, (a white noise process is a random process of random variables that are uncorrelated, have mean zero, and a finite variance which is denoted σ^2), i.e., $\alpha_t \in NID(0, \sigma_a^2)$, where NID denotes Normally Independent Distributed. Equation (3.2) permits new values of y_t to be calculated from current random white noise α_t and previous values of y_{t-i}. The hourly wind speeds incorporating the wind speed time series can be generated using Equation (3.1).

The time series ARMA model described in Equations (3.1) and (3.2) was used in the wind speed simulation. The main steps are briefly described as follows:

1. The white noise α_t is first simulated.
2. y_t is subsequently generated from the present white noise α_t and previous values of y_{t-1} using time series model Equation (3.2).
3. The simulated wind speeds at time point is then obtained using Equation (3.1).

4. Obtain hourly wind speed data through step 1 to step 3 for a calendar year.
5. Repeat step 1 to step 4 for a long period.

   For $t \le 0$, y_t and α_t are assumed to be zero.

The tabulating technique of normal distribution sampling [34] is used to generate the white noise α_t. The ARMA time series models for different locations are different as the different sites experience different wind regimes. The wind speed model and data for the Swift Current site located in the province of Saskatchewan, Canada have been used in the studies described in this thesis. The mean and the standard deviation of the wind speed at the Swift Current site are 19.46 km/h and 9.7km/h respectively. The hourly mean and standard deviation of wind speeds from a 20-year database (from 1 Jan.1984 to 31 Dec. 2003) for the Swift Current location were obtained from Environment Canada. These data were used to build the ARMA time series models. The ARMA (4, 3) model is the optimal time series model for the Swift Current site and the parameters are shown in Equation (3.3):

Swift Current: ARMA (4, 3):

$$y_t = 1.1772 y_{t-1} + 0.1001 y_{t-2} - 0.3572 y_{t-3} + 0.0379 y_{t-4} + \alpha_t - 0.5030 \alpha_{t-1} - 0.2924 \alpha_{t-2} + 0.1317 \alpha_{t-3} \qquad (3.3)$$

$$\alpha_t \in NID(0, 0.524760^2)$$

Figure 3.1 shows the simulated hourly wind speed for a representative day using the Swift Current data and Equation (3.3).

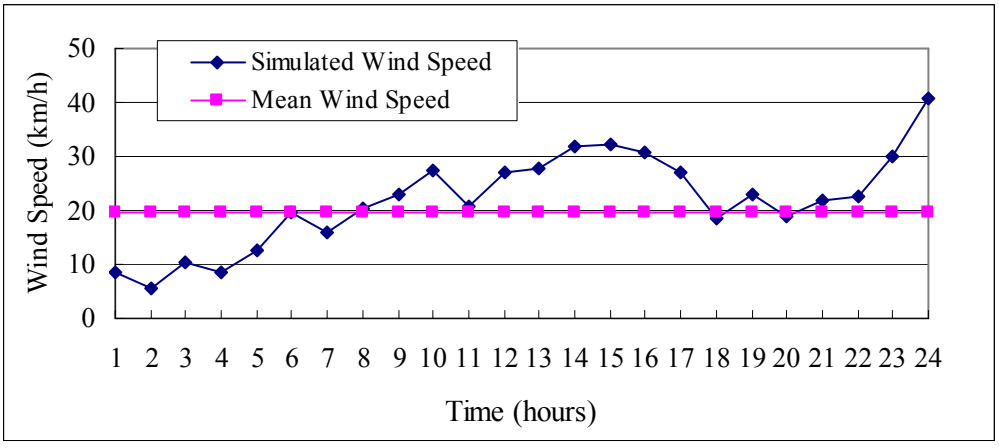

Figure 3.1: Simulated wind speeds for the third day of a sample year (Swift Current data)

Figure 3.2 and Figure 3.3 respectively show the hourly mean wind speed obtained using the ARMA model and 8,000 simulated years, and for the original 20 years of data. The two figures show that the hourly mean wind speed for Swift Current is variable around the average value of 19.46 km/h.

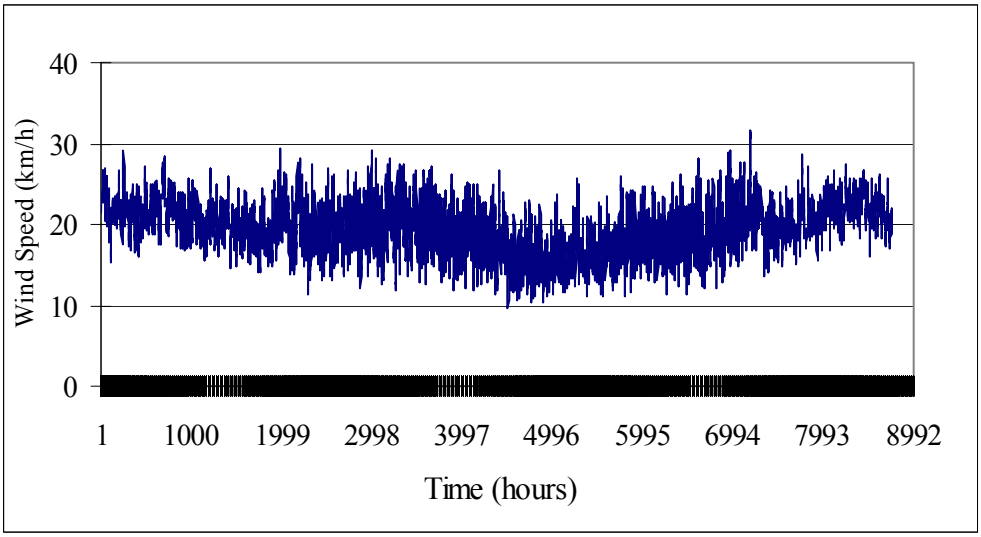

Figure 3.2: Simulated hourly mean wind speeds for 8000 sample years (Swift Current data)

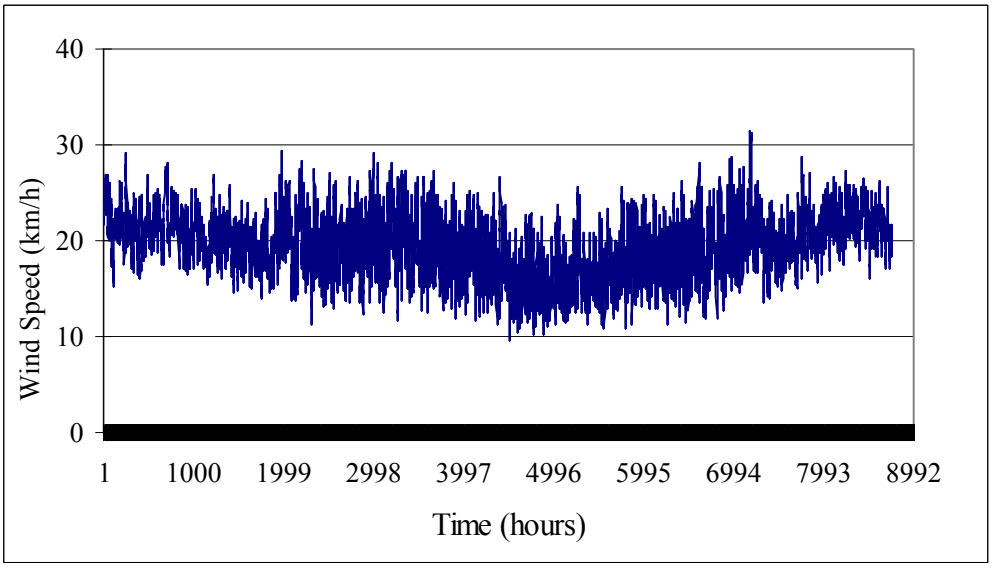

Figure 3.3: The hourly mean wind speed for the actual 20 years of Swift Current data

Figure 3.4 shows a comparison of the observed wind speed probability distribution and the simulated wind speed probability distribution. The observed average wind speed is

19.46 km/h, and the simulated value is 19.53 km/h. The observed wind speed probability distribution is not as continuous as the simulated distribution as it is based on only 20 years of data.

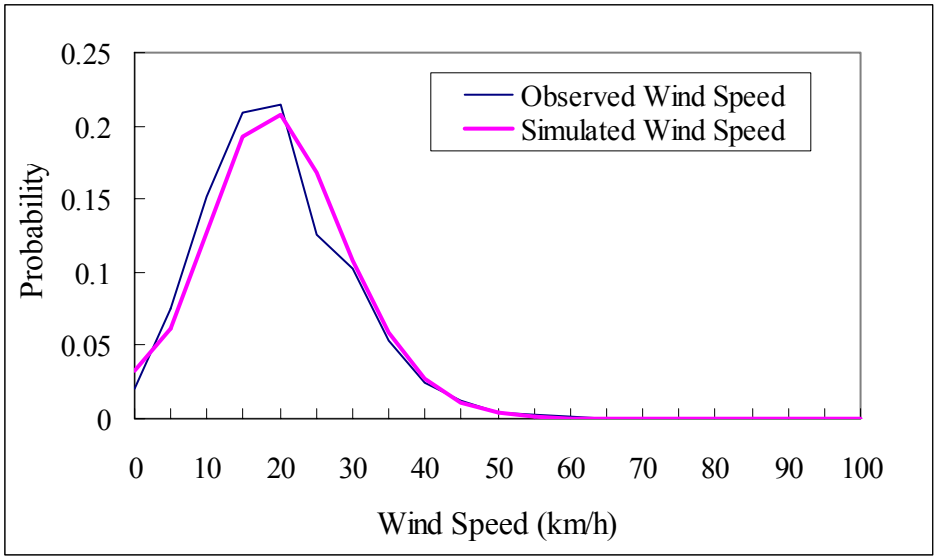

Figure 3.4: Observed and simulated wind speed distributions for the Swift Current site

Figures 3.2 to 3.4 illustrate that the ARMA (4, 3) model provides a valid representation of the actual wind regime. Simulation results are used to generate wind speed probability distributions in the system adequacy studies described in this thesis.

3.2.2 Modeling Wind Turbine Generators

The power output characteristics of a WTG are quite different from those of the conventional generating unit. The output of a WTG depends strongly on the wind regime as well as on the performance characteristics and the efficiency of the generator.

After the hourly wind speed is obtained, the next step is to determine the power output of the WTG as a function of the wind speed. This function is described by the operational parameters of the WTG. The parameters commonly used are the cut-in wind speed (at which the WTG starts to generate power), the rated wind speed (at which the WTG generates its rated power) and the cut-out wind speed (at which the WTG is shut

down for safety reasons). Equation (3.4) is used to obtain the hourly power output of a WTG from the simulated hourly wind speed.

$$P(SW_t) = \begin{cases} 0 & 0 \le SW_t < V_{ci} \\ (A + B \times SW_t + C \times SW_t^{\,2}) \times P_r & V_{ci} \le SW_t < V_r \\ P_r & V_r \le SW_t < V_{co} \\ 0 & SW_t \ge V_{co} \end{cases} \tag{3.4}$$

where P_r, V_{ci}, V_r and V_{co} are the rated power output, the cut-in wind speed, the rated wind speed and the cut-out wind speed of the WTG respectively [35]. The constants A, B, and C depend on V_{ci}, V_r and V_{co} as expressed in Equation (3.5) [35].

$$\begin{aligned} A &= \frac{1}{(V_{ci} - V_r)^2}\left\{V_{ci}(V_{ci} + V_r) - 4V_{ci}V_r\left[\frac{V_{ci} + V_r}{2V_r}\right]^3\right\}, \\ B &= \frac{1}{(V_{ci} - V_r)^2}\left\{4(V_{ci} + V_r)\left[\frac{V_{ci} + V_r}{2V_r}\right]^3 - (3V_{ci} + V_r)\right\}, \\ C &= \frac{1}{(V_{ci} - V_r)^2}\left\{2 - 4\left[\frac{V_{ci} + V_r}{2V_r}\right]^3\right\}. \end{aligned} \tag{3.5}$$

The relationship can also be illustrated graphically as shown in Figure 3.5 and is often referred to as the "Power Curve".

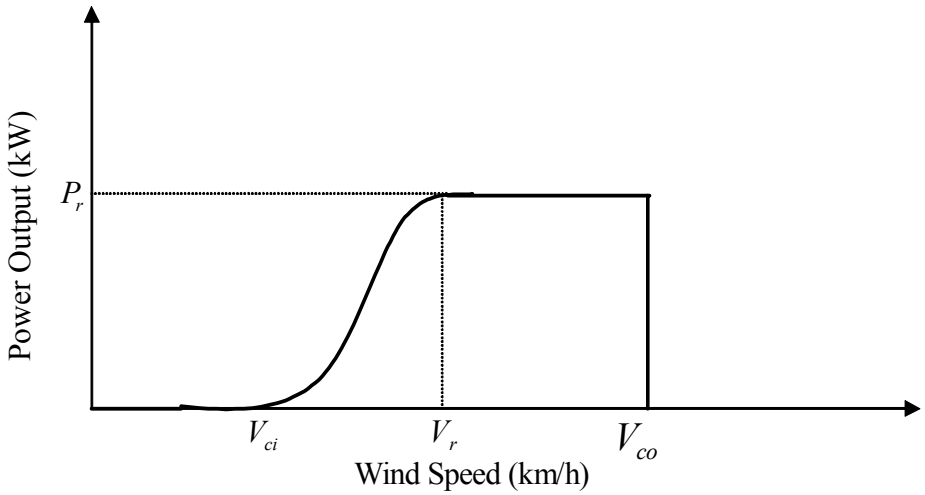

Figure 3.5: Wind turbine generator power curve

At a specific time, the hourly output power of a WTG can be obtained from the simulated hourly wind speed using Equation (3.4). Figure 3.6 presents the simulated output power of a 2 MW WTG with cut-in speed of 14.4 km/h, rated speed of 36 km/h and cut-out wind speeds of 80 km/h over a one week period.

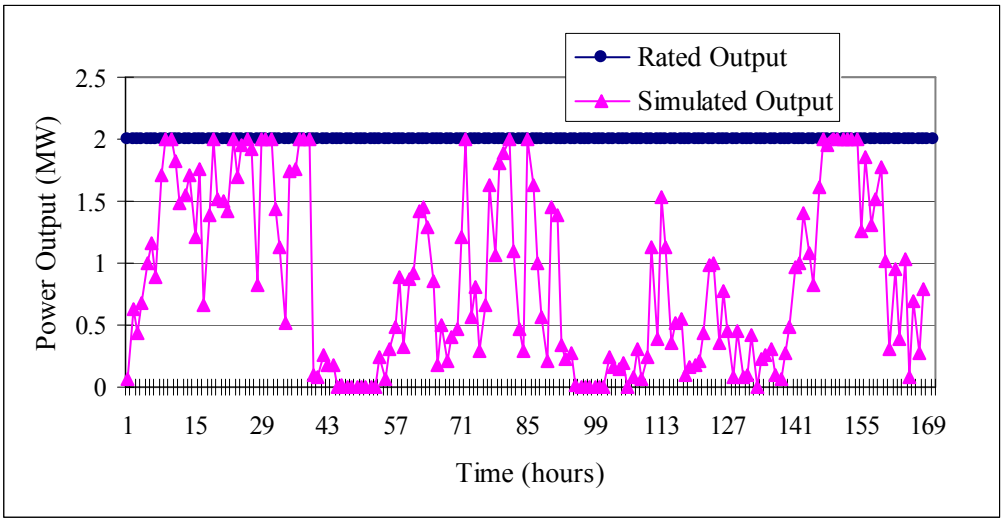

Figure 3.6: Simulated output power of a 2 MW WTG for a sample week (Swift Current data)

Figure 3.6 shows that the output power of the generator reaches its rated value for only a few hours in the week. The reason is the fact that the simulated wind speeds are seldom between the rated and cut-out wind speeds of the WTG during the sample week when the WTG unit is in the operating state. It can also be seen from Figure 3.6 that there is no power output from the WTG unit in some hours of the sample week. The possible reason for no power output is that the simulated wind speed is either lower than the cut-in wind speed or higher than the cut-out wind speed of the WTG at these time points.

3.2.3 The Capacity Outage Probability Table of the WTG

The hourly mean wind speeds and output power for the WTG unit without considering its FOR are generated based on the ARMA time series model and the power curve respectively. The capacity outage probability table (COPT) of a WTG unit can be created by applying the hourly wind speed to the power curve. The procedure is briefly described in the following:

(1) Define the output states for a WTG unit as segments of the rated power.
(2) Determine the total number of times that the wind speed results in a power output falling within one of the output states.
(3) Divide the total number of occurrences for each output state by the total number of data points to estimate the probability of each state.

The COPT is formed using this approach. Two cases are illustrated in this section. The first case utilizes the observed 20 years of Swift Current data. The second case uses the 8,000 simulated year data. Table 3.1 shows the COPT of the WTG unit for these two cases. The class interval width is 5% in this table and the indicated capacity outage level is the midpoint of the class. Figure 3.7 graphically illustrates the two capacity outage probability distributions.

Table 3.1: Capacity outage probability table for the WTG unit

Observed Wind Data		Simulated Wind Data	
Average speed=19.46 (km/h)		Average speed=19.53 (km/h)	
Capacity Outage (%)	Probability	Capacity Outage (%)	Probability
0	0.0578	0	0.0513
2.5	0	2.5	0.0064
7.5	0.0165	7.5	0.0073
12.5	0	12.5	0.0083
17.5	0	17.5	0.0094
22.5	0.0275	22.5	0.0107
27.5	0.0143	27.5	0.0122
32.5	0.0139	32.5	0.0140
37.5	0	37.5	0.0159
42.5	0.0353	42.5	0.0182
47.5	0	47.5	0.0208
52.5	0.0447	52.5	0.0240
57.5	0	57.5	0.0275
62.5	0.0505	62.5	0.0318
67.5	0	67.5	0.0367
72.5	0.0512	72.5	0.0426
77.5	0.0678	77.5	0.0496
82.5	0	82.5	0.0580
87.5	0.1494	87.5	0.0683
92.5	0.0772	92.5	0.0815
97.5	0.0886	97.5	0.1004
100	0.3052	100	0.3051

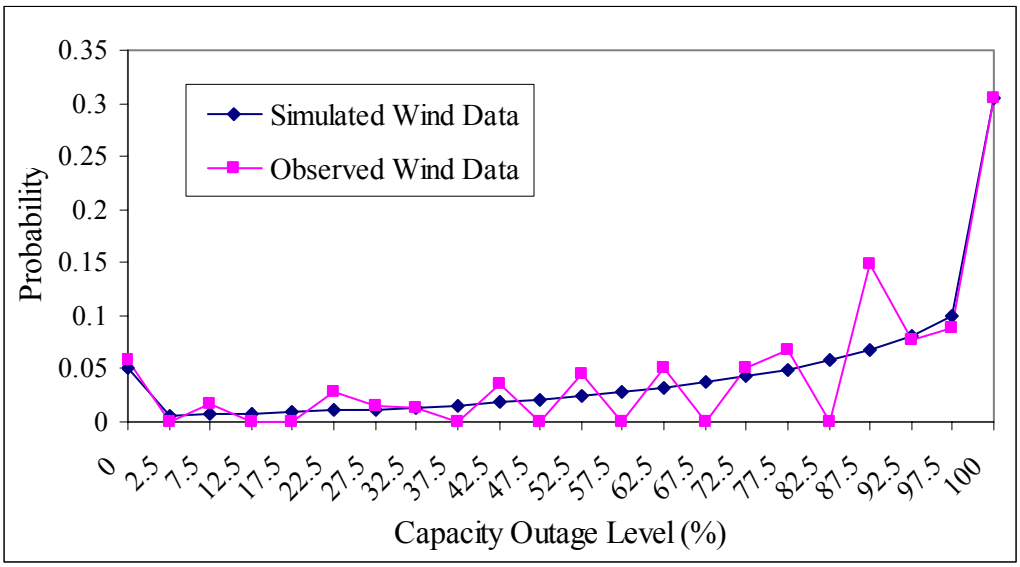

Figure 3.7: Capacity outage probability profile for the WTG unit

Table 3.1 and Figure 3.7 illustrate that the observed probability profile is discontinuous due to the limited wind data collection and the simulated wind data provides a reasonable representation for adequacy assessment. The power output characteristics of a WTG are very different from those of conventional generating units.

As noted earlier, the power output of a WTG unit depends strongly on the wind resource at the specific location. In order to illustrate the effect of site resources on the WTG unit, the average wind speed used in the ARMA model was modified from 19.46 km/h to 38.92 km/h using a simple multiplication factor of 2.0. The results are illustrated graphically in Figure 3.8 which shows that the power output of a WTG is extremely dependent on the wind regime and will increase if the facilities are located at a point where a higher wind velocity is available. Table C.1 shows the data on the capacity outage levels and probabilities for a WTG with a 38.92 km/h mean wind speed.

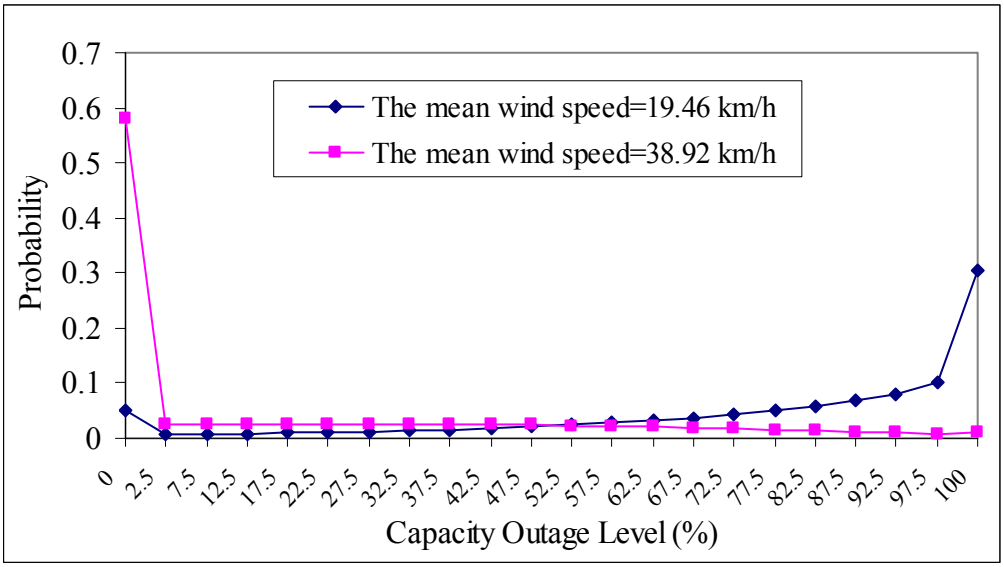

Figure 3.8: Comparison of capacity outage probability profiles for the WTG unit

3.2.4 Seasonal Wind Speed and Power Output of a WTG unit

Seasonal variations in the speed and direction of the wind result from the seasonal changes in the relative inclination of the earth towards the sun. In general, monthly and seasonal variations have a significant effect on wind power plant performance. The degree and timing of seasonal variations depend upon the region. This research investigated the difference in the seasonal wind speeds and power outputs of a WTG using data from selected Saskatchewan wind sites.

It is assumed that a year includes only two seasons: summer and winter. Summer runs from April to September and contains 4392 hours, and winter consists of two parts: January to March, and October to December. The total number of hours in winter is 4368 hours.

The four wind sites used in the study are located in Swift Current, Regina, Saskatoon and North Battleford. The ARMA time series models for the four sites were developed by the Power System Research Group at the University of Saskatchewan and are listed

in Appendix D. The original annual mean wind speed and the wind standard deviation data are divided into seasonal segments. The cut-in, rated and cut- out wind speed of a 2 MW WTG for each site are considered to be 14.4km/h, 36km/h and 80km/h respectively.

Table 3.2 shows the annual and seasonal average wind speed for the four wind sites. The wind speed probability distributions for the four wind sites are shown in Figures 3.9, 3.11, 3.13 and 3.15. It can be seen from Table 3.2 that although the average winter wind speed is higher than that of summer in the Swift Current and Regina sites, and the average summer wind speed is greater than that of winter at the Saskatoon and North Battleford sites, there is not a great difference between the two seasonal wind speeds for the four sites. The wind speed probability distributions at these locations do not change significantly from winter to summer.

The wind power output distributions for the four wind farms are shown in Figures 3.10, 3.12, 3.14 and 3.16. They demonstrate that there is very little difference for the whole year, summer and winter periods. The annual profile is an average of the summer and winter profiles. The conclusion can be drawn that the annual wind profile is an acceptable representation and that annual studies can be done directly using this profile.

Table 3.2: The average wind speed for the four wind sites

Site		Average Wind Speed (km/h)		
		Annual	Summer	Winter
Swift Current	Observed	19.458	18.281	20.642
	Simulated	19.528	18.359	20.704
Regina	Simulated	19.596	19.126	20.067
Saskatoon	Simulated	16.847	17.284	16.408
North Battleford	Simulated	14.869	15.503	14.233

Swift Current

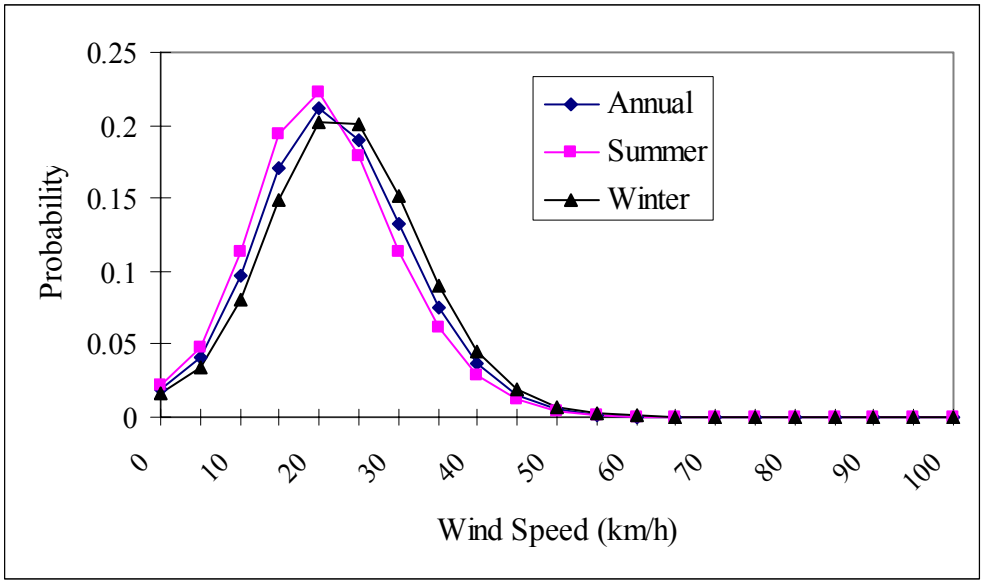

Figure 3.9: Wind speed probability distributions at Swift Current

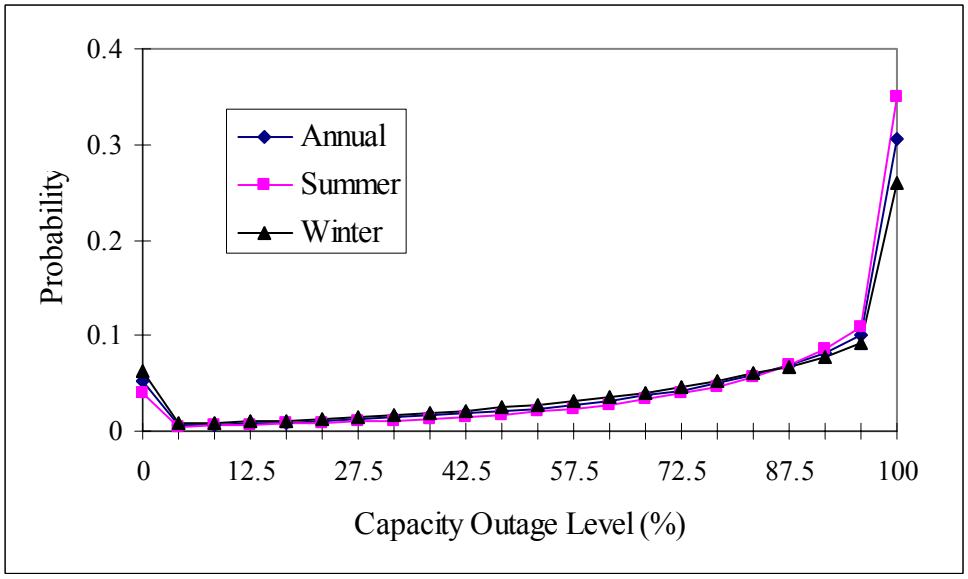

Figure 3.10: WTG unit capacity outage levels and probability distributions (Swift Current data)

Regina

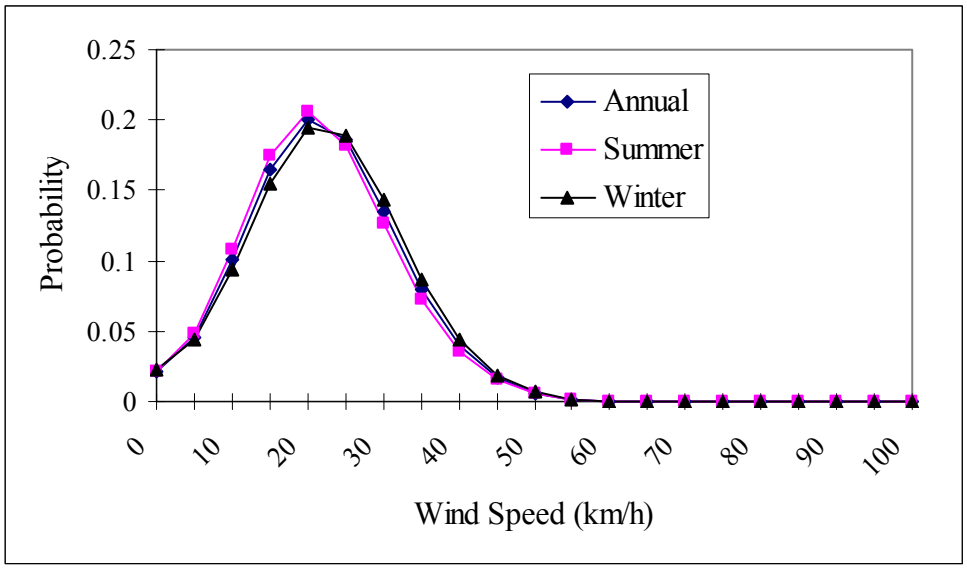

Figure 3.11: Wind speed probability distributions at Regina

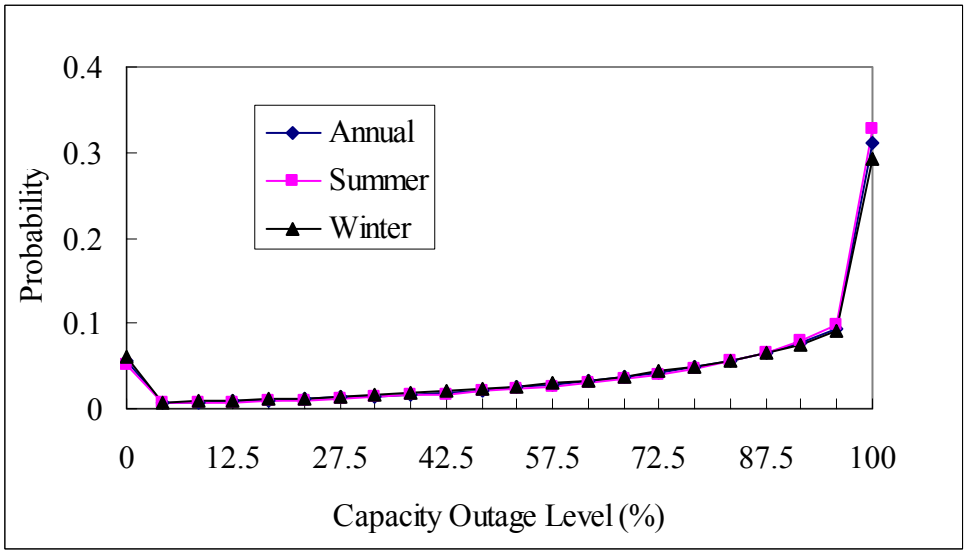

Figure 3.12: WTG unit capacity outage levels and probability distributions (Regina data)

Saskatoon

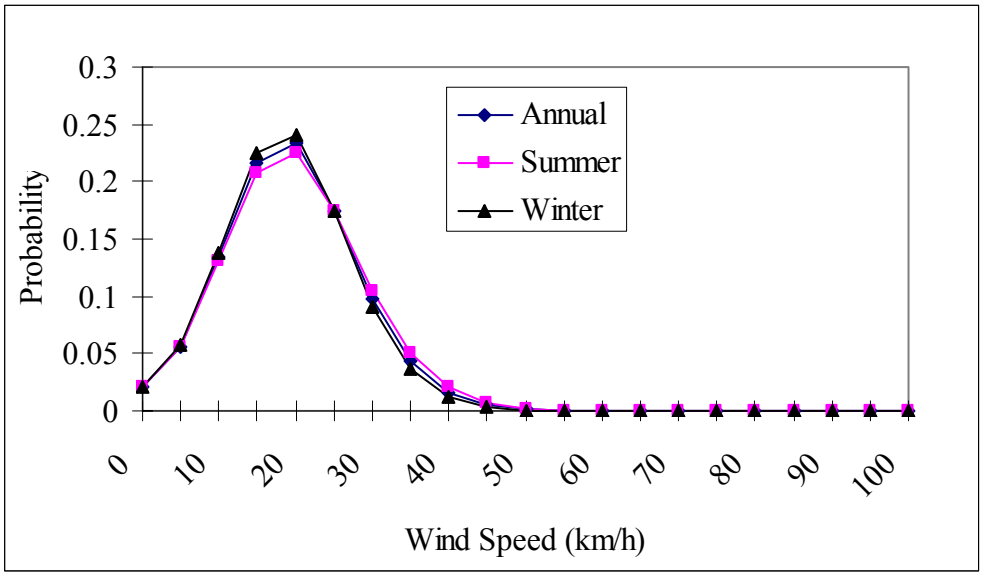

Figure 3.13: Wind speed probability distributions at Saskatoon

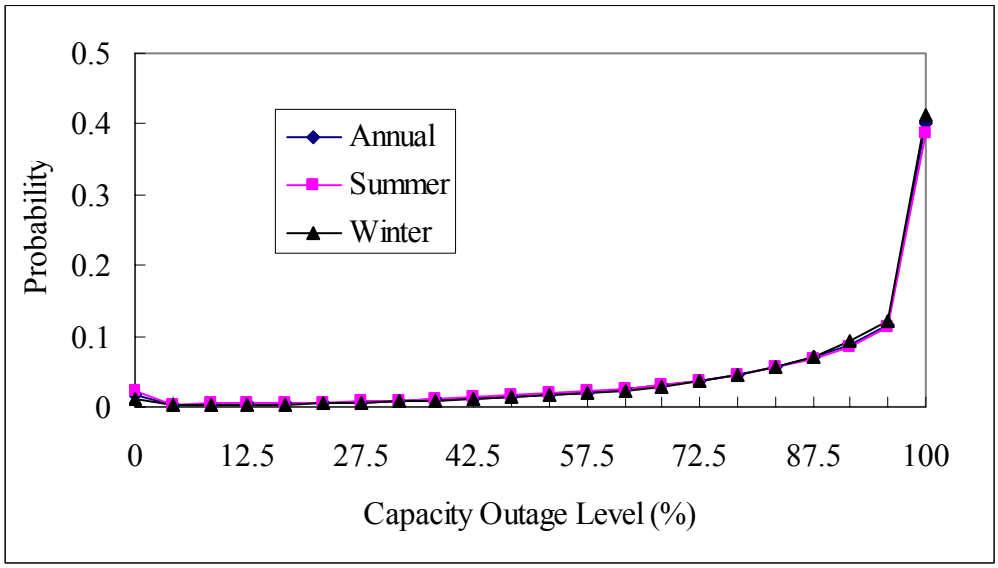

Figure 3.14: WTG unit capacity outage levels and probability distributions (Saskatoon data)

North Battleford

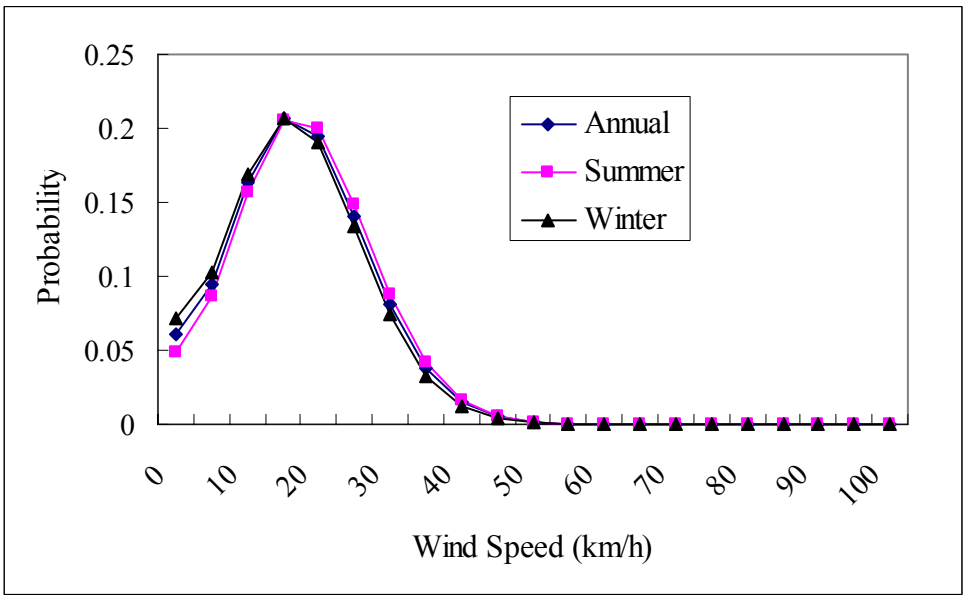

Figure 3.15: Wind speed probability distributions at North Battleford

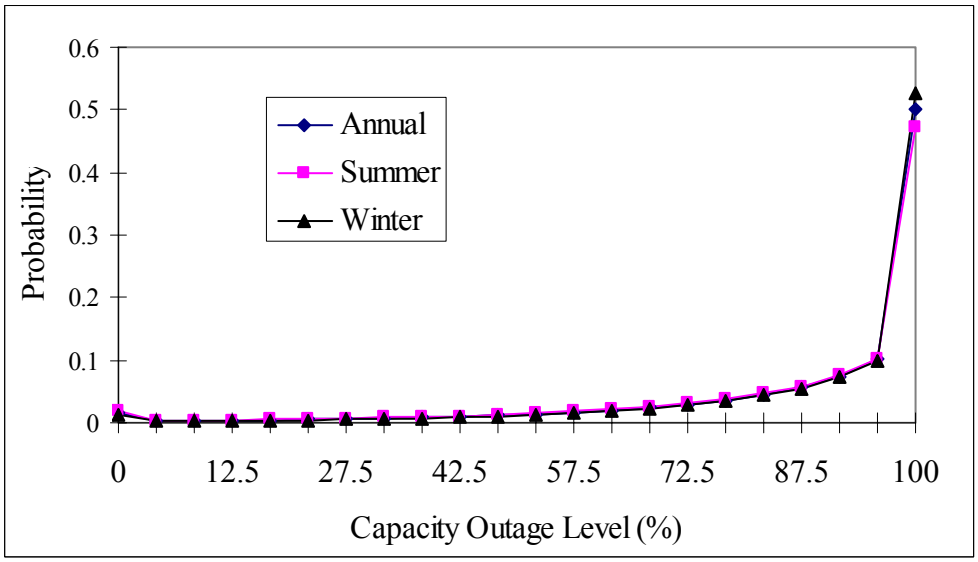

Figure 3.16: WTG unit capacity outage levels and probability distributions (North Battleford data)

3.3 Building a Multi-state WECS Model Using the Apportioning Method

There are many derated states in which a generating unit can reside in the course of its operating history [27]. The requirement in adequacy assessment is to represent a generating unit by an acceptable reduced number of derated states. A pre-convolution capacity rounding method was used in previous research [18] to determine the multi-state model of a wind generation unit. This method can involve the creation of new states for a unit and introduces certain inaccuracies in the adequacy indices. The apportioning method [27, 28] is relatively more flexible and accurate than the rounding method because it does not create new states. This method has been used in this thesis to create the selected multi-state models for a WTG and the WECS. An analytical procedure that incorporates the WTG FOR is presented and used to build a multi-state WECS model.

3.3.1 The Apportioning Method

The state reduction method is based on apportioning the residence times of the actual derated states between the assigned derated state and the up (normal) or down (outage) states. The closer an "absorbed" state is to the assigned state, the more contribution it makes to the probability of the existence of that state. The apportioning concept and the symbols used are presented in the following.

X_N: the Nth original derated state capacity in percent of full capacity

Y_N: the Nth designated derated state capacity in percent of full capacity

$Y_{dn(0)}$: generating unit in the down state

$Y_{up(100)}$: generating unit in the up state

N=1, 2, 3, ……..

N: the number of derated states

$\Delta_X t_N$: residence time of the original derated state of X_N

$\Delta t(Y_i)_N$: apportioned time of the determined derated state Y_i from the original derated state of X_N. (i=1, 2…)

$\Delta t(Y_{up})_N$: apportioned time of the up state from the original derated state of X_N.

$\Delta t(Y_{dn})_N$: apportioned time of the down state from the original derated state of X_N.

T: total time spent in the up, derated and down states

T_{up}: time spent in the up state

T_{dn}: time spent in the down state

$PFOR_{X_N}$: the Partial Forced Outage Rate (PFOR) for the Nth derated state capacity in percent of full capacity. PFOR for a given derated state is obtained by dividing the number of hours the unit is operated in the given forced derated state by the total number of hours the unit is exposed to outage.

P_{dn}: probability of the generating unit in the down state

P_{up}: probability of the generating unit in the up state

P_{dei}: probability of the generating unit in the ith determined derated state

Note: $\Delta_X t_N = PFOR_{X_N} \times T$ (3.6)

The application of these concepts to create a two-state model is illustrated in Figure 3.17.

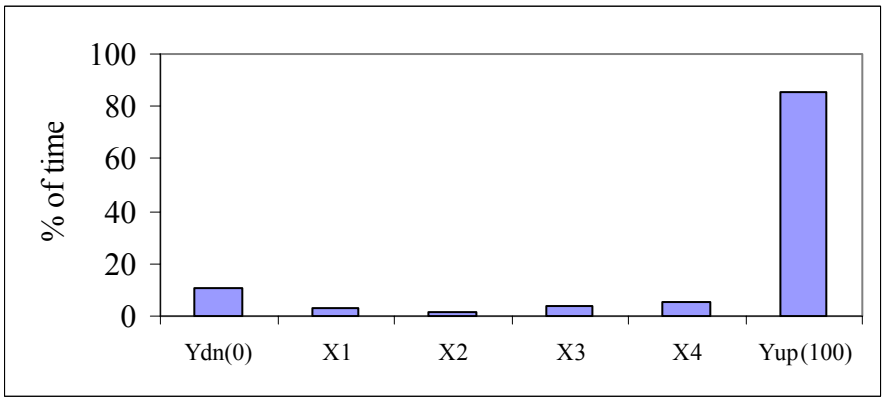

Figure 3.17: A two-state generating unit model containing no derated states

The procedure used to establish the "single-derated state" generating unit model shown in Figure 3.18 is as follows. This is illustrated in Figure 3.18.

Assume: $Y_1 \le X_N \le Y_{up}$

$$\Delta_X t(Y_1)_N = \frac{Y_{up} - X_N}{Y_{up} - Y_1} \times \Delta_X t_N \quad (3.7)$$

$$\Delta_X t\left(Y_{up}\right)_N = \frac{X_N - Y_1}{Y_{up} - Y_1} \times \Delta_X t_N \tag{3.8}$$

and when $X_N \le Y_1 \le Y_{up}$

$$\Delta_X t\left(Y_1\right)_N = \frac{X_N - Y_{dn}}{Y_1 - Y_{dn}} \times \Delta_X t_N \tag{3.9}$$

$$\Delta_X t\left(Y_{dn}\right)_N = \frac{Y_1 - X_N}{Y_1 - Y_{dn}} \times \Delta_X t_N \tag{3.10}$$

Then P_{up}, P_{dn} and P_{de} are obtained as follows:

$$P_{up} = \frac{T_{up} + \sum_{N=1}^{n} \Delta_X t\left(Y_{up}\right)_N}{T} \tag{3.11}$$

$$P_{dn} = \frac{T_{dn} + \sum_{N=1}^{n} \Delta_X t\left(Y_{dn}\right)_N}{T} \tag{3.12}$$

$$P_{de} = \frac{\sum_{N=1}^{n} \Delta_X t\left(Y_1\right)_N}{T} \tag{3.13}$$

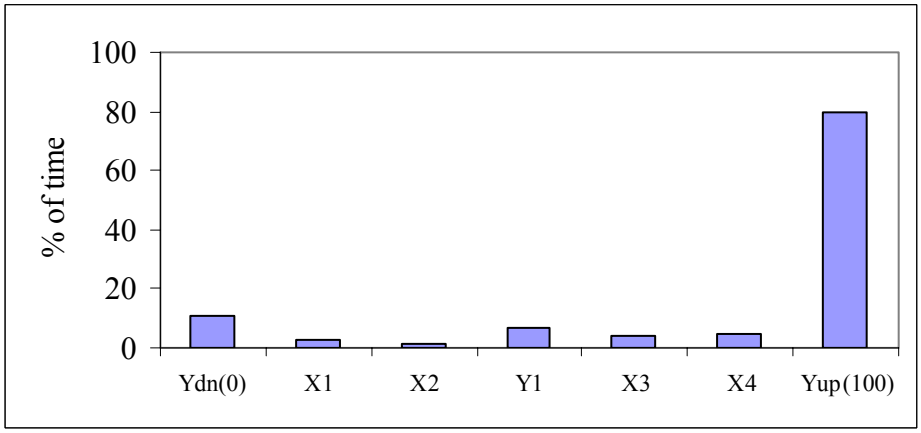

Figure 3.18: A "single-derated state" generating unit model

The procedure used to establish the "two-derated state" generating unit model is as follows. This is illustrated in Figure 3.19.

assume: $Y_1 \ge Y_2$

when $Y_1 \le X_N \le Y_{up}$

$$\Delta_X t\left(Y_1\right)_N = \frac{Y_{up} - X_N}{Y_{up} - Y_1} \times \Delta_X t_N \tag{3.14}$$

$$\Delta_X t\left(Y_{up}\right)_N = \frac{X_N - Y_1}{Y_{up} - Y_1} \times \Delta_X t_N \tag{3.15}$$

when $X_N \le Y_2 \le Y_{up}$

$$\Delta_X t\left(Y_2\right)_N = \frac{X_N - Y_{dn}}{Y_2 - Y_{dn}} \times \Delta_X t_N \tag{3.16}$$

$$\Delta_X t\left(Y_{dn}\right)_N = \frac{Y_2 - X_N}{Y_2 - Y_{dn}} \times \Delta_X t_N \tag{3.17}$$

and when $Y_2 \le X_N \le Y_1$

$$\Delta_X t\left(Y_1\right)_N = \frac{X_N - Y_2}{Y_1 - Y_2} \times \Delta_X t_N \tag{3.18}$$

$$\Delta_X t\left(Y_2\right)_N = \frac{Y_1 - X_N}{Y_1 - Y_2} \times \Delta_X t_N \tag{3.19}$$

Therefore, P_{up} and P_{dn} are obtained using Equations (3.11) and (3.12), and P_{de1} and P_{de2} are obtained as follows:

$$P_{de1} = \frac{\sum_{N=1}^{n} \Delta_X t\left(Y_1\right)_N}{T} \tag{3.20}$$

$$P_{de2} = \frac{\sum_{N=1}^{n} \Delta_X t\left(Y_2\right)_N}{T} \tag{3.21}$$

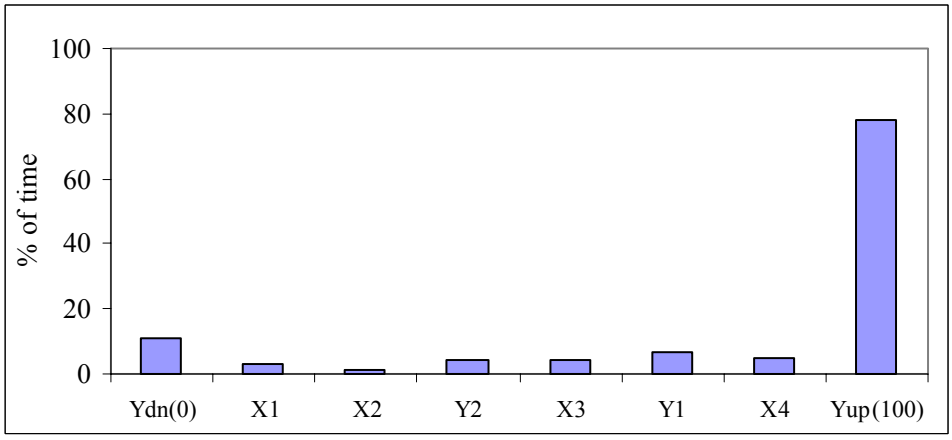

Figure 3.19: A "two-derated state" generating unit model

The two-state generating unit representation shown in Figure 3.17 has been used in many conventional generating capacity adequacy studies. The probability of a unit

residing in the full down state is known as the Derating Adjusted Forced Outage Rate (DAFOR) [36]. The term DAFOR is used by Canadian electric power utilities. In the United States, the designation for this statistic is the "equivalent forced outage rate" (EFOR). The EFOR or DAFOR is obtained using the apportioning method in which the residence times of the actual derated states are apportioned between the up (normal) and down (outage) states and there are no assigned derated states. The DAFOR of a generating unit is obtained using Equation (3.22).

$$DAFOR = \frac{T_{dn} + \sum_{N=1}^{n} \Delta_X t(Y_1)_N}{T} \tag{3.22}$$

3.3.2 Multi-state WTG Models

The WTG COPT shown in Table 3.1 based on simulated wind speeds can be reduced to form different multi-state capacity outage probability tables using the apportioning method. A state capacity outage probability table is designated as a SCOPT. A 5SCOPTW is a 5-state WTG capacity outage probability table. Table 3.3 shows the effect of reducing the COPT in Table 3.1 to a series of different SCOPTW. These tables do not include the effect of WTG FOR. The effects of wind variability can be aggregated to produce a DAFOR statistic similar in form that used for conventional generating units. This statistic is designated as DAFORW and is 0.76564 for the COPT shown in Table 3.1. The DAFORW is the same for each SCOPTW shown in Table 3.3.

Table 3.3: Multi-state WTG COPT (SCOPTW) without FOR

2-state (2SCOPTW)		3-state (3 SCOPTW)		4-state (4 SCOPTW)		5-state (5 SCOPTW)	
Capacity Outage (%)	Prob.	Capacity Outage (%)	Prob.	Capacity Outage (%)	Prob.	Capacity Outage (%)	Prob.
0	0.23436	0	0.09993	0	0.06576	0	0.07021
100	0.76564	50	0.26885	20	0.05696	25	0.05944
		100	0.63122	50	0.24606	50	0.11688
				100	0.63122	75	0.24450
						100	0.50897
DAFORW=0.76564							

Cont---

Table 3.3: Multi-state WTG COPT (SCOPTW) without FOR

6-state (6 SCOPTW)		7-state (7 SCOPTW)		8-state (8 SCOPTW)		9-state (9 SCOPTW)	
Capacity Outage (%)	Prob.	Capacity Outage (%)	Prob.	Capacity Outage (%)	Prob.	Capacity Outage (%)	Prob.
0	0.06576	0	0.06576	0	0.06169	0	0.06169
20	0.04115	20	0.04115	15	0.03284	15	0.02681
40	0.06993	40	0.04742	35	0.05087	30	0.03973
60	0.12213	50	0.07488	50	0.06815	45	0.05938
80	0.22433	70	0.16391	65	0.10445	60	0.07145
100	0.47670	90	0.20615	80	0.12934	70	0.07985
		100	0.40073	90	0.15193	80	0.10843
				100	0.40681	90	0.15453
						100	0.40681
DAFORW=0.76564							

Cont---

10-state (10 SCOPTW)		11-state (11 SCOPTW)	
Capacity Outage (%)	Prob.	Capacity Outage (%)	Prob.
0	0.06169	0	0.05796
15	0.02681	10	0.01560
30	0.03155	20	0.02021
40	0.03427	30	0.02629
50	0.04503	40	0.03427
60	0.05969	50	0.04503
70	0.07985	60	0.05969
80	0.10843	70	0.07985
90	0.15193	80	0.10843
100	0.40073	90	0.15193
		100	0.40073
DAFORW=0.76564			

3.3.3 Wind Energy Conversion System Model

A wind energy conversion system (WECS) can contain one or more WTG. A WECS has two parts: one is the wind resource and the other is the actual WTG units. If the WECS consists of identical WTG units with zero FOR, the WECS multi-state models are the same as those of a single WTG unit shown in Table 3.3. If the FOR of the WTG units is not zero, the WECS derated state capacity outage probability tables are not the same as those of a single WTG unit. An analytical procedure has been used to create WECS multi-state models including WTG FOR. The designation MSCOPTW is used to

indicate a SCOPTW modified to include the WTG FOR. A 2MSCOPTW is a 2-state WECS model including the WTG FOR. The following cases are used to illustrate the procedure.

Case 1: Consider a WECS containing one 2 MW WTG unit with a 4% FOR. The wind condition is represented by the 2-state model (2SCOPTW) shown in Table 3.3. The wind condition and the actual WTG unit form a simple series system as shown in Figure 3.20.

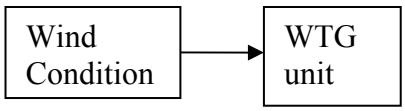

Figure 3.20: Single unit model

The availability of the WTG unit is 0.96 and unavailability is 0.04.

$$P_{WECS\,up} = P_{up} \times A = 0.23436 \times 0.96 = 0.22499$$

$$P_{WECSdown} = P_{down} + U - P_{down} \times U = 0.76564 + 0.04 - 0.76564 \times 0.04 = 0.77501$$

The COPT for the single unit WECS is shown in Table 3.4.

Table 3.4: 2MSCOPTW for Case 1

Capacity Outage (MW)	Probability
0	0.22499
2	0.77501

Case 2: Consider the WECS to consist of two identical 2 MW WTG units with a 4% FOR. The wind condition is represented by the 2SCOPTW shown in Table 3.3. The system model is shown in Figure 3.21.

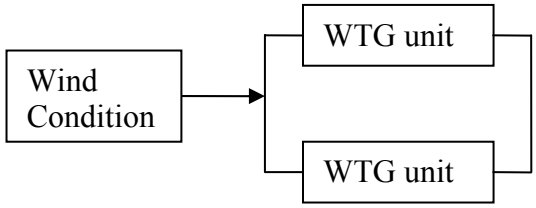

Figure 3.21: Two WTG unit model

The WTG COPT is formed using the binomial distribution and is shown in Table 3.5.

Table 3.5: Two WTG unit COPT

Capacity Outage (MW)	Probability
0	0.9216
2	0.0768
4	0.0016

The wind condition and the WTG unit COPT are combined to create a model to represent the WECS. The WECS COPT is shown in Table 3.6.

$$P_{WECSup} = P_{up} \times A = 0.9216 \times 0.23436 = 0.21599$$

$$P_{WECSderated} = P_{derated} \times A = 0.0768 \times 0.23436 = 0.01800$$

$$P_{WECSdown} = P_{down} + U - P_{down} \times U = 0.0016 + 0.76564 - 0.0016 \times 0.76564 = 0.76601$$

Table 3.6: The COPT of the WECS

Capacity Outage (MW)	Probability
0	0.21599
2	0.01800
4	0.76601

The three-state WECS COPT shown in Table 3.6 can be reduced using the apportioning method to create the two-state model illustrated in Table 3.7, if desired.

Table 3.7: 2MSCOPTW for Case 2

Capacity Outage (MW)	Probability
0	0.22499
4	0.77501

Case 3: A 20 MW WECS containing 10 identical 2 MW WTG units is represented in Figure 3.22. The WTG units are considered to have either a zero FOR or a FOR of 4%. The procedure used to develop the WECS COPT is briefly described in the following.

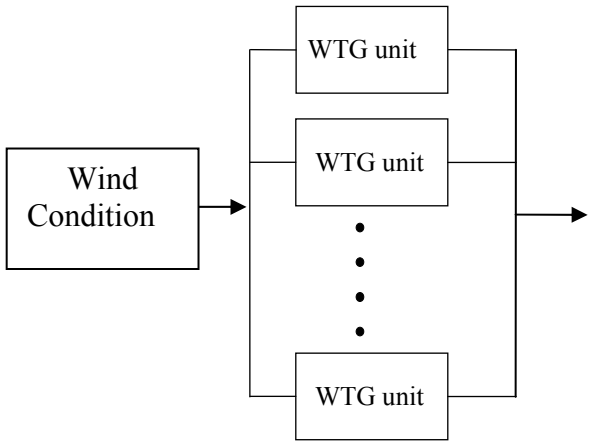

Figure 3.22: Multiple WTG unit model

Step 1: The wind condition models are represented by the SCOPTW shown in Table 3.3.
Step 2: The identical WTG units with 0% and 4% FOR are combined to create the COPT shown in Table 3.8.

Table 3.8: The WTG unit COPT with different FOR

Capacity Outage (MW)	Probability	
	FOR=0	FOR=0.04
0	1	0.66483
2	0	0.27701
4	0	0.05194
6	0	0.00577
8	0	0.00042
10	0	0.00002
12	0	0.00000
14	0	0.00000
16	0	0.00000
18	0	0.00000
20	0	0.00000

Step 3: The wind condition and the WTG unit COPT are combined to create the multi-state WECS COPT shown in Table 3.9.

Table 3.9: The WECS COPT models for different wind condition models

COPT for 2SCOPTW			COPT for 3SCOPTW			COPT for 4SCOPTW		
Cap. Outage (MW)	Probability		Cap. Outage (MW)	Probability		Cap. Outage (MW)	Probability	
	FOR =0%	FOR =4%		FOR =0%	FOR =4%		FOR =0%	FOR =4%
0	0.23436	0.15581	0	0.09993	0.06644	0	0.06576	0.04372
2	0.00000	0.06492	2	0.00000	0.02768	2	0.00000	0.01822
4	0.00000	0.01217	4	0.00000	0.00519	4	0.05696	0.04128
6	0.00000	0.00135	6	0.00000	0.00058	5.6	0.00000	0.01578
8	0.00000	0.00010	8	0.00000	0.00004	6	0.00000	0.00038
10	0.00000	0.00000	10	0.26885	0.17874	7.2	0.00000	0.00296
12	0.00000	0.00000	11	0.00000	0.07448	8	0.00000	0.00003
14	0.00000	0.00000	12	0.00000	0.01396	8.8	0.00000	0.00033
16	0.00000	0.00000	13	0.00000	0.00155	10	0.24606	0.16359
18	0.00000	0.00000	14	0.00000	0.00011	10.4	0.00000	0.00002
20	0.76564	0.76564	15	0.00000	0.00001	11	0.00000	0.06816
			16	0.00000	0.00000	12	0.00000	0.01278
			17	0.00000	0.00000	13	0.00000	0.00142
			18	0.00000	0.00000	13.6	0.00000	0.00000
			19	0.00000	0.00000	14	0.00000	0.00010
			20	0.63122	0.63122	15	0.00000	0.00001
						15.2	0.00000	0.00000
						16	0.00000	0.00000
						16.8	0.00000	0.00000
						17	0.00000	0.00000
						18	0.00000	0.00000
						18.4	0.00000	0.00000
						19	0.00000	0.00000
						20	0.63122	0.63122

Cont---

Table 3.9: The WECS COPT models for different wind condition models

COPT for 5SCOPTW			COPT for 6SCOPTW			COPT for 7SCOPTW		
Cap. Outage (MW)	Probability		Cap. Outage (MW)	Probability		Cap. Outage (MW)	Probability	
	FOR =0%	FOR =4%		FOR =0%	FOR =4%		FOR =0%	FOR =4%
0	0.07021	0.04668	0	0.06576	0.04372	0	0.06576	0.04372
2	0.00000	0.01945	2	0.00000	0.01822	2	0.00000	0.01822
4	0.00000	0.00365	4	0.04115	0.03077	4	0.04115	0.03077
5	0.05944	0.03952	5.6	0.00000	0.01140	5.6	0.00000	0.01140
6	0.00000	0.00041	6	0.00000	0.00038	6	0.00000	0.00038
6.5	0.00000	0.01647	7.2	0.00000	0.00214	7.2	0.00000	0.00214
8	0.00000	0.00312	8	0.06993	0.04652	8	0.04742	0.03155
9.5	0.00000	0.00034	8.8	0.00000	0.00024	8.8	0.00000	0.00024
10	0.11688	0.07771	9.2	0.00000	0.01937	9.2	0.00000	0.01314
11	0.00000	0.03240	10	0.00000	0.00000	10	0.07488	0.04978
12	0.00000	0.00607	10.4	0.00000	0.00365	10.4	0.00000	0.00248
12.5	0.00000	0.00000	11.6	0.00000	0.00040	11	0.00000	0.02074
13	0.00000	0.00067	12	0.12213	0.08120	11.6	0.00000	0.00027
14	0.00000	0.00005	12.8	0.00000	0.03386	12	0.00000	0.00389
15	0.24450	0.16255	13.6	0.00000	0.00634	12.8	0.00000	0.00002
15.5	0.00000	0.06773	14	0.00000	0.00000	13	0.00000	0.00043
16	0.00000	0.01270	14.4	0.00000	0.00070	13.6	0.00000	0.00000
16.5	0.00000	0.00141	15.2	0.00000	0.00005	14	0.16391	0.10901
17	0.00000	0.00010	16	0.22433	0.14914	14.6	0.00000	0.04541
17.5	0.00000	0.00001	16.4	0.00000	0.06214	15	0.00000	0.00000
18	0.00000	0.00000	16.8	0.00000	0.01165	15.2	0.00000	0.00851
18.5	0.00000	0.00000	17.2	0.00000	0.00129	15.8	0.00000	0.00095
19	0.00000	0.00000	17.6	0.00000	0.00009	16	0.00000	0.00000
19.5	0.00000	0.00000	18	0.00000	0.00000	16.4	0.00000	0.00007
20	0.50897	0.50897	18.4	0.00000	0.00000	16.8	0.00000	0.00000
			18.8	0.00000	0.00000	17	0.00000	0.00000
			19.2	0.00000	0.00000	17.6	0.00000	0.00000
			19.6	0.00000	0.00000	18	0.20615	0.13706
			20	0.47670	0.47670	18.2	0.00000	0.05711
						18.4	0.00000	0.01071
						18.6	0.00000	0.00119
						18.8	0.00000	0.00009
						19	0.00000	0.00000
						19.2	0.00000	0.00000
						19.4	0.00000	0.00000
						19.6	0.00000	0.00000
						19.8	0.00000	0.00000
						20	0.40073	0.40073

Table 3.9: The WECS COPT models for different wind condition models

COPT for 8SCOPTW					
Capacity Outage (MW)	Probability		Capacity Outage (MW)	Probability	
	FOR =0%	FOR =4%		FOR =0%	FOR =4%
0	0.06169	0.04101	15.1	0.00000	0.00060
2	0.00000	0.01709	15.8	0.00000	0.00004
3	0.03284	0.02183	16	0.12934	0.08599
4	0.00000	0.00320	16.1	0.00000	0.00000
4.7	0.00000	0.00910	16.4	0.00000	0.03583
6	0.00000	0.00036	16.5	0.00000	0.00000
6.4	0.00000	0.00171	16.6	0.00000	0.00000
7	0.05087	0.03382	16.8	0.00000	0.00672
8	0.00000	0.00003	17	0.00000	0.00000
8.1	0.00000	0.00019	17.2	0.00000	0.00075
8.3	0.00000	0.01409	17.4	0.00000	0.00000
9.6	0.00000	0.00264	17.6	0.00000	0.00005
9.8	0.00000	0.00001	17.9	0.00000	0.00000
10	0.06815	0.04531	18	0.15193	0.10101
10.9	0.00000	0.00029	18.2	0.00000	0.04209
11	0.00000	0.01888	18.3	0.00000	0.00000
11.5	0.00000	0.00000	18.4	0.00000	0.00789
12	0.00000	0.00354	18.6	0.00000	0.00088
12.2	0.00000	0.00002	18.7	0.00000	0.00000
13	0.10445	0.06984	18.8	0.00000	0.00006
13.2	0.00000	0.00000	19	0.00000	0.00000
13.5	0.00000	0.00000	19.2	0.00000	0.00000
13.7	0.00000	0.02893	19.3	0.00000	0.00000
14	0.00000	0.00003	19.4	0.00000	0.00000
14.4	0.00000	0.00543	19.6	0.00000	0.00000
14.8	0.00000	0.00000	19.8	0.00000	0.00000
14.9	0.00000	0.00000	20	0.40681	0.40073
15	0.00000	0.00000			

Cont--

Table 3.9: The WECS COPT models for different wind condition models

COPT for 9SCOPTW					
Capacity Outage (MW)	Probability		Capacity Outage (MW)	Probability	
	FOR =0%	FOR =4%		FOR =0%	FOR =4%
0	0.06169	0.04101	14.5	0.00000	0.00000
2	0.00000	0.01709	14.6	0.00000	0.02212
3	0.02681	0.01782	14.9	0.00000	0.00000
4	0.00000	0.00320	15.2	0.00000	0.00418
4.7	0.00000	0.00743	15.6	0.00000	0.00000
6	0.03973	0.02677	15.8	0.00000	0.00046
6.4	0.00000	0.00139	16	0.10843	0.07209
7.4	0.00000	0.01101	16.4	0.00000	0.03007
8	0.00000	0.00003	16.6	0.00000	0.00000
8.1	0.00000	0.00015	16.7	0.00000	0.00000
8.8	0.00000	0.00206	16.8	0.00000	0.00563
9	0.05938	0.03948	17	0.00000	0.00000
9.8	0.00000	0.00001	17.2	0.00000	0.00063
10	0.00000	0.00000	17.6	0.00000	0.00005
10.1	0.00000	0.01645	17.8	0.00000	0.00000
10.2	0.00000	0.00023	18	0.15453	0.10101
11.2	0.00000	0.00308	18.2	0.00000	0.04209
11.5	0.00000	0.00000	18.3	0.00000	0.00000
11.6	0.00000	0.00002	18.4	0.00000	0.00789
12	0.07145	0.04750	18.6	0.00000	0.00088
12.3	0.00000	0.00034	18.8	0.00000	0.00006
12.8	0.00000	0.01979	18.9	0.00000	0.00000
13	0.00000	0.00000	19	0.00000	0.00000
13.2	0.00000	0.00000	19.2	0.00000	0.00000
13.4	0.00000	0.00002	19.4	0.00000	0.00000
13.6	0.00000	0.00371	19.6	0.00000	0.00000
14	0.07985	0.05309	19.8	0.00000	0.00000
14.4	0.00000	0.00041	20	0.40681	0.40073

Cont—

Table 3.9: The WECS COPT models for different wind condition models

COPT for 10SCOPTW					
Capacity Outage (MW)	Probability		Capacity Outage (MW)	Probability	
	FOR =0%	FOR =4%		FOR =0%	FOR =4%
0	0.06169	0.04101	14.4	0.00000	0.00034
2	0.00000	0.01709	14.6	0.00000	0.02212
3	0.02681	0.01783	14.9	0.00000	0.00000
4	0.00000	0.00320	15	0.00000	0.00000
4.7	0.00000	0.00743	15.2	0.00000	0.00417
6	0.03155	0.02133	15.8	0.00000	0.00046
6.4	0.00000	0.00139	16	0.10843	0.07209
7.4	0.00000	0.00874	16.4	0.00000	0.03007
8	0.03427	0.02281	16.6	0.00000	0.00000
8.1	0.00000	0.00015	16.8	0.00000	0.00563
8.8	0.00000	0.00164	17	0.00000	0.00000
9.2	0.00000	0.00949	17.2	0.00000	0.00063
9.8	0.00000	0.00001	17.6	0.00000	0.00005
10	0.04503	0.02994	18	0.15193	0.10101
10.2	0.00000	0.00018	18.2	0.00000	0.04209
10.4	0.00000	0.00178	18.3	0.00000	0.00000
11	0.00000	0.01247	18.4	0.00000	0.00789
11.5	0.00000	0.00000	18.6	0.00000	0.00088
11.6	0.00000	0.00021	18.8	0.00000	0.00006
12	0.05969	0.04202	19	0.00000	0.00000
12.8	0.00000	0.01655	19.2	0.00000	0.00000
13	0.00000	0.00026	19.4	0.00000	0.00000
13.2	0.00000	0.00000	19.6	0.00000	0.00000
13.6	0.00000	0.00310	19.8	0.00000	0.00000
14	0.07985	0.05311	20	0.40073	0.40073

Cont—

Table 3.9: The WECS COPT models for different wind condition models

COPT for 11SCOPTW					
Capacity Outage (MW)	Probability		Capacity Outage (MW)	Probability	
	FOR =0%	FOR =4%		FOR =0%	FOR =4%
0	0.05796	0.03853	14.6	0.00000	0.02212
2	0.01560	0.02643	15	0.00000	0.00000
3.8	0.00000	0.00432	15.2	0.00000	0.00417
4	0.02021	0.01645	15.8	0.00000	0.00046
5.6	0.00000	0.00641	16	0.10843	0.07209
6	0.02629	0.01781	16.4	0.00000	0.03007
7.2	0.00000	0.00105	16.8	0.00000	0.00563
7.4	0.00000	0.00737	17	0.00000	0.00000
8	0.03427	0.02281	17.2	0.00000	0.00063
8.8	0.00000	0.00148	17.6	0.00000	0.00005
9.2	0.00000	0.00950	18	0.15193	0.10101
10	0.04503	0.02994	18.2	0.00000	0.04209
10.2	0.00000	0.00015	18.4	0.00000	0.00789
10.4	0.00000	0.00179	18.6	0.00000	0.00088
11	0.00000	0.01247	18.8	0.00000	0.00006
11.6	0.00000	0.00021	19	0.00000	0.00000
12	0.05969	0.04202	19.2	0.00000	0.00000
12.8	0.00000	0.01655	19.4	0.00000	0.00000
13	0.00000	0.00026	19.6	0.00000	0.00000
13.6	0.00000	0.00310	19.8	0.00000	0.00000
14	0.07985	0.05311	20	0.40073	0.40073
14.4	0.00000	0.00034			

Step 4: The WECS COPT shown in Table 3.9 can be reduced if desired using the apportioning method. When the FOR is equal to 0, the MSCOPTW is the same as SCOPTW shown in Table 3.3. Table 3.10 shows the MSCOPTW when the WTG FOR is 4%. The modified Derating Adjusted Forced Outage Rate of the WECS (MDAFORW) obtained using Equation (3.22) is 0.77501. The MDAFORW is the same for each MSCOPTW as shown in Table 3.10.

Table 3.10: Multi-state models for a 20 MW WECS with 4% WTG FOR

2-state (2MSCOPTW)		3-state (3MSCOPTW)		4-state (4MSCOPTW)		5-state (5MSCOPTW)	
Capacity Outage (MW)	Prob.	Capacity Outage (MW)	Prob.	Capacity Outage (MW)	Prob.	Capacity Outage (MW)	Prob.
0	0.22499	0	0.09194	0	0.05283	0	0.05908
20	0.77501	10	0.26609	4	0.06367	5	0.06335
		20	0.64197	10	0.24244	10	0.11475
				20	0.64106	15	0.24408
						20	0.51875
MDAFORW=0.77501							

Cont---

6-state (6MSCOPTW)		7-state (7MSCOPTW)		8-state (8MSCOPTW)		9-state (9MSCOPTW)	
Capacity Outage (MW)	Prob.	Capacity Outage (MW)	Prob.	Capacity Outage (MW)	Prob.	Capacity Outage (MW)	Prob.
0	0.05283	0	0.05283	0	0.04671	0	0.04671
4	0.04734	4	0.04734	3	0.04120	3	0.03457
8	0.06823	8	0.04341	7	0.04868	6	0.03932
12	0.12080	10	0.07777	10	0.06777	9	0.05824
16	0.22513	14	0.16194	13	0.10387	12	0.06882
20	0.48567	18	0.20774	16	0.12875	14	0.08157
		20	0.40898	18	0.15620	16	0.10942
				20	0.40681	18	0.15453
						20	0.40681
MDAFORW=0.77501							

Cont--

10-state (10MSCOPTW)		11-state (11MSCOPTW)	
Capacity Outage (MW)	Prob.	Capacity Outage (MW)	Prob.
0	0.04671	0	0.03853
3	0.03457	2	0.02686
6	0.03035	4	0.02162
8	0.03414	6	0.02557
10	0.04418	8	0.03329
12	0.05949	10	0.04408
14	0.07981	12	0.05948
16	0.10941	14	0.07981
18	0.15454	16	0.10941
20	0.40681	18	0.15454
		20	0.40681
MDAFORW=0.77501			

The analytical procedure used to build WECS multi-state models including the WTG FOR is briefly described using the three cases. The resulting MSCOPTW are very dependent on the wind speed profile. Tables C.2 and C.3 in Appendix C respectively show the SCOPTW and the MSCOPTW when the mean wind speed is increased from 19.46 km/h to 38.92km/h.

3.4 Application of WECS Multi-state Models in Generating Capacity Adequacy Assessment

3.4.1 The Impact of WECS Multi-state Models at HL-I

The WECS multi-state models shown in Table 3.10 are used first to investigate the impact of the different WECS models on RBTS generating system adequacy assessment. The 20-step load model introduced in Chapter 2 is utilized in this study. The annual system adequacy indices of the RBTS including the 20 MW WECS obtained using the analytical method and by using MECORE are shown in Table 3.11 and 3.12 respectively. The annual system LOLE obtained using the sequential MCS approach are shown in Table E.2. The annual system LOLE for a peak load of 185 MW are presented in Figure 3.23. This figure shows that the LOLE fluctuate slightly due to the different number of states used in the analysis and that the use of a two-state representation provides a pessimistic appraisal of the system adequacy [1]. This is consistent with the use of DAFOR to represent large conventional generator units. The results clearly show that WECS should be modelled with at least three states.

It can be seen from Figure 3.23 that the annual system LOLE obtained using MECORE and the analytical method utilizing a 20-step load model are higher than those obtained using the sequential technique which utilizes a chronological load model. The effect of the load model, as shown in Chapter 2, exists in this analysis and explains the difference between the annual system indices obtained using the three evaluation methods.

Table 3.11: The RBTS HL-I annual system indices including a 20 MW WECS for a peak load of 185 MW obtained using the analytical method

State model	LOLE (hrs/yr)	LOEE (MWh/yr)
2-state	0.93105	9.57469
3-state	0.86830	8.83698
4-state	0.86763	8.81198
5-state	0.87156	8.56968
6-state	0.87339	8.53211
7-state	0.89890	8.51176
8-state	0.87217	8.37025
9-state	0.88771	8.48550
10-state	0.88750	8.48103
11-state	0.88832	8.47984

Table 3.12: The RBTS HL-I annual system indices including a 20 MW WECS for a peak load of 185 MW obtained using MECORE

State model	EDLC (hrs/yr)	EENS (MWh/yr)
2-state	0.89742	9.05546
3-state	0.84050	8.38680
4-state	0.84527	8.44542
5-state	0.85129	8.14529
6-state	0.85668	8.18077
7-state	0.88136	8.15332
8-state	0.85484	8.02324
9-state	0.86697	8.07232
10-state	0.86405	8.04131
11-state	0.87275	8.14372

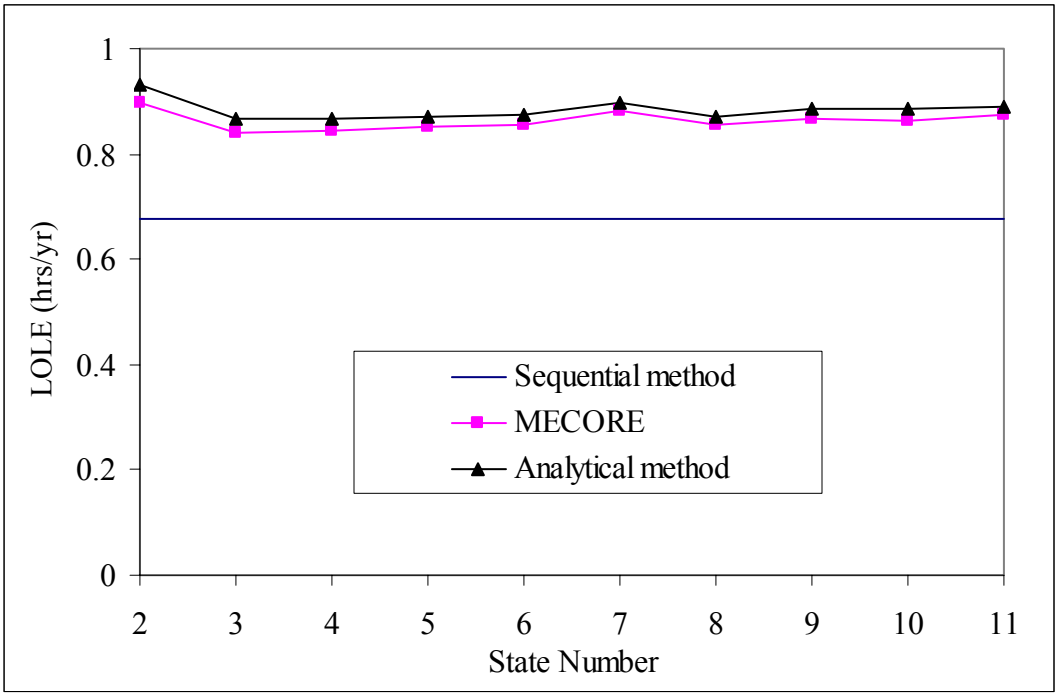

Figure 3.23: The RBTS HL-I annual system LOLE for a peak load of 185 MW for different WECS state models

3.4.2 The Effects of System Peak Load Variation

The effects of using different WECS multi-state models when the peak load is varied were analyzed using the RBTS and the RTS. The MECORE program was used to conduct these analyses and the WECS was added at Bus 3 of the RBTS and Bus 19 of the RTS respectively.

RBTS System Analysis

Figure 3.24 shows the effects of adding different WECS models to the RBTS with various system peak loads. Tables F.1 and F.3 contain the corresponding numerical data. Figure 3.24 also shows that the benefit associated with adding the 20 MW WECS to the RBTS increases as the peak load increases. This benefit is relatively small at the system design peak of 185 MW.

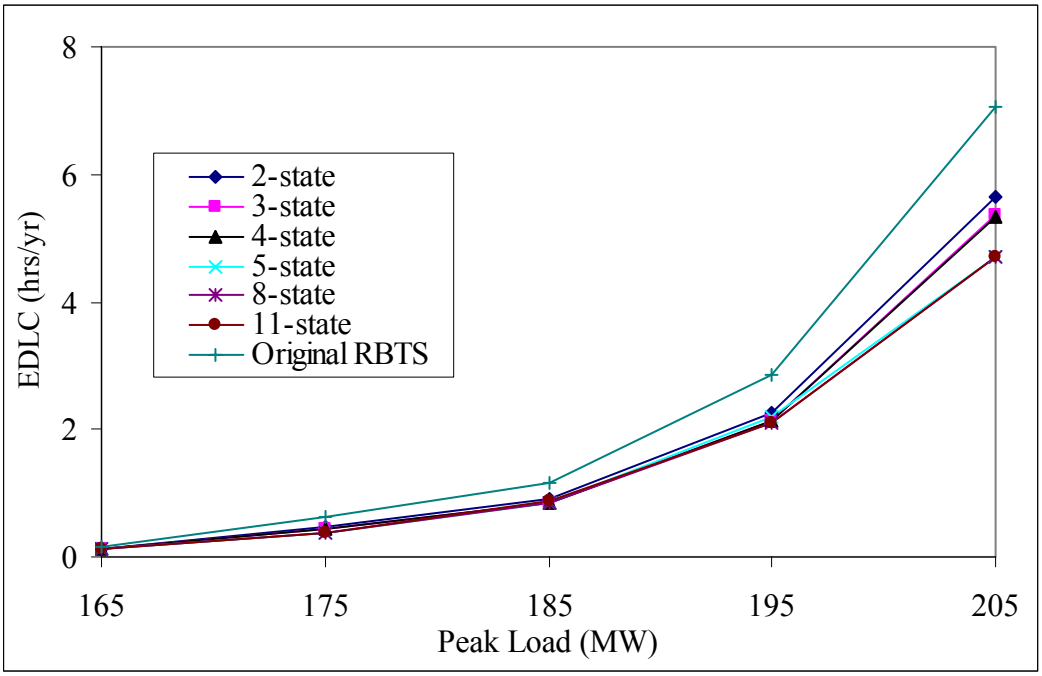

Figure 3.24: The HL-I annual system EDLC with WECS multi-state models versus peak load

Tables 3.11, 3.12 and Figure 3.23 show that the annual system indices are relatively close using a model with three or more states to represent the WECS when the peak load is 185 MW. Figure 3.24 shows that additional states are required in the WECS model when the peak load increases significantly. The system LOLE in these situations may be unacceptably high.

RTS System Analysis

The WECS addition in this case is 400 MW, obtained using 200×2 MW WTG units. The WECS multi-state models shown in Table 3.13 are used in the RTS analyses. The series of 400 MW WECS multi-state models are very similar to the 20 MW WECS multi-state models shown in Table 3.10, as both WECS consist of the same wind turbine generators.

Table 3.13: Multi-state models for a 400 MW WECS with 4% WTG FOR

2-state (2MSCOPTW)		3-state (3MSCOPTW)		4-state (4MSCOPTW)		5-state (5MSCOPTW)	
Capacity Outage (MW)	Prob.	Capacity Outage (MW)	Prob.	Capacity Outage (MW)	Prob.	Capacity Outage (MW)	Prob.
0	0.22498	0	0.09194	0	0.05261	0	0.05898
400	0.77501	200	0.26609	80	0.06404	100	0.06354
		400	0.64198	200	0.24230	200	0.11466
				400	0.64106	300	0.24407
						400	0.51875

Cont---

6-state (6MSCOPTW)		7-state (7MSCOPTW)		8-state (8 MSCOPTW)		9-state (9MSCOPTW)	
Capacity Outage (MW)	Prob.	Capacity Outage (MW)	Prob.	Capacity Outage (MW)	Prob.	Capacity Outage (MW)	Prob.
0	0.05261	0	0.05261	0	0.04524	0	0.04524
80	0.04772	80	0.04772	60	0.04371	60	0.03719
160	0.06812	160	0.04262	140	0.04764	120	0.03839
240	0.12075	200	0.07877	200	0.06788	180	0.05809
320	0.22513	280	0.16157	260	0.10379	240	0.06873
400	0.48567	360	0.20774	320	0.12874	280	0.08170
		400	0.40898	360	0.15620	320	0.10934
				400	0.40681	360	0.15452
						400	0.40681

Cont---

10-state (10MSCOPTW)		11-state (11MSCOPTW)	
Capacity Outage (MW)	Prob.	Capacity Outage (MW)	Prob.
0	0.04526	0	0.03479
60	0.03719	40	0.03317
120	0.02879	80	0.01936
160	0.03488	120	0.02540
200	0.04425	160	0.03341
240	0.05915	200	0.04425
280	0.07982	240	0.05915
320	0.10934	280	0.07982
360	0.15452	320	0.10934
400	0.40681	360	0.15452
		400	0.40681

The HL-I annual system indices for a peak load of 2850 MW are shown in Table 3.14. The annual system EDLC is shown graphically in Figure 3.25. This figure illustrates that the system EDLC at a peak load of 2850 MW are relatively constant when the WECS is represented by models containing five or more states.

Table 3.14: The RTS HL-I annual system indices for a peak load of 2850 MW

State model	EDLC (hrs/yr)	EENS (MWh/yr)
2-state	10.10922	1292.94200
3-state	9.08871	1156.12200
4-state	9.05665	1151.28300
5-state	8.66396	1086.24451
6-state	8.58357	1083.17494
7-state	8.60446	1085.15732
8-state	8.54932	1080.21329
9-state	8.54679	1077.19637
10-state	8.54202	1076.59705
11-state	8.55422	1079.09970

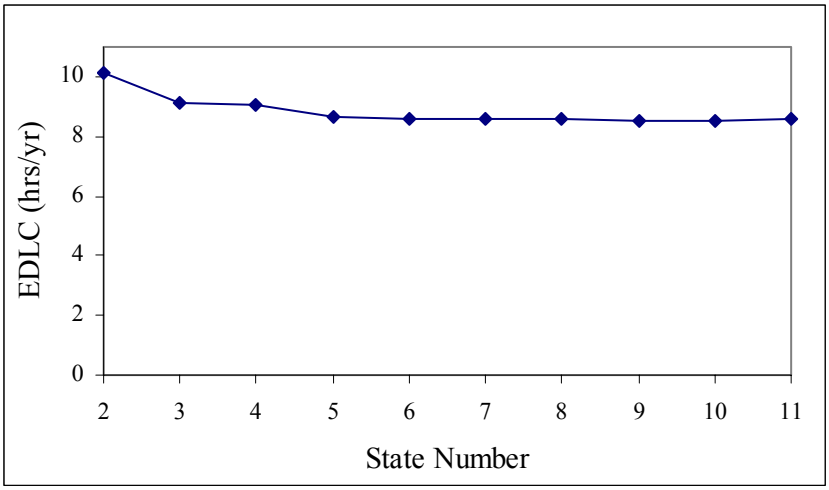

Figure 3.25: The RTS HL-I annual system EDLC for a peak load of 2850 MW with different WECS multi-state models

Figures 3.26 and 3.27 respectively show the annual system EDLC and EENS with different WECS multi-state models. Tables G.1-G.4 in Appendix G contain the corresponding numerical data. The annual system EDLC and EENS for different peak

loads obviously decrease when 400 MW of WECS is added to the RTS. Figures 3.25 to 3.27 indicate that the WECS 5-state model can be used to represent a WECS in an acceptable adequacy assessment of the RTS.

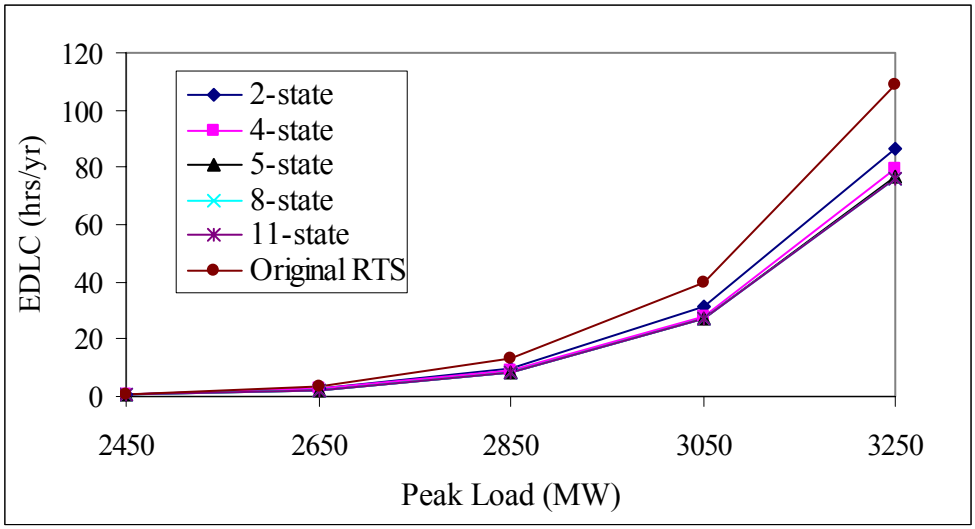

Figure 3.26: The HL-I annual system EDLC with different WECS models versus peak load

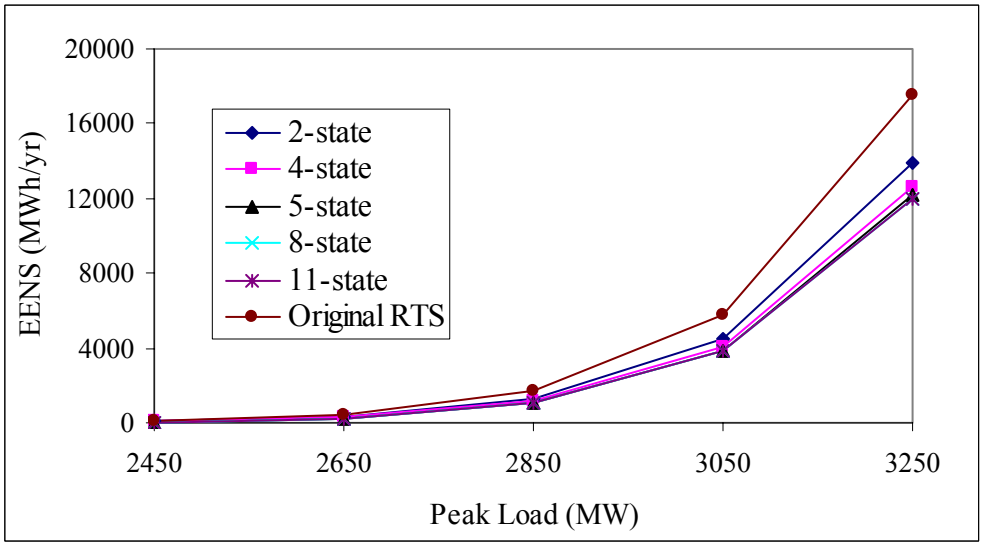

Figure 3.27: The HL-I annual system EENS with different WECS models versus peak load

The conclusion can be drawn based on the analyses of the RBTS and the RTS, that using a 5-state WECS model can provide a reasonable adequacy assessment of similar power

systems containing a WECS and this model can be applied in practical studies using the analytical method or MECORE. This WECS model is used in the composite system evaluations described later in this thesis.

3.5 The Effect of WTG Forced Outage Rate

In the previous sections, a WTG unit with 0% and 4% FOR are used to create the MSCOPTW. The effect on the generating system adequacy of varying the WTG unit FOR is analyzed for the RBTS system including a 20 MW WECS and the RTS containing 400 MW WECS. The system peak loads are 185 MW and 2850 MW respectively. The MECORE software and the analytical approach are used in the RTS analysis. These two methods and the sequential MCS technique are used in the RBTS study. The WECS 5MSCOPTW and MDAFORW for FOR varying from 0% to 10% are shown in Table 3.15 and 3.16 respectively.

Table 3.15: 5MSCOPTW and MDAFORW for different FOR (10×2 MW WECS)

Capacity Outage (MW)	Probability						
	FOR =0%	FOR =1%	FOR =2%	FOR =4%	FOR =6%	FOR =8%	FOR =10%
0	0.07021	0.06738	0.06461	0.05908	0.05368	0.04849	0.04352
5	0.05944	0.06047	0.06147	0.06335	0.06497	0.06624	0.06710
10	0.11688	0.11633	0.11578	0.11475	0.11382	0.11303	0.11237
15	0.24450	0.24440	0.24428	0.24408	0.24389	0.24371	0.24360
20	0.50897	0.51142	0.51386	0.51875	0.52364	0.52853	0.53342
MDAFORW	0.76564	0.76798	0.77033	0.77501	0.77970	0.78439	0.78908

Table 3.16: 5MSCOPTW and MDAFORW for different FOR (200×2 MW WECS)

Capacity Outage (MW)	Probability						
	FOR =0%	FOR =1%	FOR =2%	FOR =4%	FOR =6%	FOR =8%	FOR =10%
0	0.07021	0.06740	0.06459	0.05898	0.05336	0.04774	0.04213
100	0.05944	0.06047	0.06149	0.06354	0.06559	0.06764	0.06969
200	0.11688	0.11633	0.11577	0.11466	0.11355	0.11245	0.11134
300	0.24450	0.24439	0.24428	0.24407	0.24386	0.24364	0.24343
400	0.50897	0.51142	0.51386	0.51875	0.52364	0.52853	0.53342
MDAFORW	0.76564	0.76799	0.77033	0.77502	0.77970	0.78440	0.78908

The RBTS adequacy indices obtained using the sequential MCS technique are shown in Table E.2. The 5MSCOPTW shown in Table 3.15 are utilized in the analytical method and MECORE. Figure 3.28 and 3.29 show the annual system LOLE with varying WTG FOR for the RBTS and the RTS respectively. It can be seen from the two figures that, the changes in FOR of the WTG units do not have a significant impact on the calculated system reliability indices.

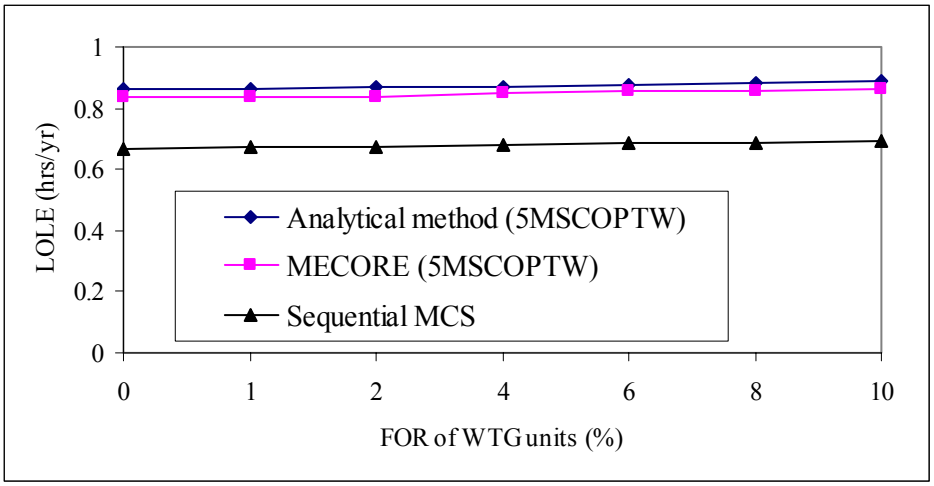

Figure 3.28: The RBTS HL-I annual system LOLE as a function of the WTG FOR for the three evaluation techniques

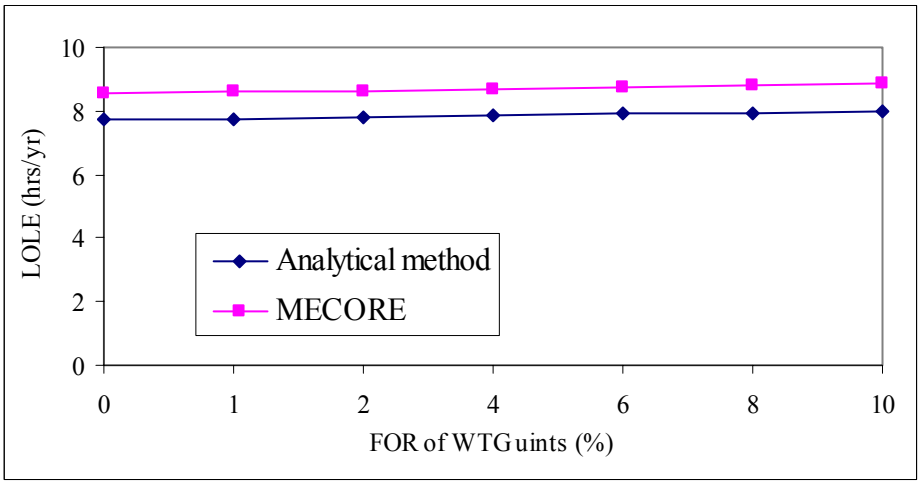

Figure 3.29: The RTS HL-I annual system LOLE as a function of the WTG FOR for the two evaluation techniques

The WTG unit FOR variations do not have a significant impact on the estimated system adequacy. While it is not possible for a WTG to have a zero FOR, this can be a

reasonable assumption in a practical system study which will simplify the analysis considerably.

3.6 Analysis of a WECS Considered as a Negative Load

In the previous studies, appropriate WECS multi-state models were obtained and utilized in adequacy assessment of generating systems incorporating wind energy. One of the significant characteristics of wind power is its variation with time. The most accurate technique for generating capacity assessment of a system including wind power is therefore the sequential MCS approach. An additional approach to incorporate the chronological nature of the wind is to model the WECS output as a negative load.

This section examines the differences in the calculated RBTS HL-I adequacy indices when the added 20 MW WECS is considered as a generating facility and when it is modeled as a negative load. The initial 20-step load model described in Chapter 2 is shown in Figure 3.30. The annual system LOLE was obtained using the analytical technique. The previous section shows that the FOR of the WTG units has relatively little impact on the system adequacy and WTG units with a 0% FOR were utilized to simplify the analysis. The following procedure was used modify the system load duration curve.

3.6.1 Modifying the RTS Load Duration Curve

The following six steps are used to modify a load duration curve (LDC) by considering the WECS power output as a negative load.

Step 1: Obtain the hourly power output of the WECS over an annual period.
Step 2: Modify the chronological system load by subtracting the hourly WECS power output over the annual period.
Step 3: The new annual system peak load is the maximum value of the modified chronological system load.
Step 4: Construct the 20-step load duration curve for each simulation year based on the

determined load levels.

Step 5: Repeat Step 1- 4 for a specified years.

Step 6: Average the new load duration curves and peak loads to create a new system load duration curve. The modified LDC for the RBTS due to adding a 20 MW WECS is shown in Figure 3.31.

The annual peak load is modified from 185 MW to 181.5 MW. The data for the modified 20-step RBTS LDC are shown in Appendix H.

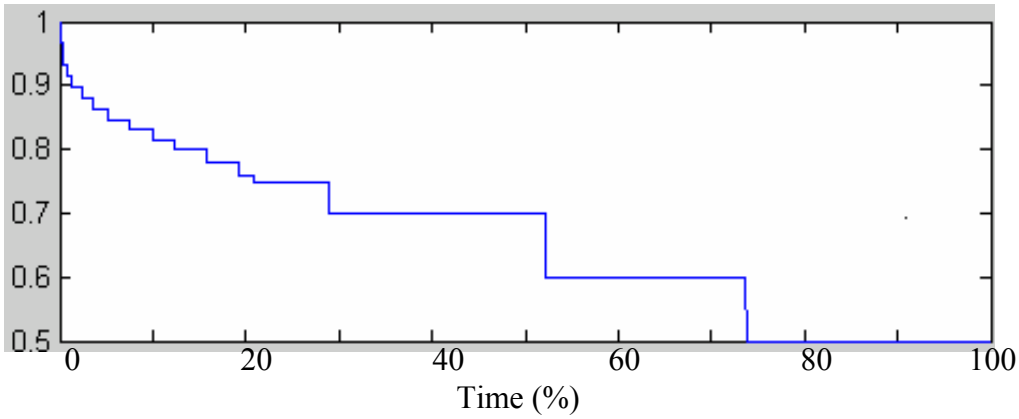

Figure 3.30: The initial 20-step RBTS load duration curve

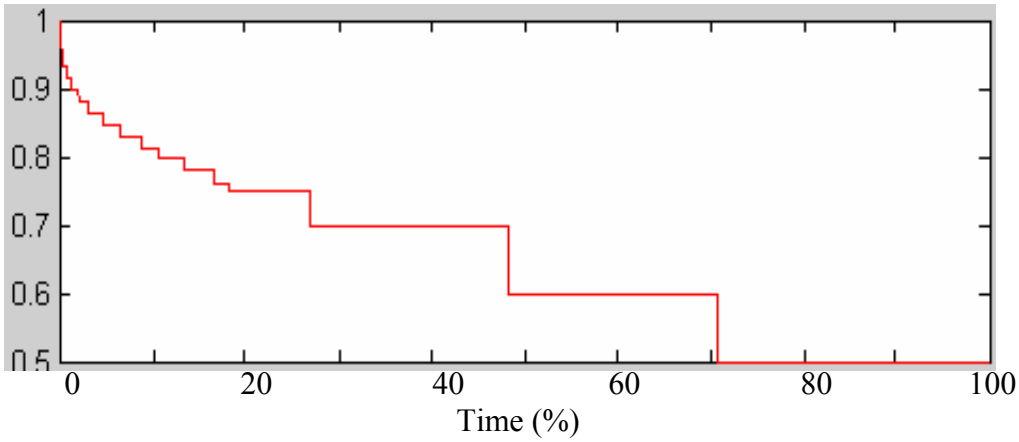

Figure 3.31: The modified 20-step RBTS load duration curve

3.6.2 Adequacy Index Comparison

The two cases described in the following are analyzed and compared.

Case 1: RBTS generating units including a 20 MW WECS and the 20-step LDC shown in Figure 3.30.
Case 2: RBTS generation units and the modified 20-step LDC shown in Figure 3.32.

The annual system LOLE for different peak loads are shown in Table 3.17 and graphically presented in Figure 3.32.

Table 3.17: The annual system indices for the two cases

Case 1		Case 2	
Peak Load (MW)	LOLE (hrs/yr)	Modified Peak Load (MW)	LOLE (hrs/yr)
165	0.12088	161.8	0.11673
175	0.39206	171.6	0.32285
185	0.86171	181.5	0.78189
195	2.21882	191.4	1.96478
205	4.70539	201.2	4.84550

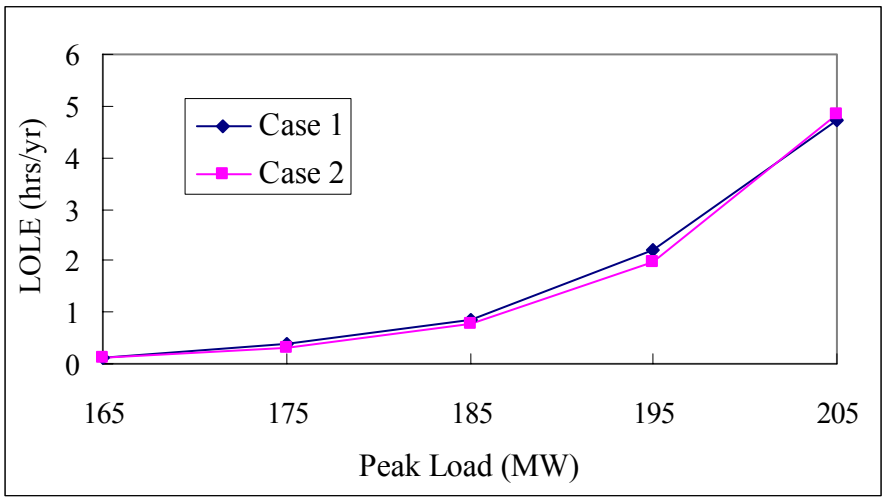

Figure 3.32: Comparison of the annual system LOLE of the two cases

Table 3.17 and Figure 3.32 show that the LOLE for these two cases are relatively close. Modelling a WECS as a negative load using the described six step procedure incorporates some of the chronological nature of wind power in the evaluation, and therefore tends to produce a slightly lower estimate of the system LOLE. A 5-state model is used to represent the WECS in Case 1.

3.7 Summary

The ARMA time series models used in this research are briefly introduced in this chapter and used to simulate wind speeds. A comparison of the observed wind speed probability distribution and the simulated wind speed probability distribution created by the ARMA model illustrates that the ARMA models provide a useful representation of the actual wind regimes. The power available from a WTG is obtained from the simulated wind speeds using a function describing the relationship between the wind speed and output power. The WTG COPT is created by applying the simulated hourly power output and the hourly wind speed relationship. A comparison between the COPT for the observed wind data and the COPT for the simulated wind data is presented which shows that the simulated wind data provides a reasonable representation for adequacy assessment.

The effect of wind speed on the WTG power output shows that the power output of a WTG is extremely dependent on the wind regime and will increase if the facilities are located at a site where higher wind velocities are experienced. Seasonal wind speeds and wind power outputs using data for four sites were analyzed. The wind speed and power output probability distributions of the four sites illustrate that in these cases, the annual profile is a valid representation of the system wind speeds and that annual studies can be done directly using this profile.

The apportioning method is introduced and used to create selected WTG multi-state models. It is assumed in this research that a WECS consists of multiple identical WTG units. Non identical units can be easily incorporated using Equation (2.3). A WECS multi-state model is the same as that of a single WTG unit when the FOR of the WTG unit is zero. The DAFOR of the WECS and the single WTG unit are also the same. An analytical procedure is introduced and used to create WECS multi-state models when the WTG FOR is incorporated.

A comparison of the analytical method, the MECORE program and the sequential Monte Carlo simulation technique using the RBTS with a WECS are presented in this

chapter. The LOLE from MECORE and the analytical method are higher than that obtained from the sequential Monte Carlo simulation technique due to the impact of the applied load model.

The analyses of generating systems including WECS indicate that a 5-state WECS model can be used to provide a reasonable assessment in practical studies using the analytical method or MECORE. Analysis conducting by considering WECS as a negative load also indicates that this approach can be used to provide reasonable assessments. The studies on the RBTS and the RTS LOLE with different WTG FOR indicate that changes in WTG FOR do not have a significant impact on the calculated reliability indices. Using a zero FOR will not significantly impact the calculated indices and can greatly simplify the WECS modelling procedure.

4. DEVELOPMENT OF PVCS MODELS FOR ADEQUACY ASSESSMENT

4.1 Introduction

Photovoltaic systems are being increasingly used for electrical power generation. The performance and operating characteristics of these systems are considerably different from those of conventional generating units. The variable nature of the energy produced by a photovoltaic conversion system (PVCS) has a different effect on the overall system reliability than the energy produced by conventional units. It is important to assess the reliability effects that PVCS will have on the overall system. Suitable PVCS models are required to evaluate these effects and the adequacy of generating and bulk systems including PVCS. Modeling the solar radiation available on the earth at a site location and modeling the PV panel power output are the two basic steps in building PVCS models. The WATGEN [29] and WATSUN-PV [30] programs developed at the University of Waterloo are briefly introduced and have been used to simulate hourly solar radiation data and hourly PV generating unit power output in this research.

The number of capacity states required in a PVCS model in order to provide a reasonable accurate adequacy assessment is examined. The analyses described in this chapter are conducted at HL-I using the RBTS and the RTS. The adequacy effects of adding a WECS or a PVCS to the RBTS and the RTS are examined.

It is assumed that a PVCS is composed of a number of identical PV cells and panels. Wiring losses, inverter losses and the energy storage facilities such as batteries are not considered in this research.

4.2 Photovoltaic Conversion System Models

The heart of any photovoltaic conversion system is the solar cell. It is the transducer that converts the sun's radiant energy directly into electricity by the "photovoltaic effect". The whole technology of converting light to electricity and using the generated power to supply various load demand is known as photovoltaics. In this thesis, the term PVCS or solar energy is used to designed those systems that convert the energy from the sun to supply electricity through the "photovoltaic effect".

Solar cells can be connected in series and parallel to create a solar panel which can be interconnected with similar panels to comprise an array. In principle, array sizes at the thousand megawatt level are possible, and are limited mainly by real estate considerations [37]. A PVCS is therefore composed of a number of photovoltaic (PV) arrays.

The amount of electric power generated by a PV array depends on a large number of factors, such as the operational constraints of the solar cell, the solar array arrangement and atmospheric conditions at the site location and the given moment. It is complex problem to model solar energy. In general, there are two steps in modeling the available solar energy when supplying power to a utility company. The first step involves the determination of the amount of radiation that arrives on the earth at the PV panel location. The second step is modeling the panel itself, considering its efficiencies, losses and physical orientation. Each step requires a model that deals with many variables, and the results of the first step are used as inputs into the second model. The following two sections present the two steps.

4.2.1 Generating Solar Radiation Data

Solar radiation on the earth's surface is complicated to model due to the number of variables inside the earth's atmosphere that affect radiation. Solar radiation outside the atmosphere is referred to as extraterrestrial radiation. The average amount of radiant energy received outside the atmosphere from the sun is known as the solar constant and

it is equal to 1353W/m^2 [38]. The solar radiation received at the surface of the earth is usually known as global radiation and produces electrical energy in a PV panel. Global radiation is a minor portion of the energy radiated from the sun. The correct prediction of the power generated by a PV array requires the determination of the intensity of the global radiation on the surface of the array at the specific site location. The global radiation is normally composed of two components designated as direct and diffuse radiation. Direct radiation is the radiation received from the sun without having been scattered by the atmosphere, while diffused radiation is scatted by clouds, water vapour and other elements in the area.

The WATGEN program [29] developed at the University of Waterloo has been used to generate synthetic global radiation data on an hourly basis for a horizontal surface. The overall model utilizes a stochastic probability transformation of the clearness index in order to obtain a Gaussian random variable which has the same mean and variance for each month. This new variable is then used in an ARMA (1, 0) model to compute the hourly radiation on a horizontal surface [39, 40]. The overall procedure for generating synthetic hourly solar radiation data in the WATGEN program is a two-step process, as shown in Figure 4.1. The first step involves generating daily radiation data from the monthly mean values such as the monthly average solar radiation, the monthly average wind speed and the monthly average ambient temperature at the particular site location. The second step is the generation of hourly solar radiation for a calendar year from the daily values generated in the first step.

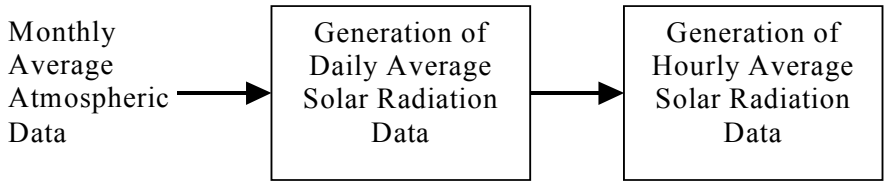

Figure 4.1: Basic steps involved in the WATGEN program

This program takes into account effects such as the average monthly temperature, wind speed and humidity. It has been used in the simulations described in this thesis.

4.2.2 Modeling Photovoltaic Panel Power Output

As stated earlier, solar cells are the basic components used to generate electricity from sunlight. A solar cell produces a direct current (DC) electrical output. The current is proportional to both the cell area and the intensity of the sunlight. The voltage of a cell depends on the type of semiconductor used to make the cell as well as the intensity of the sunlight.

The power output from a solar cell can be estimated from its current and voltage (I-V) curves, as shown in Figure 4.2. This data is available from the manufacturer. The curve is the locus of the operating point of the solar cell. The largest rectangle that fits under the I-V curve will touch the curve at the maximum power point (MPP). The curve shifts vertically upwards (the output current increases) with increase in solar insolation and extends horizontally outwards (the voltage level increases) with a decrease in temperature. The I-V curve for a PV panel can be obtained from the I-V curve of the individual cells in the panel.

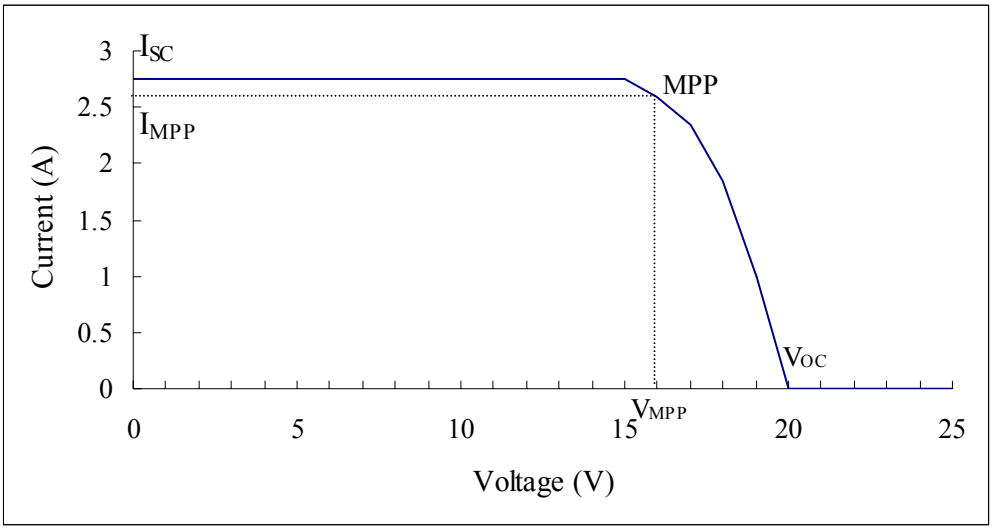

Figure 4.2: The solar cell I-V characteristics

The modeling program known as WATSUN-PV decomposes the hourly global irradiation on the horizontal earth's surface into diffuse, beam, and reflected components and evaluates the total radiation incident on the titled array surface [22]. An iterative

method is used to calculate the power output of the PV array with an initial estimate using Equation (4.1).

$$P = (V_{MPP_{REF}} \times I_{MPP_{REF}} \times H_T)/(H_{T_{REF}} \times A) \quad (4.1)$$

where $V_{MPP_{REF}}$ and $I_{MPP_{REF}}$ are the reference module voltage and current at the MPP, H_T is the insolation level for the hour, $H_{T_{REF}}$ is the reference insolation level, and A is the module area.

The power estimated from Equation (4.1) is used to obtain an estimate of the cell temperature using the solar cell thermodynamic model described in [30]. An I-V curve is constructed for the estimated insolation level and cell temperature for the particular hour using the module ratings. The program then calculates the maximum power from the I-V curve utilizing Equation (4.2).

$$P_{MPP} = (P_{MPP_{REF}} \times V_{OC} \times I_{SC})/(V_{OC_{REF}} \times I_{SC_{REF}}) \quad (4.2)$$

where P_{MPP} and $P_{MPP_{REF}}$ are the maximum and the reference module power, $V_{OC_{REF}}$ and $I_{SC_{REF}}$ the reference open circuit voltage and short circuit current.

The power output obtained from Equation (4.2) further affects the cell temperature. An iterative calculation of the cell temperature and output power is used to determine the power output for the particular hour. The total power output of a PV array is the sum of the power outputs of all the modules existing in the array.

4.2.3 Case Studies

The power output of a PV generating unit is determined by the atmospheric conditions at the actual site. It is assumed in the studies described in this thesis that the PVCS is located at Swift Current, Saskatchewan.

The hourly solar radiation is simulated using the program WATGEN. This program uses monthly average meteorological data for the specific site as the input data for the simulation of the solar radiation process at that site. The data required are the monthly

average values of solar radiation on a horizontal surface, the wind speed and the ambient temperature. The monthly average data for the Swift Current site are shown in Table 4.1.

Table 4.1: Monthly average weather data at Swift Current (50.3 degree north)

Month	Jan	Feb	Mar	Apr	May	Jun	Jul	Aug	Sep	Oct	Nov	Dec
Wind Speed (m/s)	24	23	22	22	22	21	18	18	20	22	22	24
Temperature (^oC)	-13.	-9.6	-4.0	4.3	10.8	15.6	18.3	17.6	11.4	5.5	-4.0	-10.8
Radiation (MJ/m^2)	4.95	8.58	13.6	18.0	21.3	23.4	24.2	20.2	14.0	9.3	5.2	3.8

The PV generating units are simulated using the data generated from the WATGEN program and the hourly output power is obtained using WATSUN-PV. Appendix I shows the solar panel parameters required to define the current-voltage relationship. A CANROM30 KW PV array [30] with a FOR of 0.05 was simulated using 3000 sample years. The simulated power output of a 30 KW PV array for a sample year is shown in Figure 4.3 and for a week in summer is shown in Figure 4.4. Figures 4.3 and 4.4 illustrate that the power output of a PV array can be more than its rated value. The power output of the PV array is zero during the nighttime due to no sunlight or due to a forced outage. The power output of the PV unit usually reaches its greatest daily value at noon. The rated value is considered to be the maximum output power in the studies described in this thesis.

As stated earlier, a PVCS is composed of a number of identical PV arrays in the studies described in this thesis. The power output characteristics of the 20 MW PVCS, therefore, are the same as those of a single PV array. The capacity outage levels and corresponding probabilities are created using the power output of the PV generating unit and the hourly average solar radiation relationship. The procedure is as follows:

(1) The output states for the PV array are divided into segments of the rated power. A step size of 5% is used in this analysis. The number of states is twenty-one, as zero power output is considered to be a unique point.

(2) The total number of times that the hourly solar radiation results in a power output falling within one of the output states is determined.

(3) The total number of occurrences for each output state is divided by the total number of data points to estimate the probability of each state.

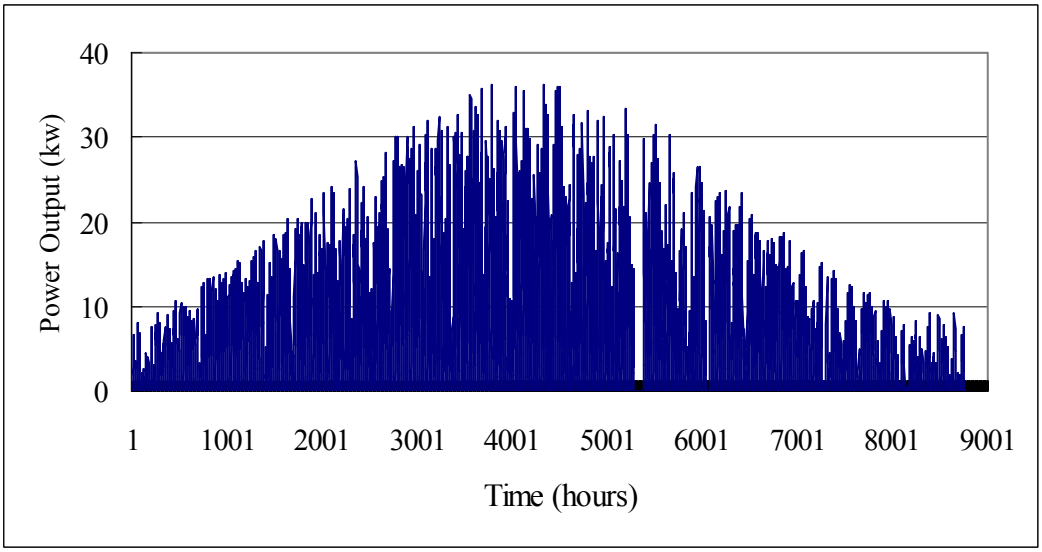

Figure 4.3: Simulated power output for a sample year using Swift Current data

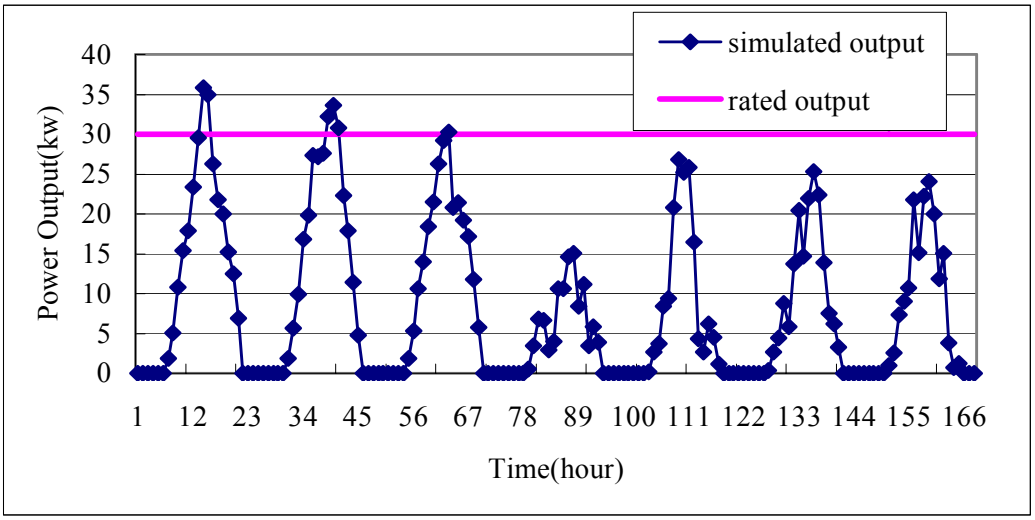

Figure 4.4: Simulated power output for a July week in a sample year using Swift Current data

Table 4.2 shows the capacity outage probability table (COPT) of a PVCS formed using this procedure. This table is used in the following studies. Figure 4.5 shows this capacity outage probability distribution.

Table 4.2: Capacity outage probability table for the PVCS

Capacity Outage (MW)	Probability
0	0.020970
1	0.007216
2	0.007663
3	0.009369
4	0.009711
5	0.012006
6	0.013089
7	0.014360
8	0.015487
9	0.017193
10	0.019883
11	0.021128
12	0.023276
13	0.027965
14	0.030533
15	0.035353
16	0.040135
17	0.038376
18	0.040593
19	0.056699
20	0.538995

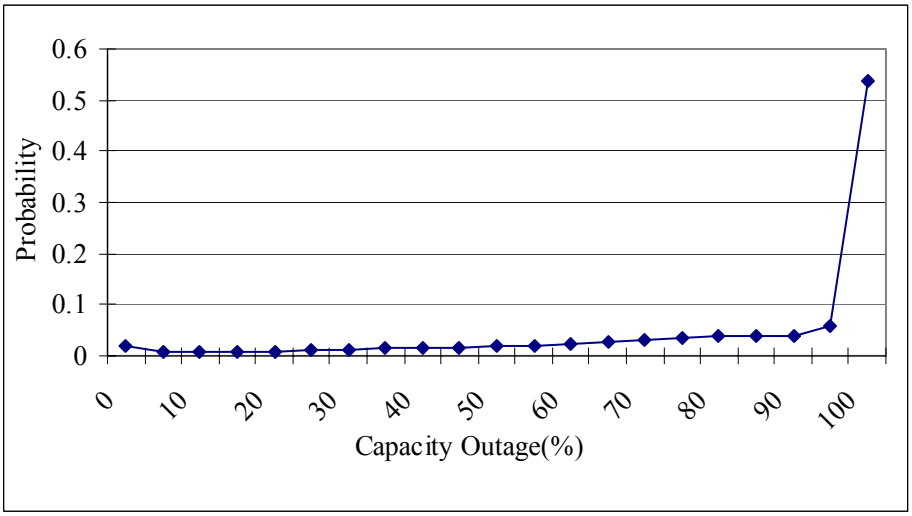

Figure 4.5: Capacity outage probability profile for the PVCS

4.3 Building PVCS Multi-state Models Using the Apportioning Method

The PVCS COPT shown in Table 4.2 was reduced to a series of multi-state models using the apportioning method described in Chapter 3. The PVCS multi-state models are shown in Table 4.3 and were used in the following studies. The DAFOR of the PVCS obtained using Equation (3.22) is 0.82607.

Table 4.3: Multi-state model of the PVCS

2-state		3-state		4-state		5-state	
Capacity Outage (MW)	Prob.	Capacity Outage (MW)	Prob.	Capacity Outage (MW)	Prob.	Capacity Outage (MW)	Prob.
0	0.17393	0	0.06634	0	0.03256	0	0.03703
20	0.82607	10	0.21517	4	0.05631	5	0.05863
		20	0.71849	10	0.19264	10	0.09945
				20	0.71849	15	0.17281
						20	0.63209

Cont---

6-state		7-state		8-state		9-state	
Capacity Outage (MW)	Prob.	Capacity Outage (MW)	Prob.	Capacity Outage (MW)	Prob.	Capacity Outage (MW)	Prob.
0	0.03256	0	0.03256	0	0.02833	0	0.02833
4	0.04151	4	0.04151	3	0.03344	3	0.02736
8	0.06392	8	0.04440	7	0.04866	6	0.03907
12	0.09844	10	0.06295	10	0.03651	9	0.05260
16	0.15216	14	0.12460	13	0.07581	12	0.05797
20	0.61141	18	0.12663	16	0.12177	14	0.06219
		20	0.56734	18	0.08813	16	0.07700
				20	0.56734	18	0.08813
						20	0.56734

Cont---

10-state		11-state	
Capacity Outage (MW)	Prob.	Capacity Outage (MW)	Prob.
0	0.02833	0	0.02458
3	0.02736	2	0.01596
6	0.03151	4	0.02040
8	0.03126	6	0.02627
10	0.03904	8	0.03126
12	0.04782	10	0.03904
14	0.06219	12	0.04782
16	0.07700	14	0.06219
18	0.08813	18	0.07700
20	0.56734	18	0.08813
		20	0.56734

4.4 Multi-state PVCS Models for Generating Capacity Adequacy Assessment

This section examines the effect of PVCS generation in the RBTS using two basically different approaches. The negative load method illustrated in the previous chapter is first applied, followed by the utilization of the different multi-state models shown in Table 4.3.

4.4.1 The PVCS Considered as Negative Load

The RBTS load duration curve was modified by considering the power output of the 20 MW PVCS as negative load. The procedure includes six steps. In the first step, the PV generating units are simulated using the WATGEN program and the PVCS hourly power output for each sample year is obtained. The remaining steps are similar to the Step 2-6 for the WECS analysis shown in Section 3.6.1. The initial and modified 20-step RBTS LDC are shown in Figure 4.6.

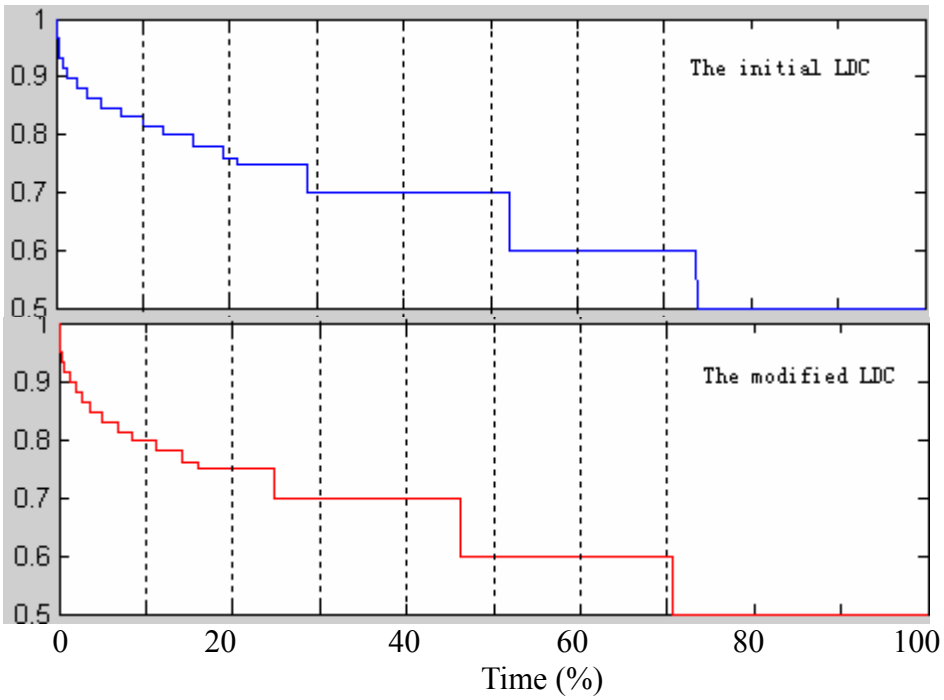

Figure 4.6: The initial and modified 20-step RBTS LDC

In the initial chronological load profile, the maximum loads occur on the 8442 and 8443

hours of a year. They occur at 6p.m and 7p.m on the 352 day. The PV power outputs, however, are zero since there is not enough solar radiation to generate PV power at that time. The modified annual system peak load is, therefore, the same as the original peak load. Figure 4.7 shows the RBTS load profile on the 352 day. The RBTS peak load of 185 MW is considered as the p.u base value. The PVCS is rated at 20 MW.

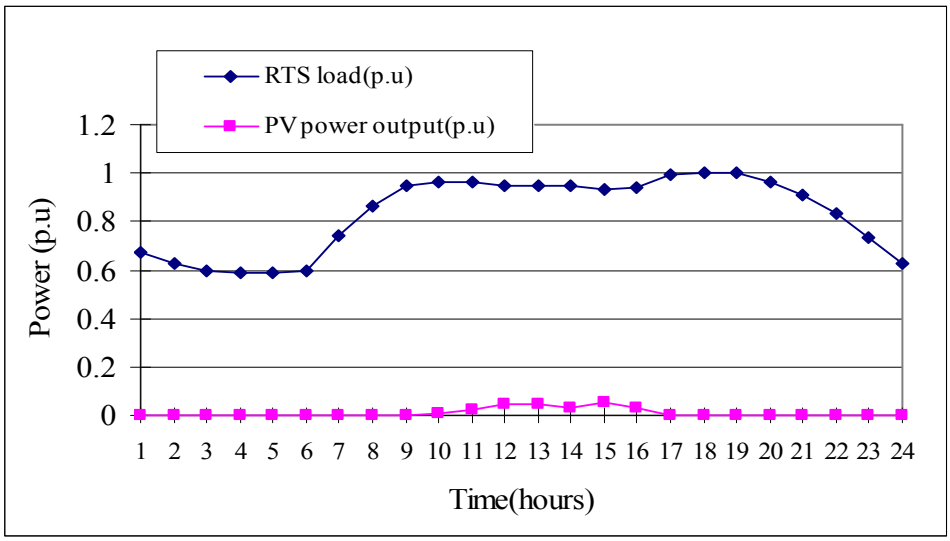

Figure 4.7: Comparison of the RBTS load and the PVCS power output on day 352

Table 4.4 shows the annual system LOLE and LOEE of the RBTS with the modified LDC obtained using the analytical method. Figure 4.8 shows that the benefit associated with adding a 20 MW PVCS as a negative load to the RBTS increases as the peak load increases.

Table 4.4: The annual system indices of the RBTS with the modified LDC

Peak Load (MW)	LOLE (hrs/yr)	LOEE (MWh/yr)
165	0.13169	1.23993
175	0.45595	3.49112
185	0.91558	9.49371
195	2.17478	23.12267
205	5.14499	53.65462

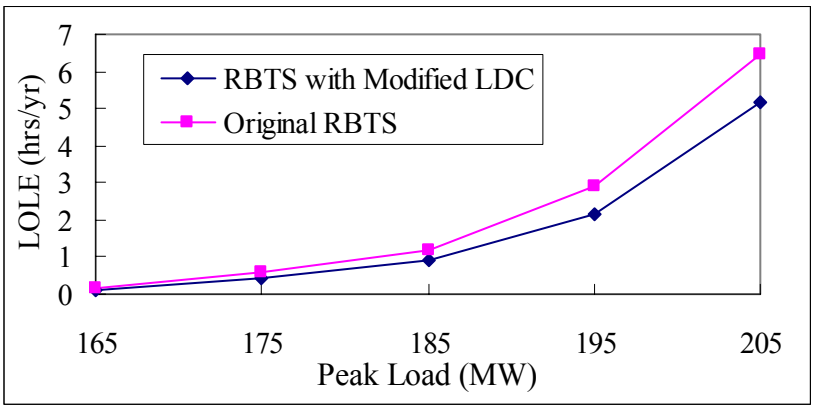

Figure 4.8: The annual RBTS LOLE as a function of the peak load

4.4.2 Multi-state PVCS Models

The 20 MW PVCS multi-state models shown in Table 4.3 were applied in a RBTS analysis. The analytical method and the MECORE program were utilized in this study. The following three cases were considered:

Case 1: The RBTS with the modified 20-step LDC shown in Figure 4.6.

Case 2: The RBTS including the PVCS using the 20-step LDC and the analytical approach.

Case 3: The RBTS including the PVCS using the 20-step LDC and MECORE.

Figure 4.9 shows the system LOLE for Cases 2 and 3 as a function of the number of states in the applied multi-state PVCS model. The LOLE for Case 1 is shown as a straight line. The results for all three cases are quite similar.

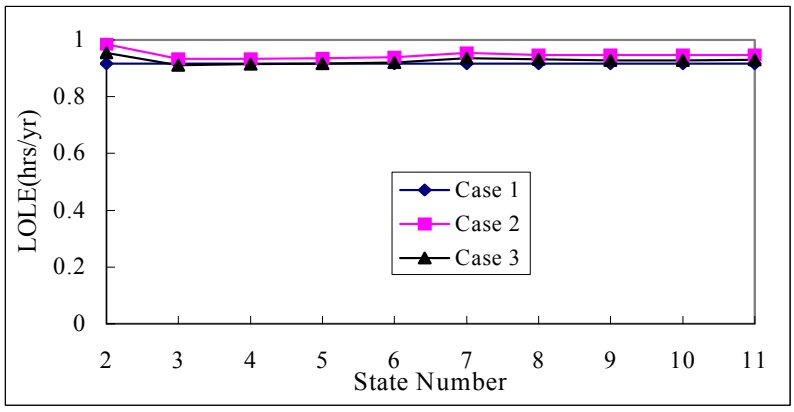

Figure 4.9: The annual system LOLE for a peak load of 185 MW

The LOLE values obtained in Case 1 using the negative load concept are slightly lower than those obtained using the PVCS multi-state model approach. The negative load approach partially recognizes the chronological characteristics of PV generation and the load following capability of the PVCS. The LOLE numerical data of Case 2 and 3 are provided in Appendix F. The differences between the LOLE estimated using the negative load approach and by applying a PVCS multi-state model are relatively small and indicate that the multi-state model method is a practical technique for incorporating PVCS in HL-I and HL-II adequacy evaluation. Figure 4.9 shows that a reasonable estimate of the annual RBTS LOLE can be obtained by using a PVCS model containing three or more states.

4.4.3 The Effects of Peak Load Variation

RBTS System Analysis

The 20 MW PVCS was added to the RBTS, as either a generating unit or as a negative load, to assess the HL-I adequacy indices as a function of the peak load. Figure 4.10 shows the results of this study using the case designations in Section 4.4.2. The LOLE values for three of the multi-state PVCS models in Case 2 are shown. Table F.4 shows the numerical data for Case 2. Figure 4.10 shows that differences in the LOLE value obtained using the negative load approach and the multi-state PVCS model are relatively small at increasing peak loads provided that three or more states are used in the PVCS model.

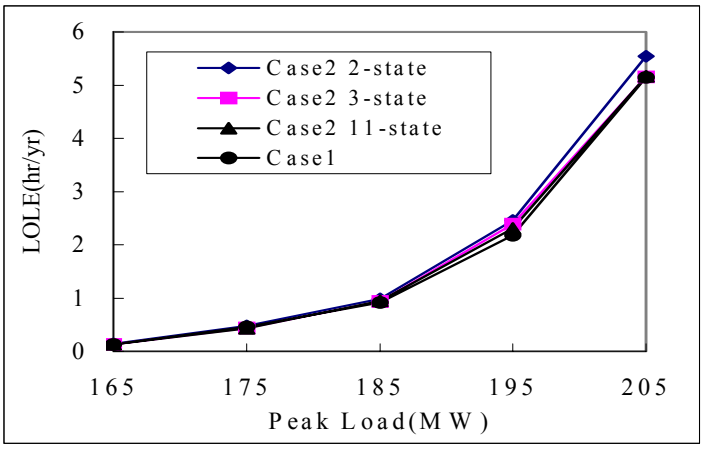

Figure 4.10: Comparison of the annual system LOLE for the two cases using the analytical method

The variation in the RBTS EDLC determined using different multi-state PVCS models as a function of the system peak load is further illustrated in Figure 4.11. The EDLC variation with the number of state is shown in this figure for specific peak loads. These studies were conducted using MECORE. The numerical data of this figure are shown in Table F.5. Figure 4.11 indicates that it may be advisable to use a PVCS model with five or more states at high peak load levels. The system risk increases as the peak load increases and the PVCS effect becomes more pronounced. This is illustrated further in the following RTS studies.

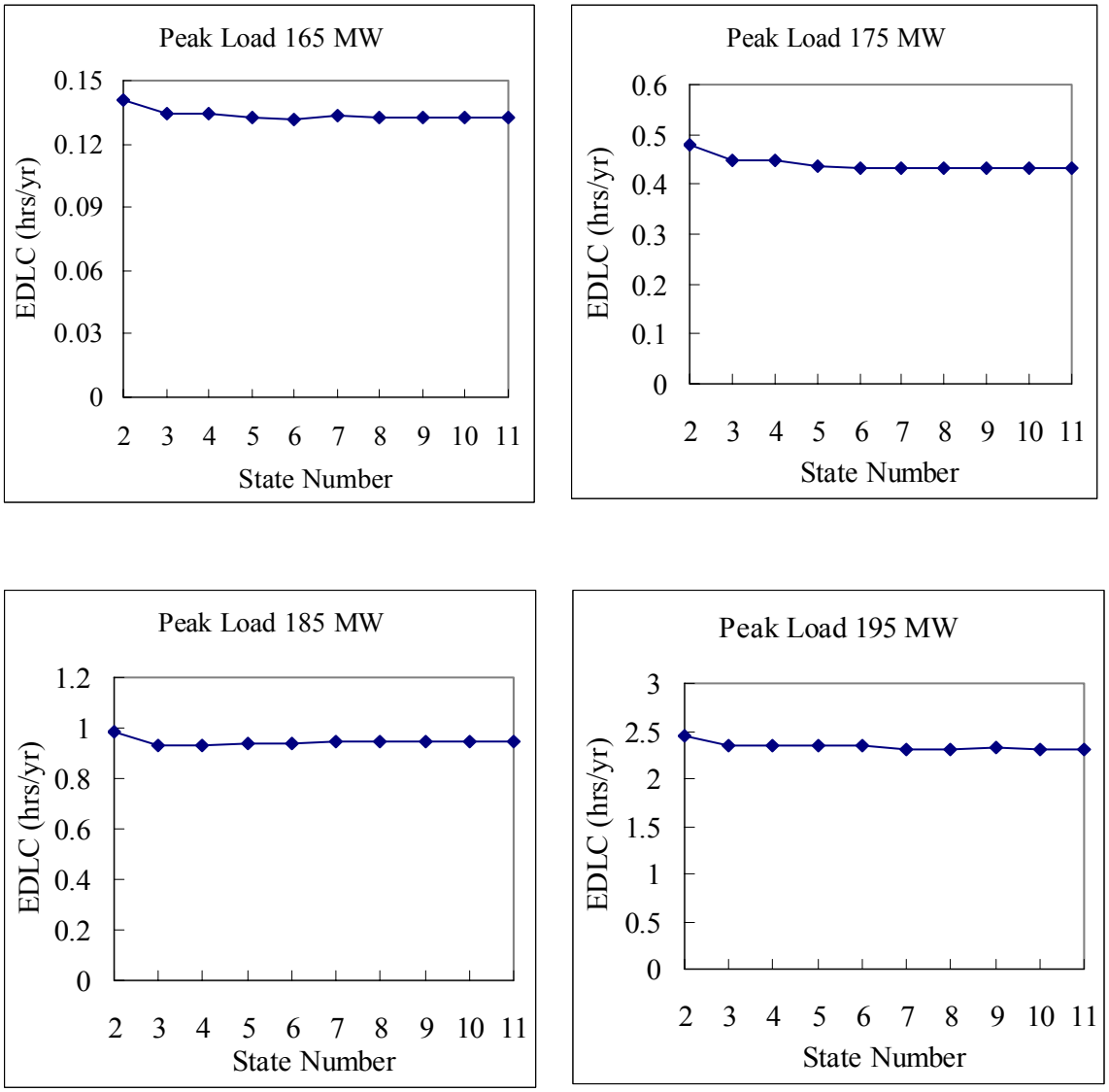

Figure 4.11: The HL-I annual RBTS EDLC with multi-state PVCS

RTS System Analysis

A 400 MW PVCS was added to the RTS. The annual system EDLC for a peak load of 2850 MW using different multi-state PVCS models is shown in Figure 4.12. The EDLC for two other load levels are shown in Figure 4.13 and corresponding data are shown in Table G.5. It can be seen from Figures 4.12 and 4.13 that the EDLC for different peak load levels are relatively constant when the PVCS is represented by models containing five or more states. These two figures also indicate that the effect of different multi-state models becomes more significant as the peak load increase. The figures indicate that a five-state model can be used to provide an acceptable adequacy assessment of the RTS.

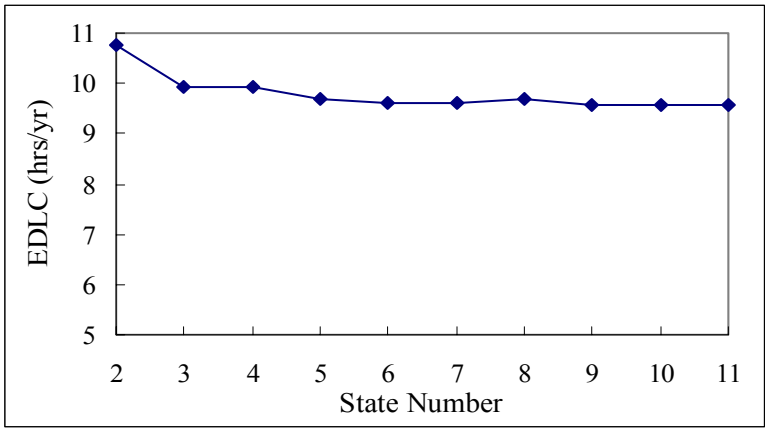

Figure 4.12: The RTS HL-I annual system EDLC for a peak load of 2850 MW with different PVCS multi-state models

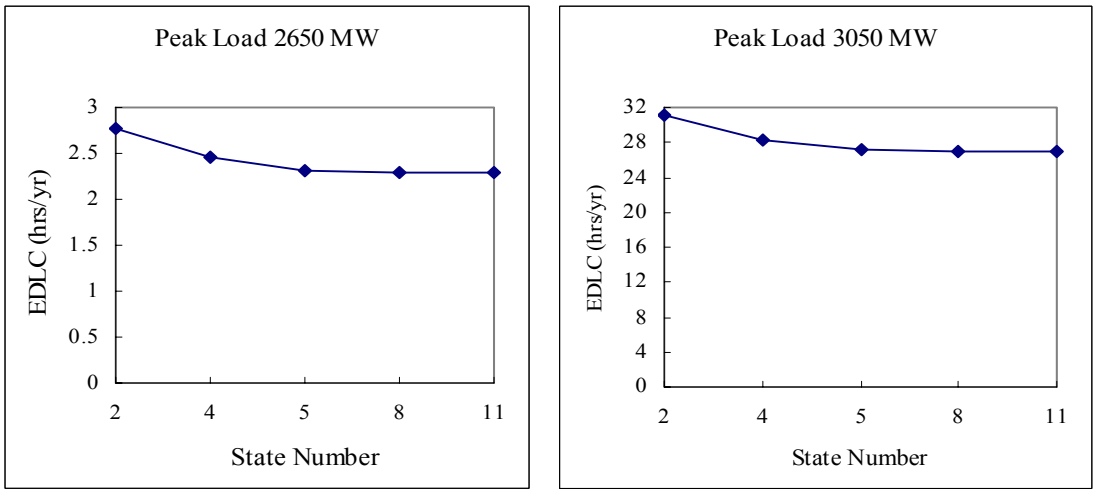

Figure 4.13: The RTS HL-I annual system EDLC with different multi-state PVCS models

The conclusion can be drawn, based on the studies of the RBTS and the RTS, that a five-state PVCS model provides a reasonable representation in power system adequacy assessment. This conclusion can be utilized in HL-I and HL-II studies using the MECORE program or an analytical method. The five-state PVCS model is used in the bulk system studies described later in this thesis.

4.5 Adequacy Comparison of WECS and PVCS

The benefits of adding WECS or PVCS to the RBTS and the RTS are illustrated in previous sections. The relative benefits of these two generating sources are shown in this section. The wind data and other weather information are from the Swift Current site. Five-state WECS and PVCS models are used in this study. The system benefits in the form of the incremental peak load carrying capability (IPLCC) are used as an index to compare the adequacy effects of adding a WECS or a PVCS in these systems.

RBTS System Analysis

The EDLC of the RBTS with an installed capacity of 240 MW and an annual peak load of 185 MW obtained using MECORE is 1.15487 hours/year. The EDLC of the RBTS incorporating WECS and PVCS respectively is shown as a function of the annual peak load in Figure 4.14. The annual peak load was varied from 175 MW to 200 MW using a 5 MW increment. It can be seen from Figure 4.14 that there are load carrying capability benefits from the WECS and PVCS additions. The analysis shows that after a 20 MW PVCS is added to the RBTS, the combined system can carry a peak load of 186.35 MW at the EDLC of 1.15487 hours/year. The IPLCC in this case is 1.35 MW. The IPLCC is approximately 2.3 MW after a 20 MW WECS is added to the RBTS.

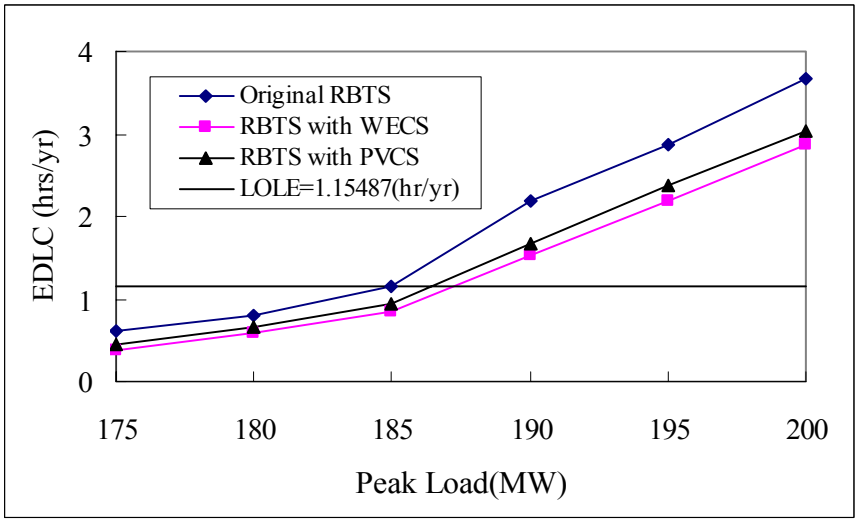

Figure 4.14: The RBTS EDLC versus annual peak load

RTS System Analysis

The EDLC for the RTS with an annual peak load of 2850 MW and an installed capacity of 3405 MW is 13.0048 hours/year. The annual peak load was varied from 2650 MW to 3050 MW using a 100 MW increment. Figure 4.15 illustrates that the IPLCC is approximately 44.5 MW after 400 MW PVCS added to the RTS. If a 400 MW WECS is incorporated in the RTS, the IPLCC is approximately 67 MW.

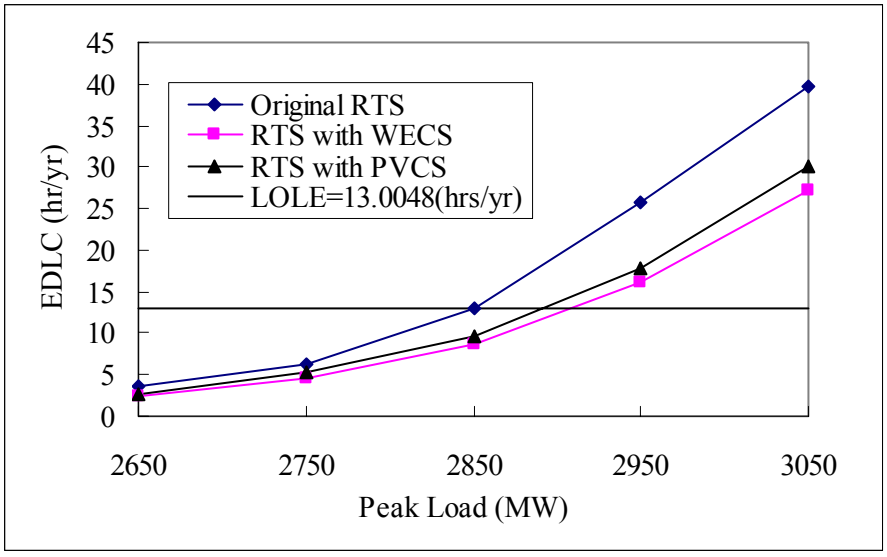

Figure 4.15: The RTS EDLC versus annual peak load

Wind data and atmospheric data from the Swift Current site are used in this study. The analyses of the RTS and the RBTS show that the WECS makes a larger contribution to the system reliability, than a PVCS with the same capacity as the WECS, at this site. This is primarily due to the fact that the PVCS produces no power during the night. It should be noted that the relative reliability benefits from renewable energy sources such as wind and solar depend on many factors, such as the wind speed and the weather characteristics at the site location. The results shown therefore do not lead to a general conclusion and each site should be analyzed using the specific weather data for that site. The procedures utilized in the studies described in this thesis can be applied to a wide range of systems.

4.6 Summary

A basic model of a PVCS is introduced in this chapter. The WATGEN and the WATSUN-PV programs were utilized to generate solar radiation data and a PV generating unit power output. The generated power of a photovoltaic generating unit was obtained based on the I-V characteristics of a solar cell using the simulated solar radiation data. It can be seen from the simulated results shown in this chapter that the output power of a PV array can be more than its rated value. The power output of a PV array is zero during the nighttime due to lack of sunlight or due to a forced outage and reaches its greatest daily value at noon. Appropriate PVCS multi-state models can be built using the apportioning approach described in this thesis.

The effect of PVCS generation on the RBTS is examined using two different methods. The first approach is designated as the negative load method, and the second as the PVCS multi-state model approach. There are only small differences between the annual system LOLE values obtained using the two methods when the PVCS model has three or more states. The variation in the LOLE for different PVCS multi-state models as a function of the system peak load was investigated using both the RBTS and the RTS. The results show that it is reasonable to use a five-state PVCS model for adequacy assessment over a range of system conditions. This conclusion is illustrated and

examined by analyses of the RTS.

The RBTS and the RTS analyses show that a WECS makes a bigger contribution to the system adequacy than a PVCS with the same capacity. This conclusion is based on the Swift Current weather data. The relative reliability benefits from renewable energy sources such as wind and solar depend on many factors, such as the wind speed and the weather characteristics at the site location. Each site should therefore be analyzed on its own merits. The techniques utilized in this research and described in this thesis can be used to examine the benefits associated with adding different WECS and PVCS additions to an electric power system.

5. ADEQUACY ASSESSMENT OF COMPOSITE POWER SYSTEMS WITH WIND AND SOLAR ENERGY

5.1 Introduction

The performance of a WECS or PVCS is quite different from that of a conventional generation system. This is due to the dispersed nature of the wind and solar energy at a specific site location. This chapter investigates the reliability contribution of wind and solar energy in bulk electric systems. The five-state WECS and PVCS models used in this chapter are described in the two previous chapters. The contribution of a single wind farm or solar park and that of multiple wind farms or solar parks are investigated using the RBTS and the RTS. The system peak load and different levels of installed unconventional unit capacity are examined. The adequacy impact of adding WECS and PVCS to composite systems are considered.

A WECS or a PVCS is assumed to be connected to the test system through a transmission line as shown in Figure 5.1.

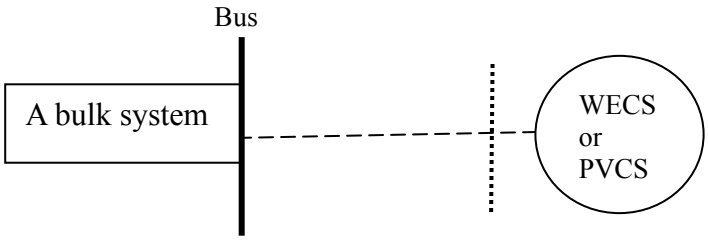

Figure 5.1: The connection diagram

5.2 Single Site Studies

5.2.1 RBTS System Analysis

The diagram of the RBTS was shown in Figure 2.5. This study focuses on the effect of a WECS or a PVCS added at different buses in the RBTS and the impact of wind or solar penetration levels on this system. The admittance, failure probability and repair time of the facility connection line is 8.3333(p.u.), 0.00114 and 10 hrs respectively. The assumed carrying capacity of the circuit is the installed capacity of the WECS or PVCS.

Location Analysis

A 20 MW WECS or PVCS was individually added at each bus in the RBTS. The basic RBTS studies in Chapter 2 show that the annual EENS values at load buses 3 and 6 are much larger than those at the other load buses and the system indices are dominated by the performance at these two buses. Table 5.1 shows the EENS indices at buses 3 and 6 with the WECS addition. The original EENS values at buses 3 and 6 are also shown in Table 5.1 in order to illustrate the reliability effects on the load points when the WECS is added at the various buses.

Table 5.1: EENS (MWh/yr) at Bus 3 and Bus 6 for a peak load of 185 MW with the addition of a WECS at different locations

Load Point	Original RBTS	WECS Location					
		Bus 1	Bus 2	Bus 3	Bus 4	Bus 5	Bus 6
Bus 3	12.561	8.798	8.806	8.745	8.747	8.746	8.748
Bus 6	137.712	127.463	127.465	127.463	127.463	127.463	90.736

The annual system EDLC and EENS for a 20MW WECS added at different points in the RBTS obtained using MECORE are shown in Table 5.2. Figures 5.2 and 5.3 respectively show the system EDLC and EENS obtained using MECORE and the sequential MCS

technique. The sequential MCS results were provided by Mr. Wijarn Wangdee and show the reliability indices for WECS additions at buses 2-5. The load point and system index data for the sequential MCS technique are shown in Tables E.3 and E.4 in Appendix E. Figure 5.2 shows that the two methods provide similar estimates for the system EDLC. Figures 5.2 and 5.3 show that there is relatively little difference in the calculated indices when the WECS is connected at buses 1-5. The figures show that there is a significant benefit by connecting the WECS to Bus 6, which is supplied by a single radial line. This conclusion is strictly from an adequacy point of view and assumes that there are no operational problems in an islanding situation at Bus 6.

Table 5.2: The RBTS indices for a peak load of 185 MW with the WECS added at different locations

	EENS (MWh/yr)	EDLC (hrs/yr)
Base Case	150.36530	11.69545
Location		
Bus 1	136.47056	10.60989
Bus 2	136.48075	10.60516
Bus 3	136.41952	10.60007
Bus 4	136.42141	10.60023
Bus 5	136.39854	10.60009
Bus 6	99.72003	9.29243

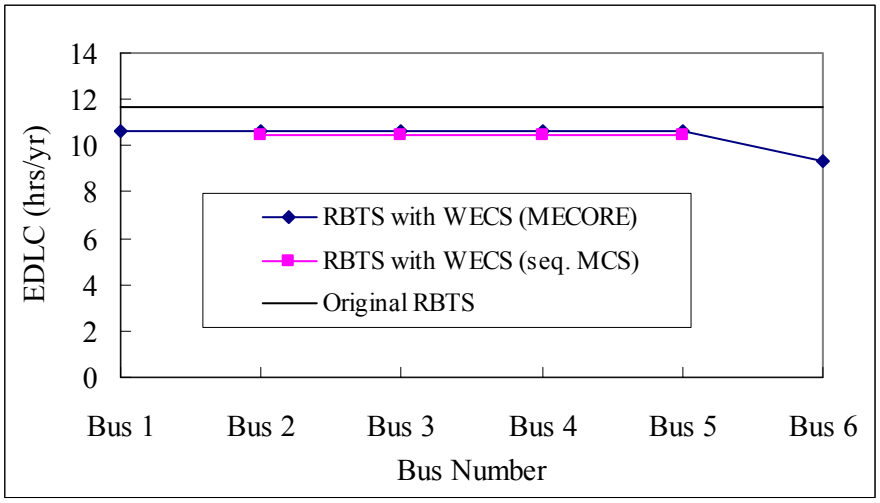

Figure 5.2: The annual system EDLC for the RBTS with the WECS added at different buses

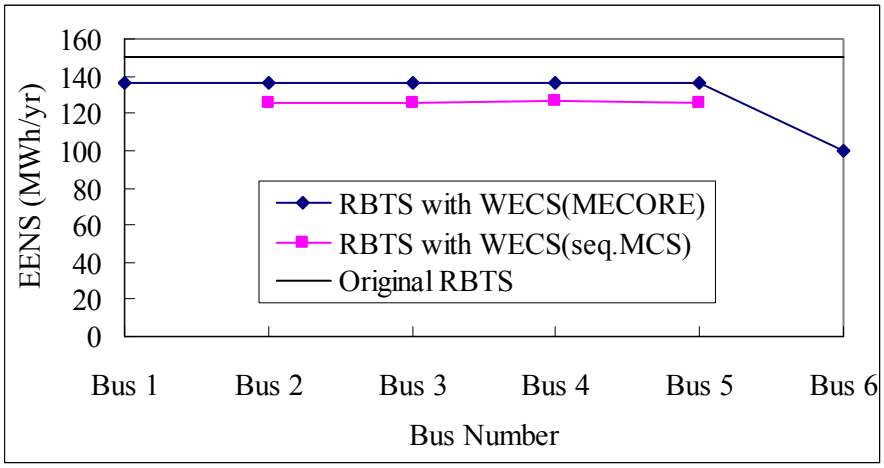

Figure 5.3: The annual system EENS for the RBTS with the WECS added at different buses

Table 5.3 shows the load point EENS with the addition of a PVCS at the individual load points in the RBTS. Figures 5.4 and 5.5 respectively show the annual RBTS EDLC and EENS with the PVCS obtained using MECORE.

Table 5.3: EENS (MWh/yr) at Bus 3 and Bus 6 for a peak load of 185 MW with the addition of a PVCS at different locations

Load Point	Base Case	PVCS Location					
		Bus 1	Bus 2	Bus 3	Bus 4	Bus 5	Bus 6
Bus 3	12.561	9.545	9.560	9.508	9.512	9.511	9.511
Bus 6	137.712	127.469	127.471	127.469	127.469	127.469	99.212

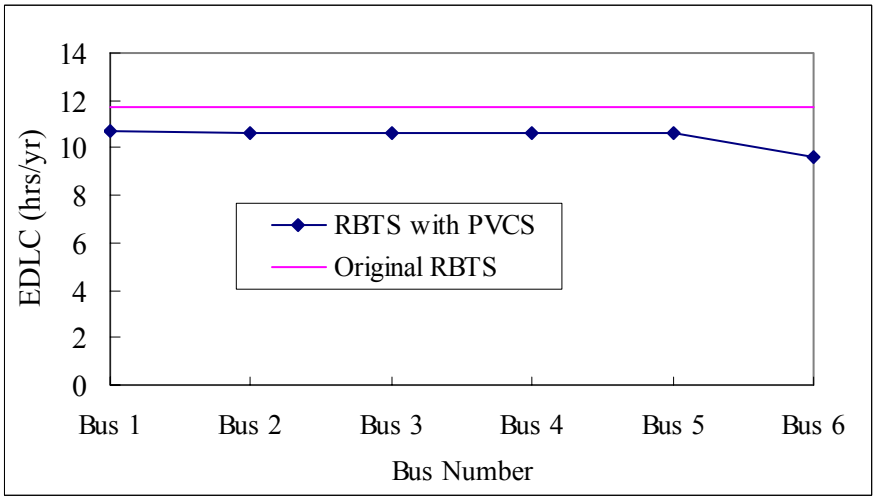

Figure 5.4: The annual system EDLC for the RBTS with the PVCS added at different buses

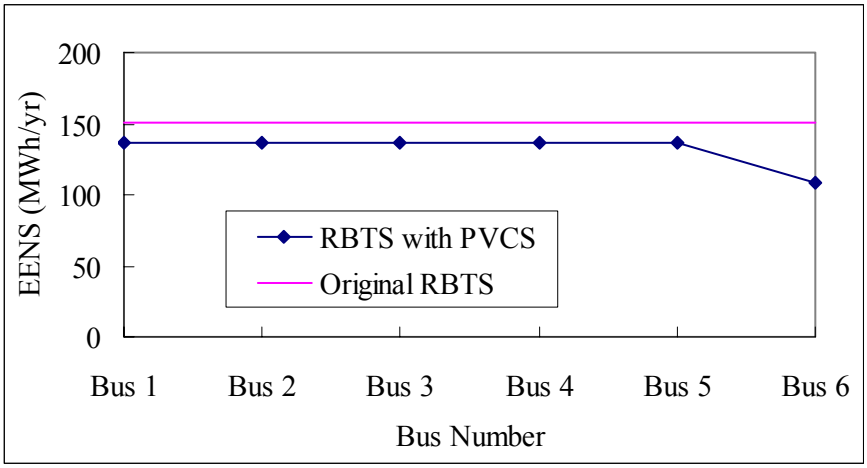

Figure 5.5: The annual system EENS for the RBTS with the PVCS added at different buses

Tables 5.1 - 5.3, and Figures 5.2 - 5.5 illustrate that the system and load point reliabilities are improved by adding WECS or PVCS. The system EENS is relatively constant when the WECS or the PVCS is added at Bus 1 to Bus 5. The EENS at Bus 3 is relatively unchanged when the WECS or the PVCS is added at different locations in the RBTS. This is also the case for Bus 6 when the WECS is added at Buses 1 - 5. The effect on the bulk system EENS of adding WECS or PVCS at Bus 6 is quite different to similar additions at other buses, since the system indices are dominated by the performance of Bus 6 which is connected to the rest of the system by a single radial line.

Penetration Level Analysis

As noted earlier, WECS or PVCS additions at Bus 1 to Bus 5 in the RBTS result in similar reliability benefits, and the condition at Bus 6 is different from the other buses. Penetration level analysis was therefore conducted at Bus 3 and Bus 6. The effects on the system EENS are illustrated.

The WECS/PVCS installed capacity was expanded from 20 MW to 180 MW by adding 40 MW increments to the original RBTS. The wind/solar penetration levels vary from 7.7% to 43%. The annual system EENS for selected peak loads as a function of the wind penetration level is shown in Figures 5.6 and 5.7. Figure 5.6 shows the case of a WECS

added at Bus 3, and Figure 5.7 shows the case of a WECS added at Bus 6. Tables F.6-F.7 in Appendix F show the numerical data of the two figures.

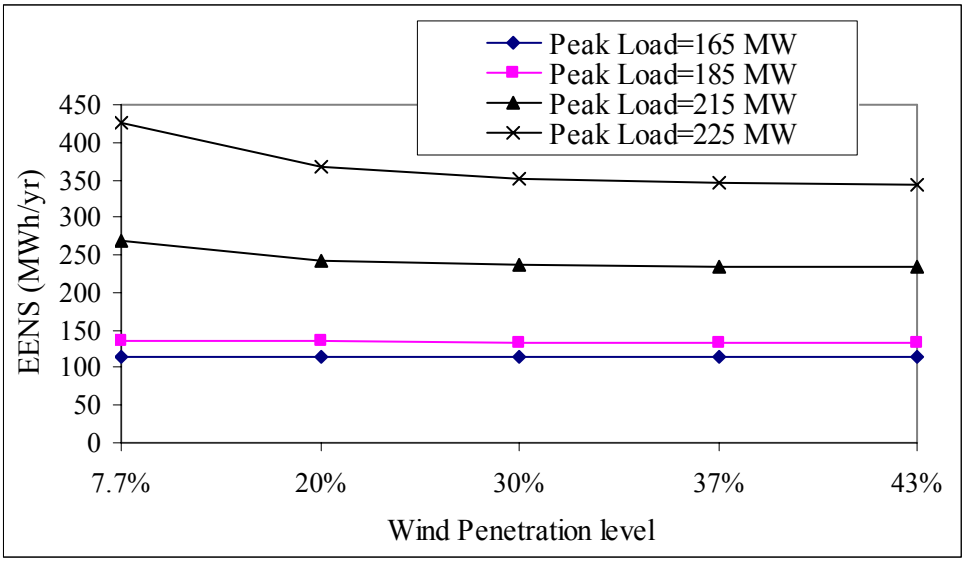

Figure 5.6: The RBTS EENS with the addition of the WECS at Bus 3 versus the wind penetration level

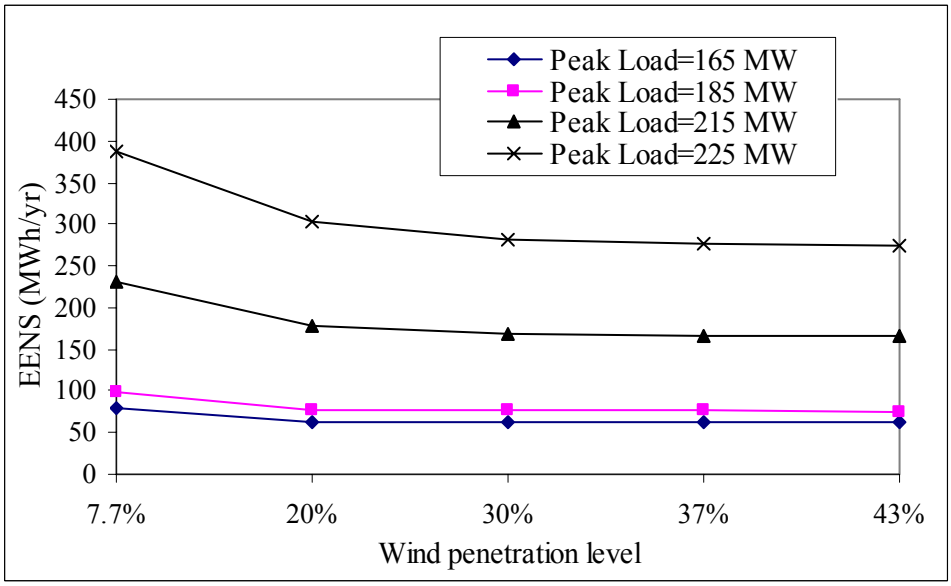

Figure 5.7: The RBTS EENS with the addition of the WECS at Bus 6 versus the wind penetration level

The annual system EENS for different peak loads with variation in the solar penetration level are shown in Figures 5.8 and 5.9. Figures 5.8 and 5.9 shows the results with the

PVCS added at Bus 3 and Bus 6 respectively. Tables F.8 – F.9 show the RBTS EENS with PVCS added at buses 3 and 6 respectively.

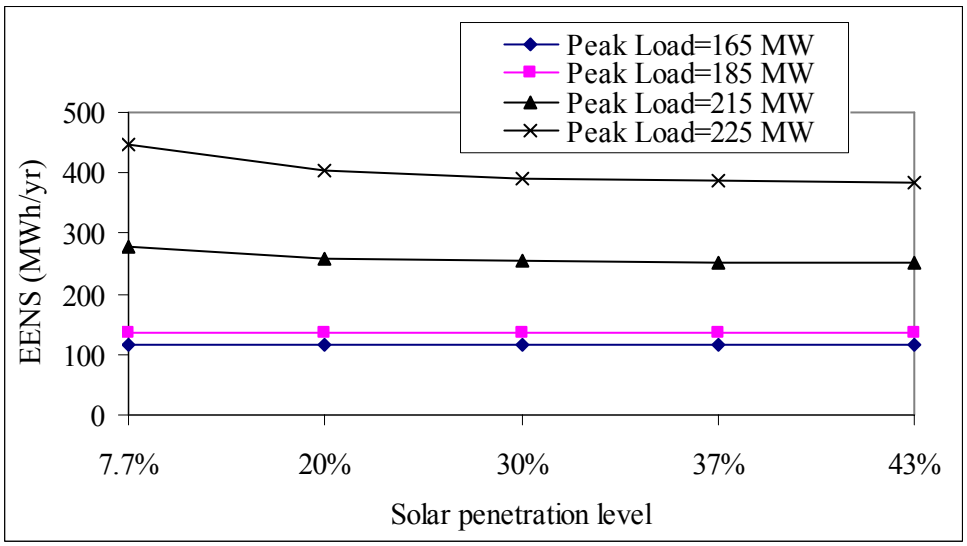

Figure 5.8: The RBTS EENS with the addition of the PVCS at Bus 3 versus the solar penetration level

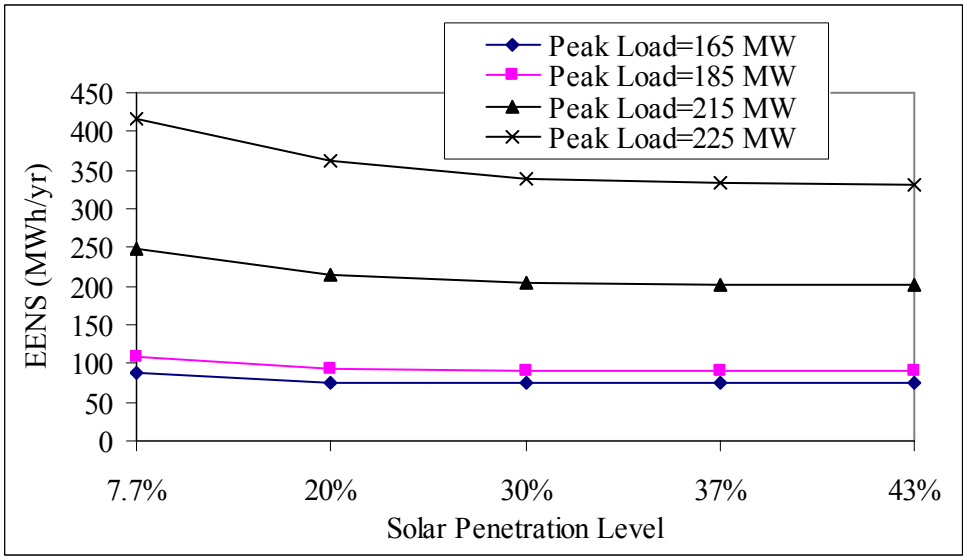

Figure 5.9: The RBTS EENS with the addition of the PVCS at Bus 6 versus the solar penetration level

Figures 5.6 - 5.9 show that the system EENS decreases as the wind or solar penetration level increases. The benefits associated with different WECS or PVCS penetration levels increase as the peak load increases. The four figures also illustrate that the reliability benefit tends to saturate as the wind/solar penetration levels continue to increase.

Similar capacity WECS and PVCS were added at Bus 3 of the RBTS in order to compare the different effect on the system EENS. The installed capacity changes from 20 MW to 180 MW in 40 MW increments. The wind or solar penetration level therefore varies from 7.7% to 43%. Figure 5.10 shows the EENS for peak loads of 185 MW and 225 MW and different WECS/PVCS installed capacities.

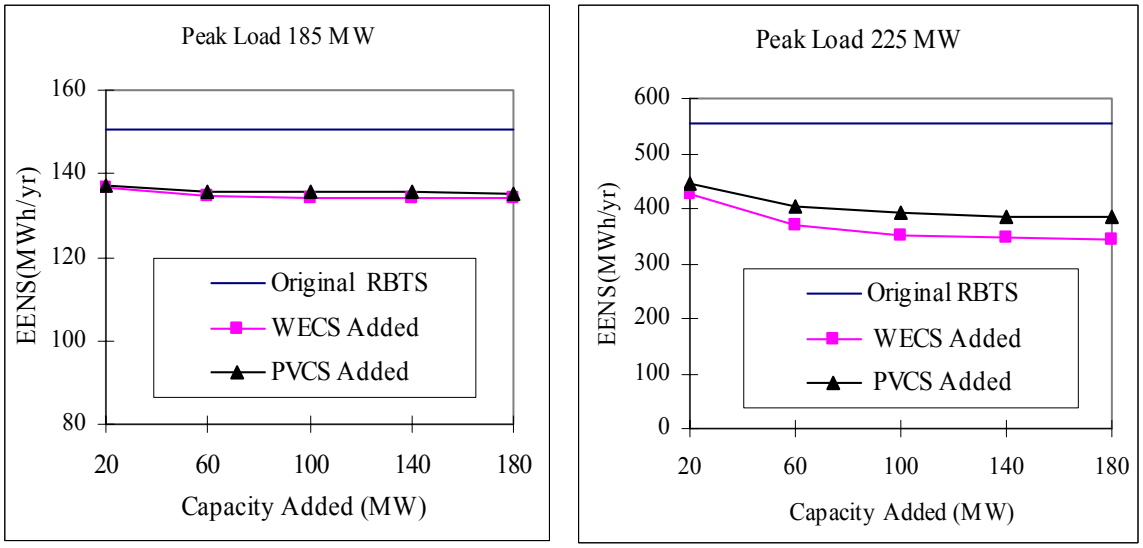

Figure 5.10: The RBTS EENS for different renewable energy installed capacity

It can be seen from Figure 5.10 that the system EENS are basically the same with WECS and PVCS additions when the annual peak load is 185 MW. In this case, the generating capacity is much greater than the load demand. When the annual peak load increases to 225 MW, the reliability benefits of adding WECS are more obvious than those obtained by adding PVCS. Figure 5.10 also indicates that the reliability benefits tend to saturate as the renewable energy capacity continue to increase.

5.2.2 RTS System Analysis

The RTS diagram is shown in Figure 2.6. The studies conducted on the RTS are similar to those on the RBTS. A 400 MW WECS or a PVCS was added through a transmission line at different buses. The admittance, failure probability and repair time of the facility connection line is 11.91895 (p.u.), 0.00050, 11 hrs respectively. The assumed carrying capacity of the line is the WECS or PVCS installed capacity. Buses 9, 15 and 19 were

selected from the 24 buses and used in the following studies. These buses have relatively large EENS values as shown in the basic RTS studies in Chapter 2.

Location Analysis

The load point EENS and system indices for a peak load of 2850 MW with the WECS added at different buses are shown in Tables 5.4 and 5.5 respectively. The two tables show that the load point EENS and system adequacy indices decrease significantly by adding the WECS to the RTS. The reliability benefits are basically the same when the WECS is located at various buses.

Table 5.4: The RTS EENS (MWh/yr) at selected load points for a peak load of 2850 MW with the addition of WECS at different locations

Load point	Base Case	WECS Location		
		Bus 9	Bus 15	Bus 19
Bus 9	428.406	277.819	277.819	277.822
Bus 14	74.296	45.778	45.778	45.778
Bus 15	332.503	211.676	211.676	211.676
Bus 19	788.182	520.934	520.941	520.931

Table 5.5: The RTS indices for a peak load of 2850 MW with the WECS added at different locations

	EENS (MWh/yr)	EDLC (hr/yr)
Base Case	1674.87700	13.01818
WECS Location		
Bus 9	1088.53698	8.69044
Bus 15	1088.56127	8.69105
Bus 19	1088.53750	8.69045

The system EENS with the addition of WECS at different buses as a function of peak load is shown in Figure 5.11. Figure 5.11 shows that the system reliability benefits increase as the peak load increases. This figure also illustrates that system EENS values with the WECS connected at various buses are relatively unchanged with increasing

peak load.

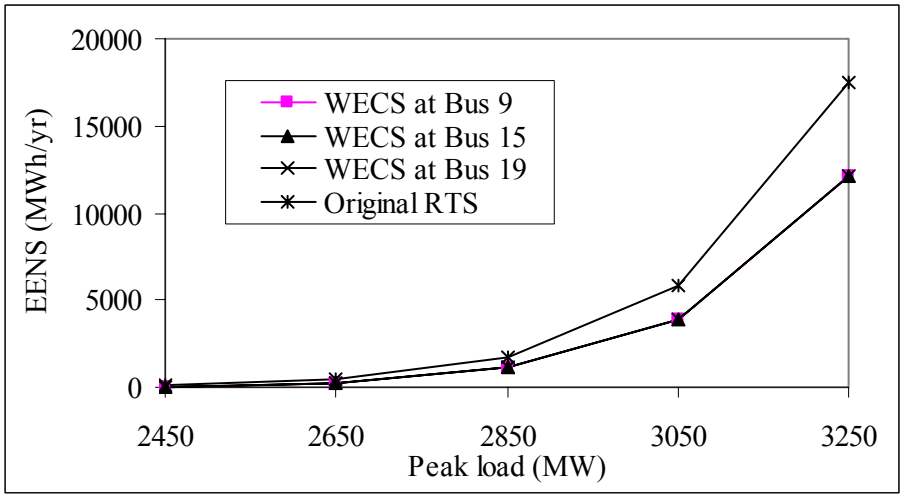

Figure 5.11: The RTS EENS with the addition of WECS at different locations versus peak load

Analyses of a PVCS addition similar to those for the WECS were conducted. The EENS at selected load points and the annual system indices for a 400 MW PVCS added at various points are shown in Tables 5.6 and 5.7 respectively.

Table 5.6: The RTS EENS (MWh/yr) at selected buses for a peak load of 2850 MW with the PVCS added at different locations

Load point	Base Case	PVCS Location		
		Bus 9	Bus 15	Bus 19
Bus 9	428.406	313.785	313.785	313.649
Bus 14	74.296	52.989	52.989	52.983
Bus 15	332.503	241.166	241.166	241.094
Bus 19	788.182	583.557	583.557	583.264

Table 5.7: The RTS indices for a peak load of 2850 MW with the PVCS added at different locations

	EENS (MWh/yr)	EDLC (hr/yr)
Base Case	1674.87700	13.01818
PVCS Location		
Bus 9	1229.09464	9.70052
Bus 15	1229.09449	9.70052
Bus 19	1228.58688	9.69520

Tables 5.6 and 5.7 show that the load point and system adequacy indices decrease when the PVCS is added to the RTS. The two tables also show that the load point and system adequacy indices are not affected by the location of the PVCS. Figure 5.12 shows the system EENS with the PVCS added at different buses versus peak load.

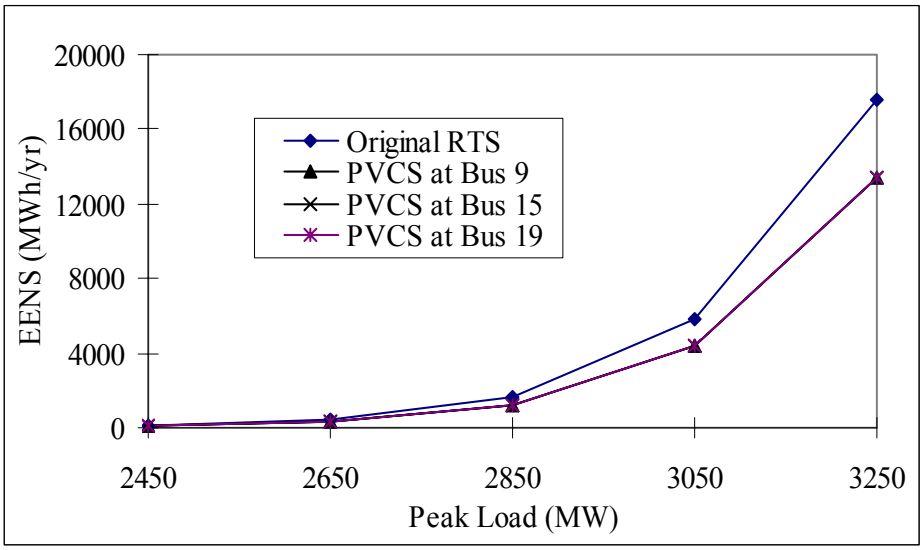

Figure 5.12: The RTS EENS with the PVCS at different locations versus peak load

The conclusion can be drawn, based on location analysis of the RTS, that the location in the RTS of adding a WECS/PVCS connection point does not materially affect the load point and system adequacy indices. This is due to the fact that the RTS has a relatively strong transmission network.

Penetration Levels Analysis

The previous RTS study shows that adding a WECS/PVCS at different buses results in similar reliability benefits. The studies in this section were conducted by adding WECS/PVCS capacity at Bus 19. The WECS/PVCS installed capacity was varied from 400 MW to 1800 MW in 200 MW increments. The wind/solar penetration level, therefore, changes from 10.5% to 35%. The system EENS values with WECS and PVCS added at Bus 19 are shown in Tables G.6 and G.7 respectively. Figures 5.13 and 5.14 show the system EENS for WECS and PVCS additions respectively for various wind/solar penetration levels as a function of the peak load.

Figures 5.13 and 5.14 indicate that the reliability benefits increases with increasing wind/solar penetration. The system EENS tends to saturate when additional WECS or PVCS capacity is added. The benefits saturate quickly at lower peak load levels as the wind penetration level increases because the load demand is much less than the installed generating capacity.

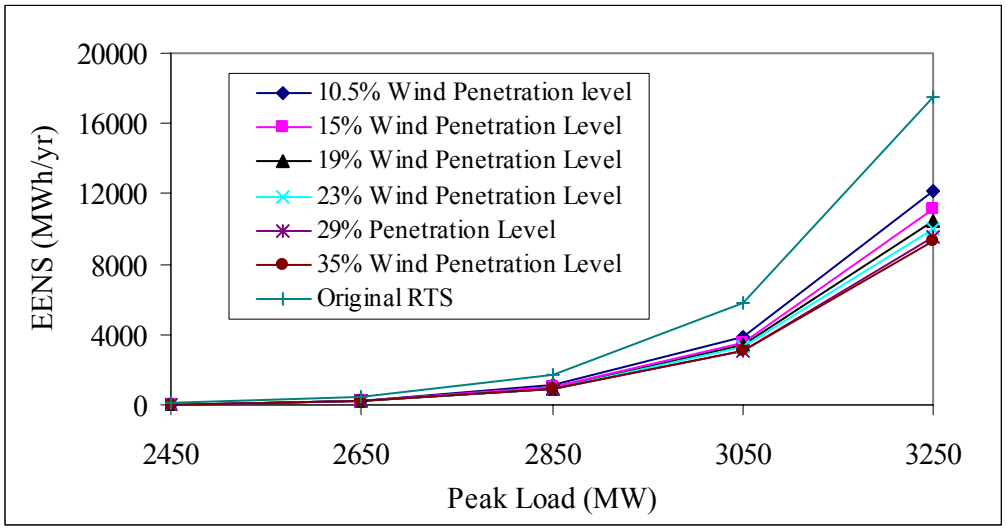

Figure 5.13: The RTS EENS with the addition of WECS for various wind penetration levels versus peak load

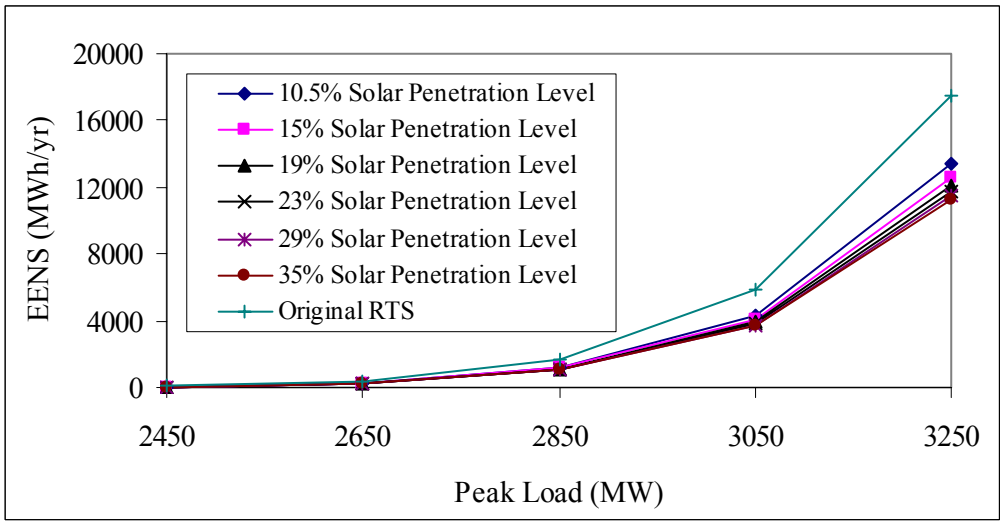

Figure 5.14: The RTS EENS with the addition of PVCS for various solar penetration levels versus peak load

Similar capacity WECS or PVCS were added at Bus 19 of the RTS in order to compare

the different impacts on the system EENS. The installed capacities were varied from 400 MW to 1800 MW. Figure 5.15 shows the system EENS for a peak load of 2850 MW with different WECS/PVCS installed capacities. Figure 5.15 shows that the reliability benefits saturate with increasing WECS or PVCS installed capacity. Figure 5.15 also indicates that the reliability benefits of adding WECS are more obvious than adding PVCS using the Swift Current site data.

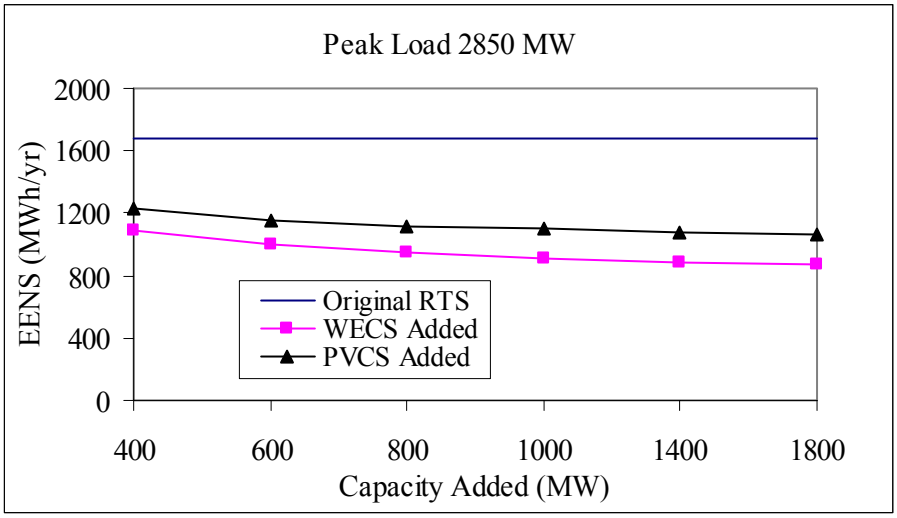

Figure 5.15: The RTS EENS for different renewable energy installed capacity

Single site studies indicate that the load point and system reliability is improved by adding a WECS/PVCS. The reliability benefits tend to saturate as the renewable energy capacity increases. Location analysis on the RTS shows that WECS/PVCS additions located at different buses results in similar load point and system adequacy indices. This is due to the RTS transmission configuration. This conclusion is not applicable to the RBTS due to the radial supply to Bus 6.

5.3 Two Site Studies

This section investigates the bulk system reliability benefits associated with two independent wind farms or solar parks. The basic Swift Current weather data was used for each wind/solar site, together with the connection transmission line data used in the previous study. The WTG units/ PV generating units are divided equally between the two independent sites.

5.3.1 RBTS System Analysis

The two wind farms/ solar parks were added at Bus 3 and Bus 6. The modified RBTS is shown in Figure 5.16.

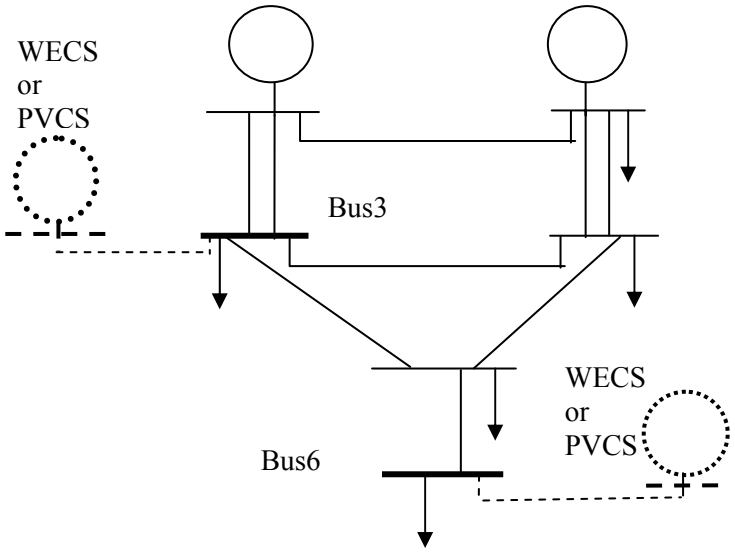

Figure 5.16: The RBTS modified by adding two wind farms/ solar parks

The system EENS for selected wind or solar penetration levels as a function of the peak load are shown in Figures 5.17 and 5.18 respectively. Tables F.10 and F.11 show the corresponding numerical data. The wind/solar penetration level changes from 7.7% to 43%.

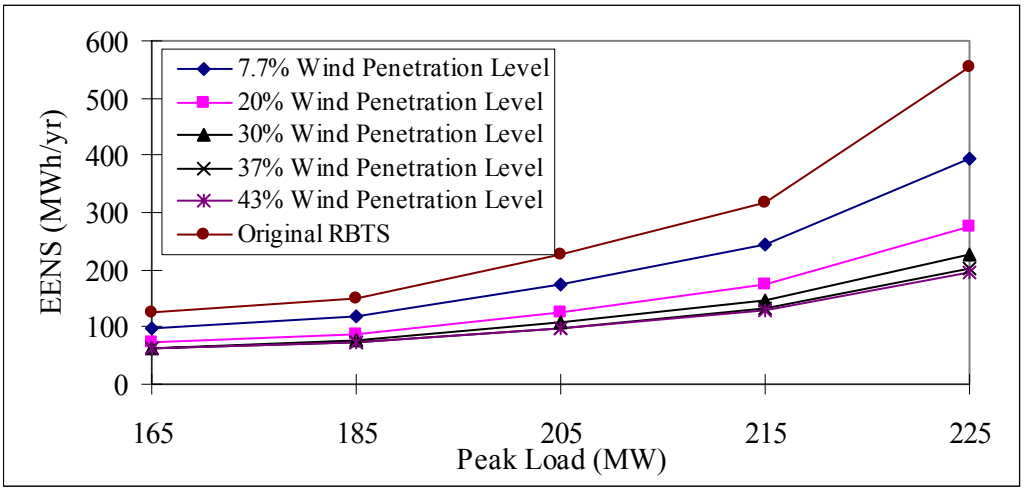

Figure 5.17: The RBTS EENS with the addition of two wind farms for different wind penetration levels versus peak load

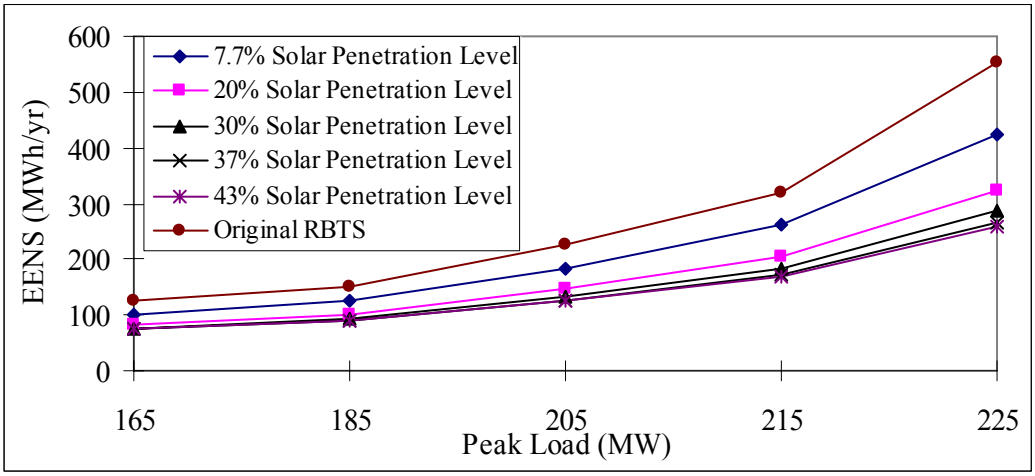

Figure 5.18: The RBTS EENS with the addition of two solar parks for different solar penetration levels versus peak load

The two figures illustrate that the system EENS decreases as the renewable energy penetration levels increase, and it saturates as the penetration levels increase.

5.3.2 RTS System Analysis

The WTG units or PV generating units are divided between two sites located at Bus 15 and Bus 19. The wind/solar penetration level varies from 10.5% to 35%. Figures 5.19 and 5.20 respectively show the annual system EENS for different wind or solar penetration levels as a function of peak load. Tables G.8 and G.9 show the detailed data of the two figures respectively.

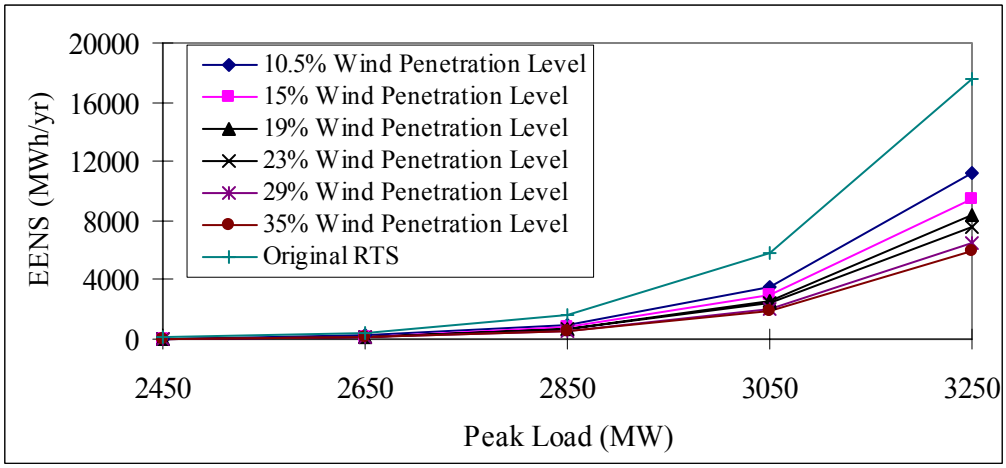

Figure 5.19: The RTS EENS with the addition of two wind farms for different wind penetration levels versus peak load

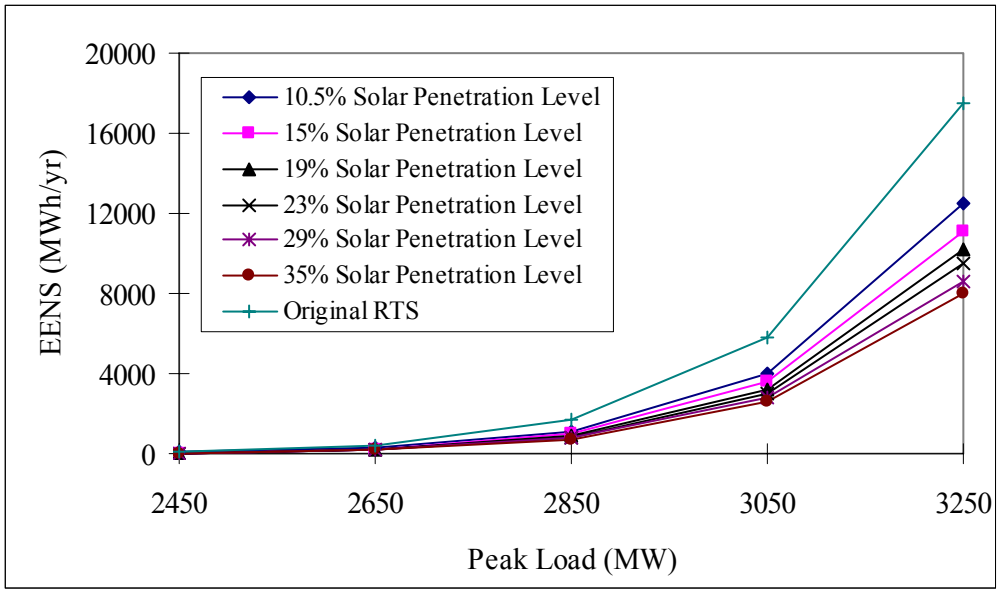

Figure 5.20: The RTS EENS with the addition of two solar parks for different solar penetration levels versus peak load

The two figures show that the system reliability improves as the renewable energy penetration levels increase. The benefits tend to decrease as the penetration level increases.

5.4 Three Site Studies

This section describes similar studies to those in the previous sections, but with three independent wind farms or solar parks added to the bulk system. The renewable energy capacity is divided equally between three wind/solar sites. Each wind farm or solar park is assumed to have the Swift Current data and is connected with the test system through the previous applied facility connection line.

5.4.1 RBTS System Analysis

The three wind farms/solar parks were added at Buses 3, 5 and 6. The modified RBTS is shown in Figure 5.21.

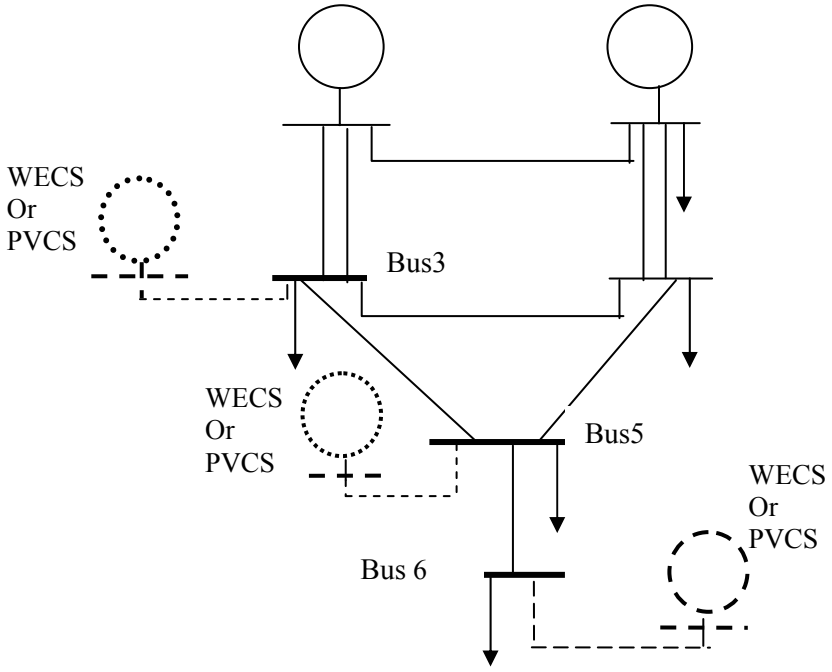

Figure 5.21: The RBTS modified by adding three wind farms/solar parks

Figures 5.22 and 5.23 respectively show the system EENS with different renewable energy penetration levels when the three wind farms or solar parks are added to the RBTS. The wind/solar penetration level changes from 7.7% to 43%. Tables F.12-F.13 show the detailed data for the two figures. The general conclusions are similar to those drawn in the two site studies.

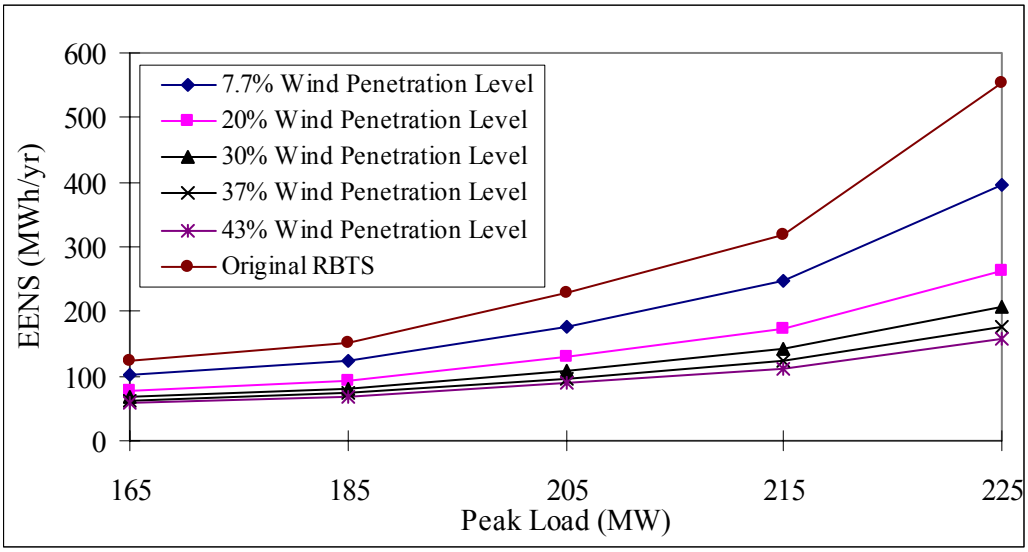

Figure 5.22: The RBTS EENS with three independent wind farms for different wind penetration levels versus peak load

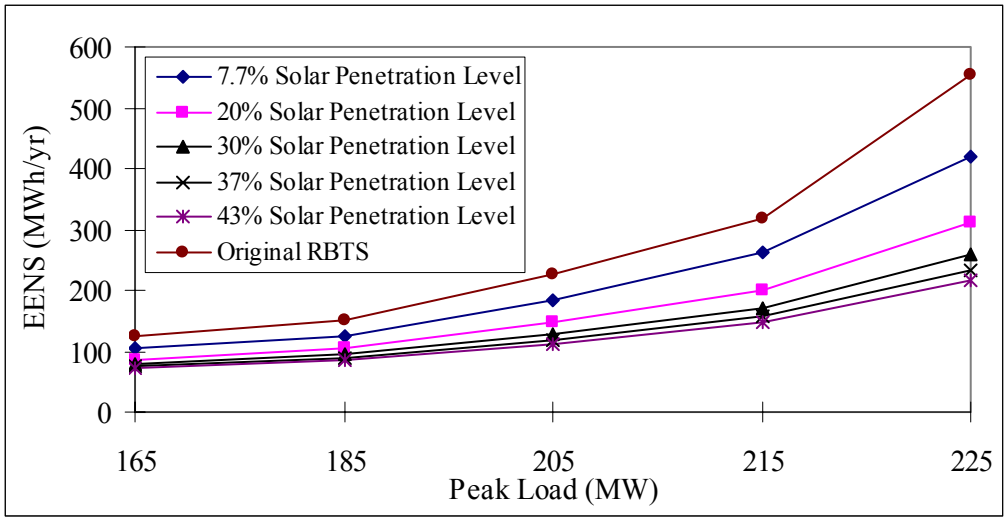

Figure 5.23: The RBTS EENS with three independent solar parks for different solar penetration levels versus peak load

5.4.2 RTS System Analysis

The WTG/PV generating units were divided equally into three wind farms/solar parks. The three sites were added at buses 1, 15 and 19. The wind/solar penetration level changes from 10.5% to 35%. The annual system EENS for the three WECS/PVCS systems are shown in Figures 5.24 and 5.25 respectively. Corresponding numerical data of the system EENS are shown in Tables G.10- G.11.

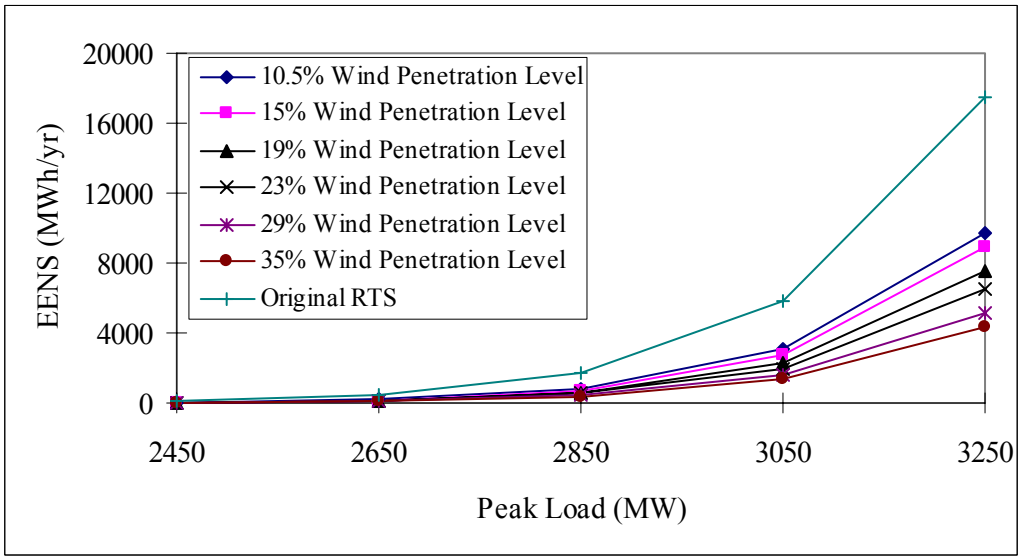

Figure 5.24: The RTS EENS with three independent wind farms for different wind penetration levels versus peak load

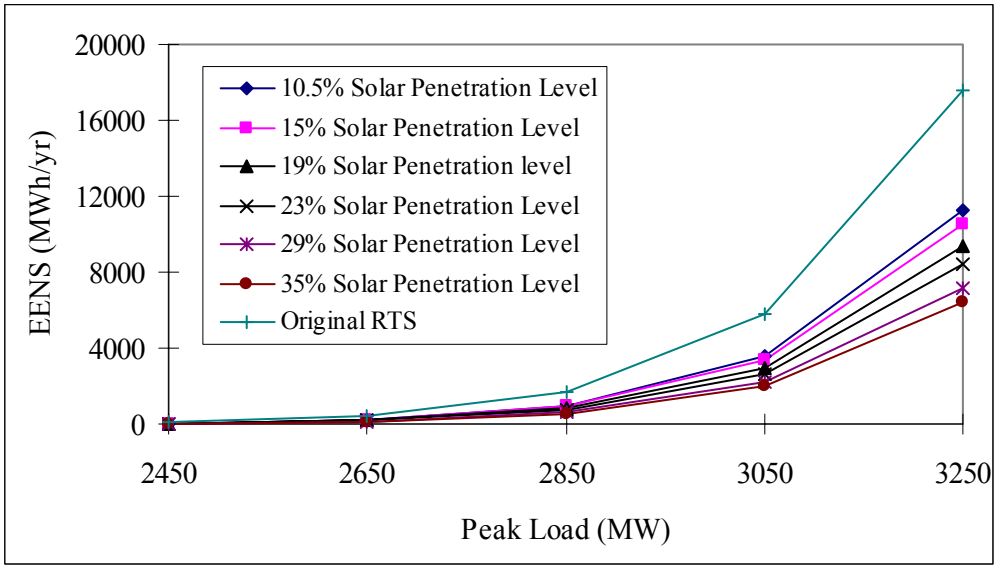

Figure 5.25: The RTS EENS with three independent solar parks for different solar penetration levels versus peak load

The analyses with three independent sites added to the RTS shows that the system reliability benefits increase significantly as the wind/solar penetration levels increase.

5.5 Comparison of single wind /solar and multiple wind /solar sites

5.5.1 RBTS System Analysis

The two and three wind farm/solar park studies confirm the conclusion drawn in the single wind farm/solar park case that wind/solar energy can make a significant reliability contribution to an existing power system. Two cases are utilized to compare the single and multiple independent WECS/PVCS reliability benefits. Two peak loads of 185 MW and 225 MW are used to present the relative benefits to the RBTS of adding single and multiple wind and solar energy sites.

Case 1: A single wind farm/solar park is added at Bus 3

Two wind farms/solar parks are added at Buses 3 and 5

Three wind farms/solar parks are added at Buses 3, 4 and 5.

Case 2: A single wind farm/solar park is added at Bus 6

Two wind farms/solar parks are added at Buses 3 and 6

Three wind farms/solar parks are added at Buses 3, 5 and 6.

The EENS numerical results for Case 1 are shown in Table F.14. Figures 5.26 and 5.27 show the results for Case 1. The two figures show the relative benefits in the RBTS of adding single and multiple wind and solar energy sites respectively.

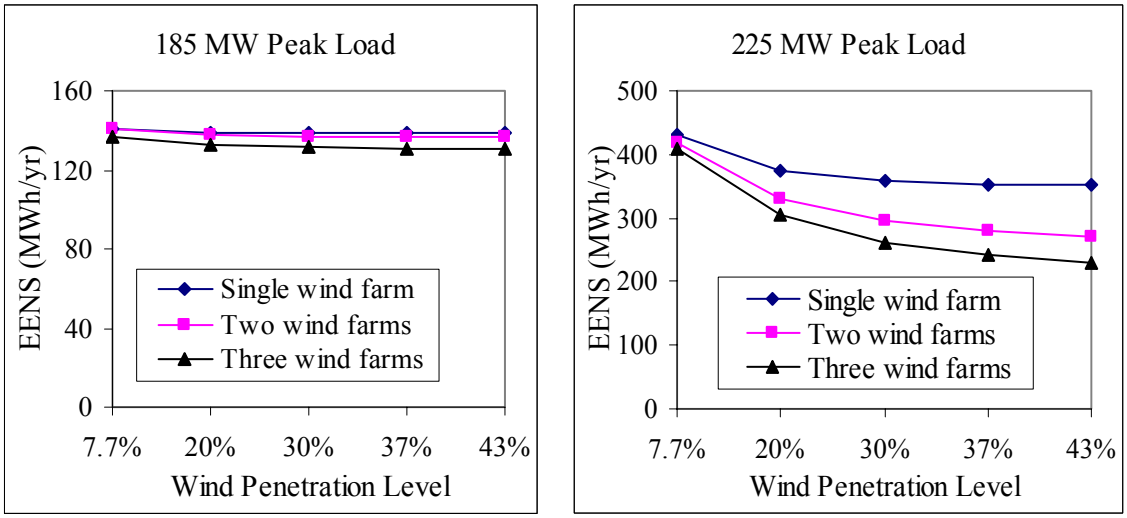

Figure 5.26: Comparison of the RBTS EENS with the addition of single and multiple wind sites (Case 1)

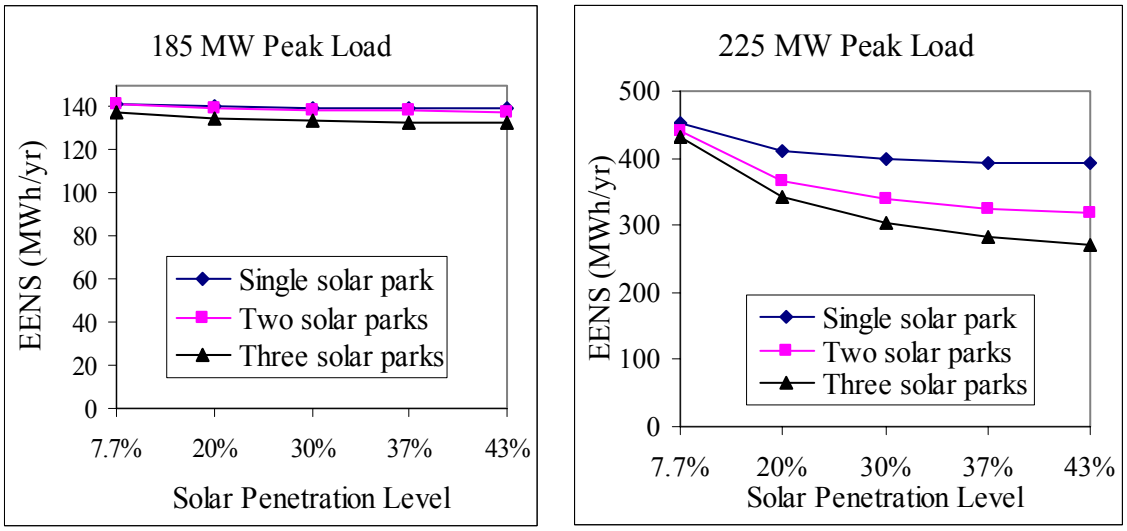

Figure 5.27: Comparison of the RBTS EENS with the addition of single and multiple solar sites (Case 1)

Figures 5.26 and 5.27 indicate that the EENS for the RBTS decreases with increase in the number of independent wind/solar sites. The reliability benefit of adding a single wind/solar site for a peak load of 225 MW tend to saturate faster than the cases with multiple sites. There is relatively little difference in the reliability contributions between adding single and multiple sites at a peak load of 185 MW. The difference increases considerably as the peak load increases.

It is important to appreciate that the probability of generating the total installed capacity from two or more independent wind farms/solar parks is less than the probability of obtaining the total installed capacity when this capacity is located in a single wind farm/solar park. This is illustrated in the following numerical example. Assume that a 60 MW WECS with the Swift Current wind regime is considered. The COPT for this WECS is shown in Table 5.8. Tables 5.9 and 5.10 respectively show the combined COPT when the 60 MW of wind capacity is installed in two and three independent WECS. Tables 5.8-5.10 show that the probability of generating 60 MW decreases as the number of independent wind sites increase. The probabilities of obtaining various generation levels from the three configurations are shown in Figure 5.28. This figure also shows that the probability of having zero capacity from the various configurations also decreases as the number of wind sites increase. The shape of these distributions is very dependent on the actual site wind profile.

Table 5.8: The COPT of a single WECS (1×60 MW)

Capacity In (MW)	Capacity Outage (MW)	Individual Probability	Cumulative Probability
60	0	0.0591	1.0000
45	15	0.0633	0.9409
30	30	0.1148	0.8776
15	45	0.2440	0.7628
0	60	0.5188	0.5188

Table 5.9: The COPT of two independent WECS (2×30 MW)

Capacity In (MW)	Capacity Outage (MW)	Individual Probability	Cumulative Probability
60	0	0.0035	1.0000
52.5	7.5	0.0075	0.9965
45	15	0.0176	0.9890
37.5	22.5	0.0434	0.9715
30	30	0.1054	0.9281
22.5	37.5	0.1217	0.8227
15	45	0.1786	0.7010
7.5	52.5	0.2532	0.5223
0	60	0.2691	0.2691

Table 5.10: The COPT of three independent WECS (3×20 MW)

Capacity In (MW)	Capacity Outage (MW)	Individual Probability	Cumulative Probability
60	0	0.0002	1.0000
55	5	0.0007	0.9998
50	10	0.0019	0.9992
45	15	0.0054	0.9972
40	20	0.0146	0.9919
35	25	0.027	0.9772
30	30	0.0501	0.9502
25	35	0.0885	0.9002
20	40	0.1368	0.8117
15	45	0.1529	0.6749
10	50	0.1854	0.522
5	55	0.197	0.3366
0	60	0.1396	0.1396

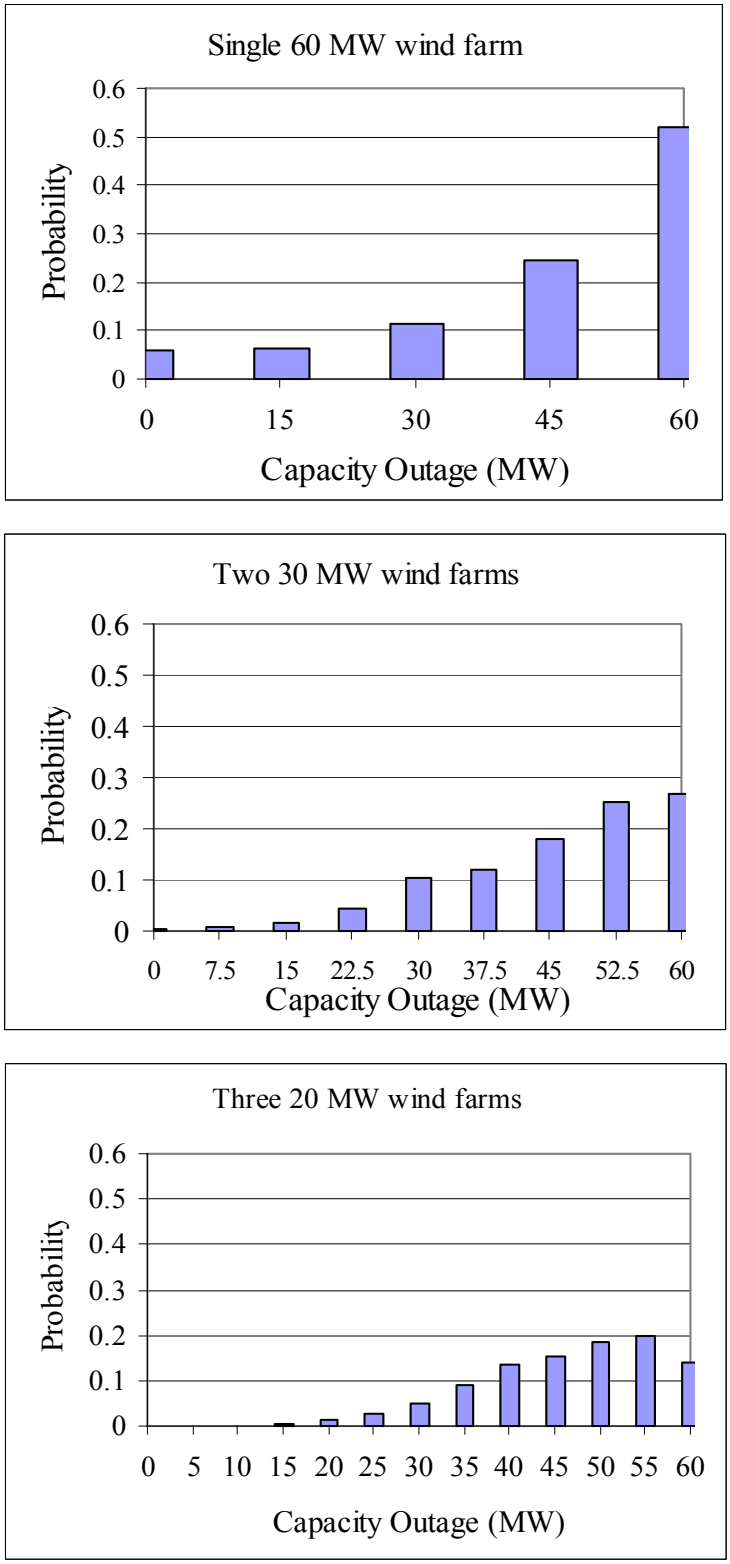

Figure 5.28: The COPT of the one, two and three independent wind farms

Figures 5.29 and 5.30 show the Case 2 results. The two figures show the relative benefits in the RBTS of adding single and multiple wind and solar energy sites respectively. As noted earlier, Bus 6 is connected to the system by a single radial line. The system EENS increases as the number of independent wind/solar sites increases. The reason is that the allocated WECS/PVCS capacity at Bus 6 decreases with increase in the number of sites. The EENS at Bus 3 is significantly impacted by the system peak load level as this bus has the lowest priority order. The EENS for a peak load of 225 MW, therefore, decreases with increase in the number of independent wind/solar sites.

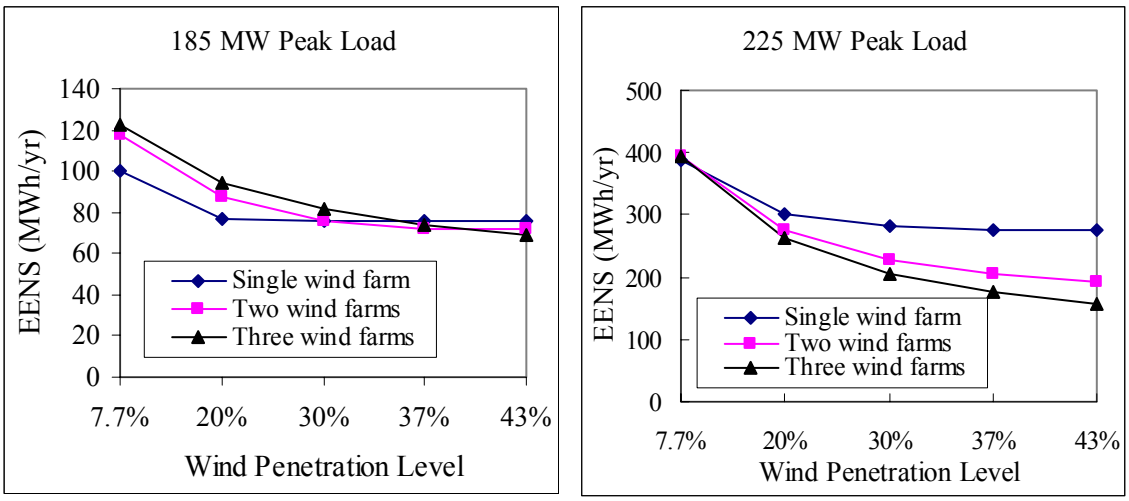

Figure 5.29: Comparison of the RBTS EENS with the addition of single and multiple wind sites (Case 2)

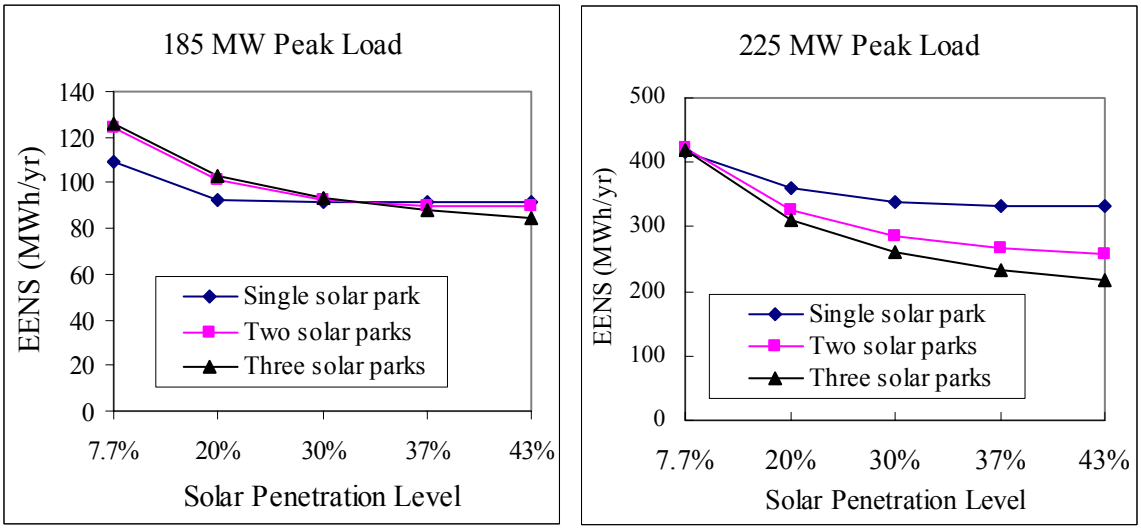

Figure 5.30: Comparison of the RBTS EENS with the addition of single and multiple solar sites (Case 2)

The results shown for the two cases illustrate the effect of connecting multiple WECS/PVCS at different locations in a composite generation and transmission system. The results shown in Figures 5.26 and 5.27 are similar in form to those obtained in an HL-I evaluation. The WECS/PVCS in this case are connected at relatively strong points in the transmission system. The results shown in Figures 5.29 and 5.30 indicate the effects when the WECS/PVCS are added at relatively weaker points in the transmission system. The reliability benefits are obviously very dependent on the actual transmission network.

5.5.2 RTS System Analysis

The RTS is a large system compared to the RBTS and has a relatively strong transmission network. The RTS EENS values obtained in sections 5.2.2, 5.3.2 and 5.4.2 are used to compare the reliability benefits when single and multiple renewable energy sites are added to the system. Figures 5.31 and 5.32 respectively show a comparison of the benefits obtained by increasing the number of independent wind farms and solar parks. Peak loads of 2850 MW and 3250 MW are used in these figures.

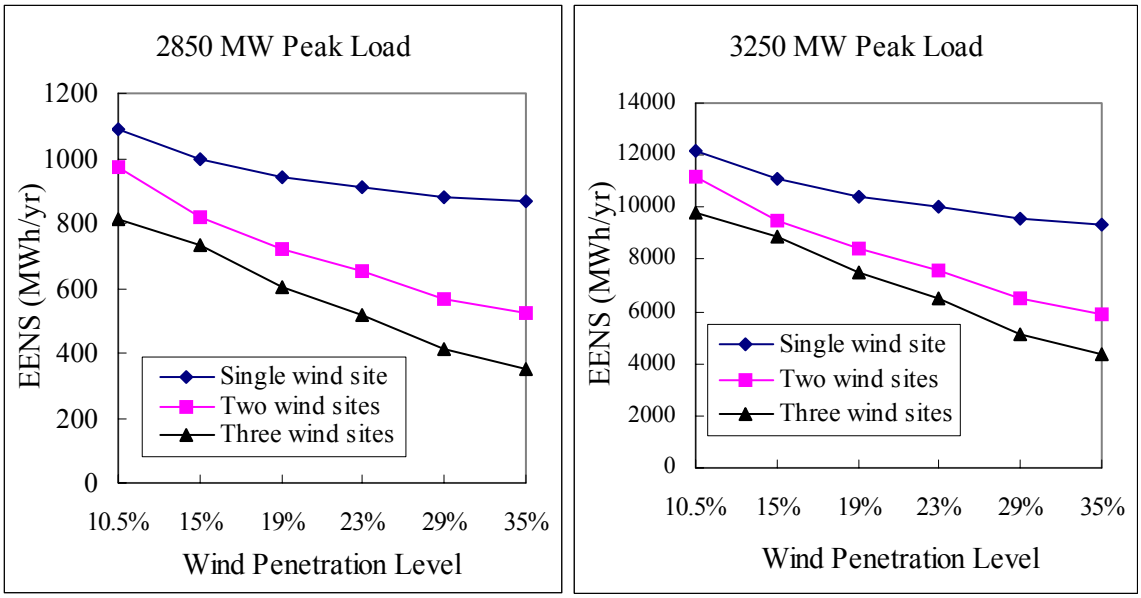

Figure 5.31: Comparison of the RTS EENS with the addition of single and multiple wind sites

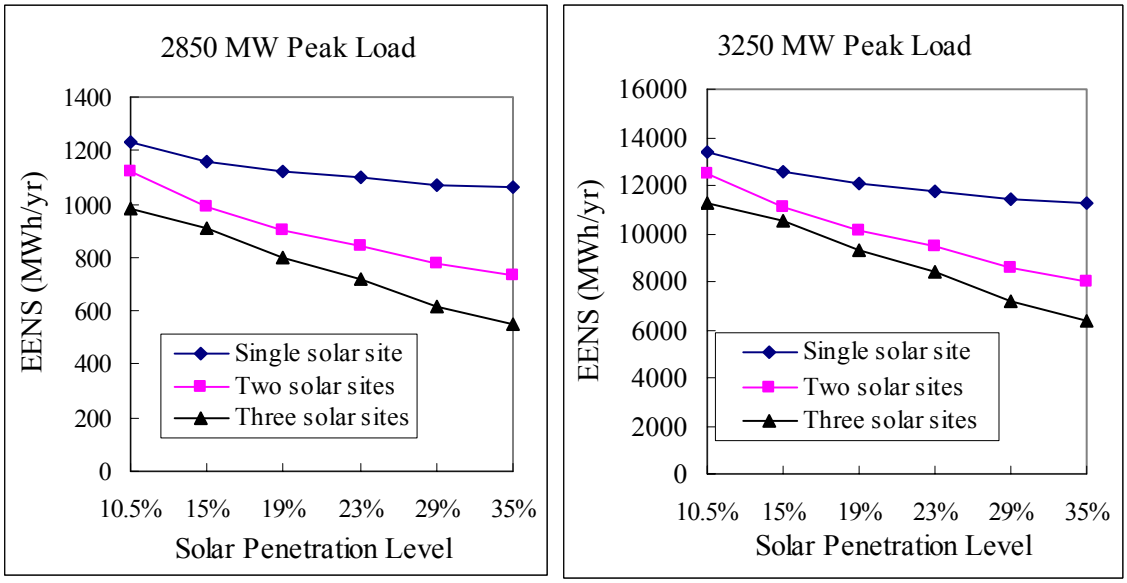

Figure 5.32: Comparison of the RTS EENS with the addition of single and multiple solar sites

The RTS is considered to have a relatively weak generation system and the studies show that multiple wind farms/solar parks make a more significant reliability contribution than a single wind farm/solar park. This study indicates that there are decreasing benefits associated with increasing the number of wind farms/solar parks in the RTS. The reliability benefits due to the addition of a single renewable energy site saturates more quickly than at multiple sites.

5.6 Summary

A series of adequacy analyses on the RBTS and the RTS were conducted in order to investigate the effect of adding WECS/PVCS at different locations and the reliability benefits of increasing the number of wind farms/solar parks in an existing power system. The multiple wind farms and solar parks were assumed to have the same Swift Current wind and PV models in order to simplify the comparisons.

The system and load point reliabilities are improved by adding WECS or PVCS to the RBTS and RTS. The system and load point indices are relatively unchanged when the

WECS or the PVCS is added at different locations other than Bus 6 in the RBTS. The effect on the bulk system EENS of adding WECS or PVCS at Bus 6 is quite different to similar additions at other buses, as the system indices are dominated by the performance of Bus 6 which is connected to the rest of the system by a single radial line. The RTS system and load point reliability benefits are relatively similar no matter where the WECS/PVCS is located.

Both the RTS and the RBTS analyses show that WECS provide a larger contribution to the system reliability than PVCS with the same capacity. This conclusion is obviously dependent on the site wind and solar conditions. The Swift Current data were used in this analysis. The differences in reliability benefits between the WECS and the PVCS are not obvious when the generation capacity is much greater than the load demand.

The studies in this chapter show the effect of connecting multiple WECS/PVCS at different locations in a composite generation and transmission system. The system EENS decreases as the number of wind farms/solar parks increase when the WECS/PVCS are connected at relatively strong points in the transmission system. This result is similar in form to those obtained in an HL-I evaluation. This conclusion is not applicable to the case that the WECS/PVCS are added at relatively weaker points in the transmission system. The benefits are obviously very dependent on the actual transmission network.

Multiple wind farms/solar parks make a more significant reliability contribution than a single wind farm/solar park in a composite generation and transmission system which has a strong transmission system and a weak generation system. There are decreasing benefits associated with increasing the number of wind farms/solar parks in a system. The reliability benefits due to the addition of a single renewable energy site saturate more quickly than for multiple sites.

6. SUMMARY AND CONCLUSIONS

The development and utilization of wind and solar energy for satisfying electrical demand has received considerable attention in recent years due to concerns on dwindling energy resources and enhanced public awareness of the potential impact of conventional energy systems on the environment. As power generation plants using wind and solar energy are integrated into existing power systems, it becomes important to evaluate the reliability of these plants and assess the effects that they will have on the overall system reliability. The purpose of this research work is to develop appropriate models and techniques for wind energy conversion systems and photovoltaic conversion systems to assess the adequacy of composite power systems containing wind or solar energy.

Chapter 1 provides a brief introduction to the basic concepts related to overall power system reliability evaluation and to power systems including renewable energy.

Chapter 2 describes some basic concepts and evaluation techniques utilized in HL-I and HL-II analysis. Adequacy at these two hierarchical levels can be assessed either by analytical techniques or by Monte Carlo simulation methods. Three basic Monte Carlo simulation techniques designated as state sampling, state transition sampling and sequential analysis are introduced. Each approach has its own advantages and disadvantages. The MECORE program is based on the state sampling approach and this program has been utilized in the research described in this thesis to conduct bulk system adequacy studies. It also has been used to conduct generating system adequacy assessments by assuming that the transmission elements in the test systems are completely reliable.

The basic indices used in generating system reliability evaluation are briefly introduced,

followed by the basic indices used in bulk power systems. The basic bulk system indices can be used to measure the reliability at an individual load bus or for the entire system. The two sets of indices complement each other in providing an overall assessment of bulk system reliability. Two composite test systems known as the RBTS and the IEEE-RTS are used in this research. The RBTS is a small system designed for education and research purposes. The IEEE-RTS is relatively large compared to the RBTS. The annualized and annual indices for the original RBTS and IEEE-RTS are given in Chapter 2. These results provide a base case reference for the system conditions covered in subsequent chapters.

The utilization of the three different techniques to determine annualized and annual reliability indices at HL-I is illustrated in Chapter 2. The results are quite similar in the case of annualized analysis. The studies presented in this chapter illustrate that the HL-I results obtained using the MECORE program with a 20-step load model are very similar to those produced using an analytical method with this load model and are slightly higher than those obtained using an analytical method or by sequential Monte Carlo simulation and a detailed load model. The 20-step load model is used in the subsequent HL-I and HL-II studies described in this thesis.

Chapter 3 develops multi-state WECS models for adequacy assessment. The ARMA time series models used to simulate wind speeds are briefly introduced. A comparison of the observed wind speed probability distribution and the simulated wind speed probability distribution created by the ARMA model illustrates that the ARMA models provide a useful representation of the actual wind regimes. The power available from a WTG is obtained from the simulated wind speeds using a function describing the relationship between the wind speed and output power. The WTG COPT is created by applying the simulated hourly power output and the hourly wind speed relationship. A comparison between the COPT for the observed wind data and the COPT for the simulated wind data is presented which shows that the simulated wind data provides a reasonable representation for adequacy assessment.

The effect of wind speed on the WTG power output shows that the power output of a

WTG is extremely dependent on the wind regime and will increase if the facilities are located at a site where higher wind velocities are experienced. Seasonal wind speeds and wind power outputs using data for four sites were analyzed. The wind speed and power output probability distributions of the four sites illustrate that in these cases, the annual profile is a valid representation of the system wind speeds and that annual studies can be done directly using this profile.

The apportioning method is introduced and used to create selected WTG multi-state models. It is assumed in this research that a WECS consists of multiple identical WTG units. Non identical units can be easily incorporated using Equation (2.3). A WECS multi-state model is the same as that of a single WTG unit when the FOR of the WTG unit is zero. An analytical procedure is introduced and used to create WECS multi-state models when the WTG FOR is incorporated.

A comparison of the analytical method, the MECORE program and the sequential Monte Carlo simulation technique using the RBTS with a WECS are also presented in Chapter 3. The LOLE from MECORE and the analytical method are higher than that obtained from the sequential Monte Carlo simulation technique due to the impact of the applied load model.

The analyses of generating systems including WECS indicate that a 5-state WECS model can be used to provide a reasonable assessment in practical studies using the analytical method or MECORE. Analysis conducting by considering WECS as a negative load also indicates that this approach can be used to provide reasonable assessments. The studies on the RBTS and the RTS LOLE with different WTG FOR indicate that changes in WTG FOR do not have a significant impact on the calculated reliability indices. Using a zero FOR will not significantly impact the calculated indices and can greatly simplify the WECS modeling procedure.

Chapter 4 develops PVCS models for adequacy evaluation. The WATGEN and WATSUN-PV programs were utilized to generate solar radiation data and PV generating

unit power outputs. The generated power of a photovoltaic generating unit was obtained based on the I-V characteristics of a solar cell using the simulated solar radiation data. Appropriate PVCS multi-state models can be built using the apportioning approach described in this thesis.

The effect of PVCS generation on the RBTS is examined using two different methods. The first approach is designated as the negative load method, and the second as the PVCS multi-state model approach. There are only small differences between the annual system LOLE values obtained using the two methods when the PVCS model has three or more states. The variation in the LOLE for different PVCS multi-state models as a function of the system peak load was investigated using both the RBTS and the RTS. The results show that it is reasonable to use a 5-state PVCS model for adequacy assessment over a range of system conditions. This conclusion is illustrated and examined by analyses of the RTS.

The RBTS and the RTS analyses show that a WECS makes a bigger contribution to the system adequacy than a PVCS with the same capacity. This conclusion is based on the Swift Current weather data. The relative reliability benefits from renewable energy sources such as wind and solar depend on many factors, such as the wind speed and the weather characteristics at the site location. Each site should therefore be analyzed on its own merits. The techniques utilized in this research and described in this thesis can be used to examine the benefits associated with adding different WECS and PVCS to an electric power system.

Chapter 5 investigates the effect of adding WECS/PVCS at different locations and the reliability benefits of increasing the number of wind farms/solar parks in an existing power system. The multiple wind farms and solar parks were assumed to have the same Swift Current wind and PV models in order to simplify the comparisons.

The system and load point reliabilities are improved by adding WECS/PVCS to the RBTS and RTS. The system and load point indices are relatively unchanged when the

WECS or the PVCS is added at different locations other than Bus 6 in the RBTS. The effect on the bulk system EENS of adding WECS or PVCS at Bus 6 is quite different to similar additions at other buses, as the system indices are dominated by the performance of Bus 6 which is connected to the rest of the system by a single radial line. The RTS system and load point reliability benefits are relatively similar no matter where the WECS/PVCS is located.

Both the RTS and the RBTS analyses show that WECS provide a larger contribution to the system reliability than PVCS with the same capacity. This conclusion is obviously dependent on the site wind and solar condition. The Swift Current data was used in this analysis. The difference in reliability benefits between the WECS and the PVCS are not obvious when the generation capacity is much greater than the load demand.

The studies in Chapter 5 show the effect of connecting multiple WECS/PVCS at different locations in a composite generation and transmission system. The system EENS decreases as the number of wind farms/solar parks increases when the WECS/PVCS are connected at relatively strong points in the transmission system. This result is similar in form to those obtained in an HL-I evaluation. This conclusion is not applicable to cases where WECS/PVCS are added at relatively weaker points in the transmission system. The benefits are obviously very dependent on the actual transmission network.

Multiple wind farms/solar parks make a more significant reliability contribution than a single wind farm/solar park in a composite generation and transmission system which has a strong transmission system and a weak generation system. There are decreasing benefits associated with increasing the number of wind farms/solar parks in a system. The reliability benefits due to the addition of a single renewable energy site saturate more quickly than for multiple sites.

In conclusion, this research shows that a five-state model can be used to reasonable represent a WECS or PVCS in an adequacy assessment using the analytical method or

MECORE. This is an important observation as it permits WECS and PVCS to be incorporated in large practical system studies without requiring excessive increases in computer solution time. The procedure developed to consider WECS and PVCS as negative loads should also prove useful in large system studies and should be studied further.

The reliability benefits of adding single or multiple wind/solar sites in a composite generation and transmission system are obviously dependent on the actual system configuration. The relative reliability benefits from renewable energy sources such as wind and solar depend on many factors, such as the wind speed and the weather characteristics at the site location. Each site should therefore be analyzed on its own merits. The techniques utilized in this research and described in this thesis can be used to examine the benefits associated with different WECS and PVCS additions to an electric power system.

It is believed that the models, methodologies, results and discussion presented in this thesis provide valuable information for system planners assessing the adequacy of composite electric power systems incorporating wind or solar energy conversion systems.

REFERENCES

1. R. Billinton and R. Allan, *Reliability evaluation of power systems*, 2nd Edition, Plenum Press, New York, 1996.
2. R.Billinton, R.Allan and L.Salvaderi, *Applied Reliability Assessment in Electric Power Systems,* IEEE Press, New York, 1991.
3. R. Allen, R. Billinton, S. M. Shahidehpour and C. Singh, "Bibliography on the Application of Probability Methods in Power System Reliability Evaluation: 1982-1987", *IEEE Transactions on Power Apparatus and Systems*, Vol3, No.4, November 1988, pp. 1555-1564.
4. R.N. Allan, R. Billinton, A.M. Breipohl, and C.H. Grigg, "Bibliography on the application of probability methods in power system reliability evaluation: 1987-1991", *IEEE Transactions on Power Systems*, Vol. 9, No. 4, February 1994, pp. 275-282.
5. R.N. Allan, R. Billinton, A.M. Breipohl, and C.H. Grigg, "Bibliography on the application of probability methods in power system reliability evaluation: 1992-1996", *IEEE Transactions on Power Systems*, Vol. 14, No. 1, February 1999, pp. 51-57.
6. R. C. Bansal, T. S. Bhatti, and D. P. Kothari, "Discussion of "Bibliography on the Application of Probability Methods in Power System Reliability Evaluation", *IEEE Transactions on Power Systems*, Vol. 17, No. 3, August 2002, pg. 924.
7. Roy Billinton, Mahmud Fotuhi-Firuzabad, and Lina Bertling, "Bibliography on the application of probability methods in power system reliability evaluation: 1996-1999", *IEEE Transactions on Power Systems*, Vol. 16, No. 4, November 2001, pp. 595-602.
8. M.Th. Schilling, R. Billinton, A.M. Leite da Silva, M.A. El-kady, "Bibliography on composite system reliability 1964-1988," *IEEE Trans. Power Systems*, vol.4, No.3,

August 1989, pp.1122-1132.

9. Nick Jenkins, Ron Allan, Peter Crossley, Daniel Kirschen and Goran Strbac, *Embedded generation*, The Institution of Electrical Engineers, London, United Kingdom, 2000.
10. Global Wind Energy Council, *www.gwec.net* (Oct.2005)
11. Solar Electric Power Association, *www.solarelectricpower.org* (Oct.2005)
12. http://www.greenhouse.gov.au/markets/mret/pubs/6_solar.pdf, (Oct.2005) Australian Greenhouse Office
13. R. Billinton, H. Chen and R. Ghajar, "Time-series Models for Reliability Evaluation of Power Systems Including Wind Energy", *Microelectron. Reliability*, Vol.36. No.9. 1996, pp1253-1261.
14. C. Singh and A. Lago-Gonzalez, "Reliability Modeling of Generation System Including Unconventional Energy Sources", *IEEE Transaction on Power Apparatus and System*, Vol. PAS-104, No.5, 1985, pp. 1049-1056.
15. Amit Jain, S.C.Tripathy and R.Balasubramanian, "Reliability and Economic Analysis of a Power Generation System Including a Photovolatic System", *Energy Conversion and Management*, Vol.36, No.3, 1995, pp183-189.
16. S.H. Karaki, R.B. Chedid, and R. Ramadan, "Probabilistic Performance Assessment of Autonomous Solar-Wind Energy Conversion Systems", *IEEE Transactions on Energy Conversion*, Vol.14, No.3, September 1999, pp.766-772.
17. R. Billinton, H. Chen and R. Ghajar, "A Sequential Simulation Technique for Adequacy Evaluation of Generating Systems Including Wind Energy", *IEEE Transactions on Energy Conversion*, Vol.11, No.4, December 1996.
18. Xiaoming Cao, *Adequacy Assessment of A Combined Generating System Containing Wind Energy Conversion System*, M.Sc thesis, University of Saskatchewan, 1994.
19. R. Billinton and G. Bai, "Generating Capacity Adequacy Associated with Wind Energy", *IEEE Transactions on Energy Conversion*, Vol. 19, No. 3, September 2004, pp.641-646.
20. Rajesh Karki and Po Hu, "Wind Power Simulation Model for Reliability Evaluation", the 2005 Canadian Conference on Electrical and Computer Engineering, Saskatoon, May 2005, pp. 527-530.

21. Bagen, *Adequacy Evaluation of Small Stand Alone Wind and Solar Energy Based Power Systems*, M.Sc thesis, University of Saskatchewan, 2002.
22. Rajesh Karki, and Roy Billinton, "Reliability/Cost Implications of PV and Wind Energy Utilization in Small Isolated Power System" *IEEE Transactions on Energy Conversion,* Vol.16, No.4, December 2001, pp.368-373.
23. T. L. Skakum, *Reliability of a Generating System Containing Photovoltaic Power Generation*, M.Sc. thesis, University of Saskatchewan, 1997.
24. W. Li, *Installation Guide and User's Manual for the MECORE Program,* July 1998.
25. R. Billinton and et al, "A Reliability Test System for Educational Purposes Basic Data"*, IEEE Transactions on Power Systems*, Vol. PWRS-3, No. 4, August 1989, pp. 1238-1244.
26. IEEE Task Force, "IEEE Reliability Test System"*, IEEE Transactions on Power Apparatus and Systems*, Vol. PAS-98, Nov/Dec. 1979, pp. 2047-2054.
27. R. Billinton and C. Wee, *Derated State Modelling of Generating Units*, Report prepared for Saskatchewan Power Corporation, September 1985.
28. Yifeng Li, *Bulk System Reliability Evaluation in A Deregulated Power Industry,* M.Sc thesis, University of Saskatchewan, 2003.
29. Watsun Simulation Laboratory, *WATGEN User's Manual*, University of Waterloo, 1.0-August 1992.
30. Watsun Simulation Laboratory, *WATSUN-PV 5.1 User's Manual and Program Documentation*: University of Waterloo, August 1995.
31. R. Billinton and W. Li, *Reliability Assessment of Electrical Power System Using Monte Carlo Methods,* Plenum Press, New York, 1994.
32. R. Billinton and W. Wangdee, "Impact of Utilizing Sequential and Non-Sequential Simulation Techniques in Bulk Electric System Reliability Assessment", *IEE Generation, Transmission and Distribution*, Vol.152, No. 5, September 2005, pp.623-628.
33. Xiaosu Tang, *Considerations in Bulk System Reliability Assessment*, M.Sc. thesis University of Saskatchewan, 2000.
34. Wenyuan Li, R. Billinton*, "*Effect of Bus Load Uncertainty and Correlation in Composite System Adequacy Evaluation*", IEEE Transaction on Power Systems,* Vol.6, No.4, 1991, pp.1522-1528.

35. P. Giorsetto and K. F. Utsurogi, “Development of A New Procedure for Reliability Modeling of Wind Turbine Generators”, *IEEE Transactions on Power Apparatus and Systems*, Vol. PAS-102, No. 1, 1983, pp.134-143.
36. Canadian Electricity Association, “2002 Generation Equipment Status Annual Report”, December 2003, pp.1-115.
37. David L. Pulfrey, *Photovoltaic Power Generation*, Litton Education Publishing, Inc. 1978.
38. Martin A. Green, *Solar Cells Operating Principles, Technology, and System Applications,* Prentice-Hall, Inc., 1982.
39. V.A. Graham, K.G.T. Hollands and T.E. Unny, “A Time Series Model For *Kt* with application to Global Synthetic Weather Generation”, *Solar Energy,* Vol.40, No.2, 1988, pp. 83-92.
40. V.A. Graham and K.G.T. Hollands, “A Method to Generate Synthetic Hourly Solar Radiation Globally”, *Solar Energy*, Vol.44, No.6, 1990, pp. 333-341.

APPENDIX A. BASIC DATA FOR THE RBTS AND THE IEEE RTS

Tables A.1-A.3 and A.4-A.6 present the bus, transmission line and generator data for the RBTS and the IEEE-RTS respectively.

Table A.1: Bus data for the RBTS

Bus No.	Load (p.u.)		P_g	Q_{max}	Q_{min}	V_0	V_{max}	V_{min}
	Active	Reactive						
1	0.00	0.0	1.0	0.50	-0.40	1.05	1.05	0.97
2	0.20	0.0	1.2	0.75	-0.40	1.05	1.05	0.97
3	0.85	0.0	0.0	0.00	0.00	1.00	1.05	0.97
4	0.40	0.0	0.0	0.00	0.00	1.00	1.05	0.97
5	0.20	0.0	0.0	0.00	0.00	1.00	1.05	0.97
6	0.20	0.0	0.0	0.00	0.00	1.00	1.05	0.97

Table A.2: Line data for the RBTS

Line	Bus		R	X	B/2	Tap	Current Rating (p.u.)	Failure Rate (occ/yr)	Repair Time (hrs)	Failure Prob.
	I	J								
1,6	1	3	0.0342	0.18	0.0106	1.0	0.85	1.50	10.0	0.00171
2,7	2	4	0.1140	0.60	0.0352	1.0	0.71	5.00	10.0	0.00568
3	1	2	0.0912	0.48	0.0282	1.0	0.71	4.00	10.0	0.00455
4	3	4	0.0228	0.12	0.0071	1.0	0.71	1.00	10.0	0.00114
5	3	5	0.0228	0.12	0.0071	1.0	0.71	1.00	10.0	0.00114
8	4	5	0.0228	0.12	0.0071	1.0	0.71	1.00	10.0	0.00114
9	5	6	0.0228	0.12	0.0071	1.0	0.71	1.00	10.0	0.00114

Table A.3: Generator data for the RBTS

Unit No.	Bus No.	Rating (MW)	Failure Rate (occ/yr)	Repair Time (hrs)	Failure Prob.
1	1	40.0	6.0	45.0	0.03
2	1	40.0	6.0	45.0	0.03
3	1	10.0	4.0	45.0	0.02
4	1	20.0	5.0	45.0	0.025
5	2	5.0	2.0	45.0	0.01
6	2	5.0	2.0	45.0	0.01
7	2	40.0	3.0	60.0	0.02
8	2	20.0	2.4	55.0	0.015
9	2	20.0	2.4	55.0	0.015
10	2	20.0	2.4	55.0	0.015
11	2	20.0	2.4	55.0	0.015

Table A.4: Bus data for the IEEE-RTS

Bus No.	Load (p.u.)		P_g	Q_{max}	Q_{min}	V_0	V_{max}	V_{min}
	Active	Reactive						
1	1.08	0.22	1.92	1.20	-0.75	1.00	1.05	0.95
2	0.97	0.20	1.92	1.20	-0.75	1.00	1.05	0.95
3	1.80	0.37	0.00	0.00	0.00	1.00	1.05	0.95
4	0.74	0.15	0.00	0.00	0.00	1.00	1.05	0.95
5	0.71	0.14	0.00	0.00	0.00	1.00	1.05	0.95
6	1.36	0.28	0.00	0.00	0.00	1.00	1.05	0.95
7	1.25	0.25	3.00	2.70	0.00	1.00	1.05	0.95
8	1.71	0.35	0.00	0.00	0.00	1.00	1.05	0.95
9	1.75	0.36	0.00	0.00	0.00	1.00	1.05	0.95
10	1.95	0.40	0.00	0.00	0.00	1.00	1.05	0.95
11	0.00	0.00	0.00	0.00	0.00	1.00	1.05	0.95
12	0.00	0.00	0.00	0.00	0.00	1.00	1.05	0.95
13	2.65	0.54	5.91	3.60	0.00	1.00	1.05	0.95
14	1.94	0.39	0.00	3.00	-0.75	1.00	1.05	0.95
15	3.17	0.64	2.15	1.65	-0.75	1.00	1.05	0.95
16	1.00	0.20	1.55	1.20	-0.75	1.00	1.05	0.95
17	0.00	0.00	0.00	0.00	0.00	1.00	1.05	0.95
18	3.33	0.68	4.00	3.00	-0.75	1.00	1.05	0.95
19	1.81	0.37	0.00	0.00	0.00	1.00	1.05	0.95
20	1.28	0.26	0.00	0.00	0.00	1.00	1.05	0.95
21	0.00	0.00	4.00	3.00	-0.75	1.00	1.05	0.95
22	0.00	0.00	3.00	1.45	-0.90	1.00	1.05	0.95
23	0.00	0.00	6.60	4.50	-0.75	1.00	1.05	0.95
24	0.00	0.00	0.00	0.00	0.00	1.00	1.05	0.95

Table A.5: Line data for the IEEE-RTS

Line No.	Bus		R	X	B/2	Tap	Current Rating (p.u.)	Failure Rate (occ/yr)	Repair Time (hrs)
	I	J							
1	1	2	0.0260	0.0139	0.2306	1.00	1.75	0.240	16.0
2	1	3	0.0546	0.2112	0.0286	1.00	1.75	0.510	10.0
3	1	5	0.0218	0.0845	0.0115	1.00	1.75	0.330	10.0
4	2	4	0.0328	0.1267	0.0172	1.00	1.75	0.390	10.0
5	2	6	0.0497	0.1920	0.0260	1.00	1.75	0.480	10.0
6	3	9	0.0308	0.1190	0.0161	1.00	1.75	0.380	10.0
7	3	24	0.0023	0.0839	0.0000	1.00	4.00	0.020	768.0
8	4	9	0.0268	0.1037	0.0141	1.00	1.75	0.360	10.0
9	5	10	0.0228	0.0883	0.0120	1.00	1.75	0.340	10.0
10	6	10	0.0139	0.0605	1.2295	1.00	1.75	0.330	35.0
11	7	8	0.0159	0.0614	0.0166	1.00	1.75	0.300	10.0
12	8	9	0.0427	0.1651	0.0224	1.00	1.75	0.440	10.0
13	8	10	0.0427	0.1651	0.0224	1.00	1.75	0.440	10.0
14	9	11	0.0023	0.0839	0.0000	1.00	4.00	0.020	768.0
15	9	12	0.0023	0.0839	0.0000	1.00	4.00	0.020	768.0
16	10	11	0.0023	0.0839	0.0000	1.00	4.00	0.020	768.0
17	10	12	0.0023	0.0839	0.0000	1.00	4.00	0.020	768.0
18	11	13	0.0061	0.0476	0.0500	1.00	5.00	0.400	11.0
19	11	14	0.0054	0.0418	0.0440	1.00	5.00	0.390	11.0
20	12	13	0.0061	0.0476	0.0500	1.00	5.00	0.400	11.0
21	12	23	0.0124	0.0966	0.1015	1.00	5.00	0.520	11.0
22	13	23	0.0111	0.0865	0.0909	1.00	5.00	0.490	11.0
23	14	16	0.0050	0.0389	0.0409	1.00	5.00	0.380	11.0
24	15	16	0.0022	0.0173	0.0364	1.00	5.00	0.330	11.0
25	15	21	0.0063	0.0490	0.0515	1.00	5.00	0.410	11.0
26	15	21	0.0063	0.0490	0.0515	1.00	5.00	0.410	11.0
27	15	24	0.0067	0.0519	0.0546	1.00	5.00	0.410	11.0
28	16	17	0.0033	0.0259	0.0273	1.00	5.00	0.350	11.0
29	16	19	0.0030	0.0231	0.0243	1.00	5.00	0.340	11.0
30	17	18	0.0018	0.0144	0.0152	1.00	5.00	0.320	11.0
31	17	22	0.0135	0.1053	0.1106	1.00	5.00	0.540	11.0
32	18	21	0.0033	0.0259	0.0273	1.00	5.00	0.350	11.0
33	18	21	0.0033	0.0259	0.0273	1.00	5.00	0.350	11.0
34	19	20	0.0051	0.0396	0.0417	1.00	5.00	0.380	11.0
35	19	20	0.0051	0.0396	0.0417	1.00	5.00	0.380	11.0
36	20	23	0.0028	0.0216	0.0228	1.00	5.00	0.340	11.0
37	20	23	0.0028	0.0216	0.0228	1.00	5.00	0.340	11.0
38	21	22	0.0087	0.0678	0.0712	1.00	5.00	0.450	11.0

Table A.6: Generator data for the IEEE-RTS

Unit No.	Bus No.	Rating (MW)	Failure Rate (occ/yr)	Repair Time (hrs)	Failure Prob.
1	22	50	4.42	20	0.01
2	22	50	4.42	20	0.01
3	22	50	4.42	20	0.01
4	22	50	4.42	20	0.01
5	22	50	4.42	20	0.01
6	22	50	4.42	20	0.01
7	15	12	2.98	60	0.02
8	15	12	2.98	60	0.02
9	15	12	2.98	60	0.02
10	15	12	2.98	60	0.02
11	15	12	2.98	60	0.02
12	15	155	9.13	40	0.04
13	7	100	7.30	50	0.04
14	7	100	7.30	50	0.04
15	7	100	7.30	50	0.04
16	13	197	9.22	50	0.05
17	13	197	9.22	50	0.05
18	13	197	9.22	50	0.05
19	1	20	19.47	50	0.10
20	1	20	19.47	50	0.10
21	1	76	4.47	40	0.02
22	1	76	4.47	40	0.02
23	2	20	9.13	50	0.10
24	2	20	9.13	50	0.10
25	2	76	4.47	40	0.02
26	2	76	4.47	40	0.02
27	23	155	9.13	40	0.04
28	23	155	9.13	40	0.04
29	23	350	7.62	100	0.08
30	18	400	7.96	150	0.12
31	21	400	7.96	150	0.12
32	16	155	9.13	40	0.04

Tables A.7-A.9 give the per-unit load model for the RBTS and IEEE-RTS.

Table A.7: The weekly peak load as a percent of annual peak

Week	Peak load	Week	Peak load	Week	Peak load	Week	Peak load
1	86.2	14	75.0	27	75.5	40	72.4
2	90.0	15	72.1	28	81.6	41	74.3
3	87.8	16	80.0	29	80.1	42	74.4
4	83.4	17	75.4	30	88.0	43	80.0
5	88.0	18	83.7	31	72.2	44	88.1
6	84.1	19	87.0	32	77.6	45	88.5
7	83.2	20	88.0	33	80.0	46	90.9
8	80.6	21	85.6	34	72.9	47	94.0
9	74.0	22	81.1	35	72.6	48	89.0
10	73.7	23	90.0	36	70.5	49	94.2
11	71.5	24	88.7	37	78.0	50	97.0
12	72.7	25	89.6	38	69.5	51	100.0
13	70.4	26	86.1	39	72.4	52	95.2

Table A.8: Daily peak load as a percentage of weekly load

Day	Peak Load
Monday	93
Tuesday	100
Wednesday	98
Thursday	96
Friday	94
Saturday	77
Sunday	75

Table A.9: Hourly peak load as a percentage of daily peak

Hour	Winter Weeks 1-8&44-52		Summer Weeks 18-30		Spring/Fall Weeks 9-17&31-43	
	Wkdy	Wknd	Wkdy	Wknd	Wkdy	Wknd
12-1am	67	78	64	74	63	75
1-2	63	72	60	70	62	73
2-3	60	68	58	66	60	69
3-4	59	66	56	65	58	66
4-5	59	64	56	64	59	65
5-6	60	65	58	62	65	65
6-7	74	66	64	62	72	68
7-8	86	70	76	66	85	74
8-9	95	80	87	81	95	83
9-10	96	88	95	86	99	89
10-11	96	90	99	91	100	92
11-noon	95	91	100	93	99	94
Noon-1pm	95	90	99	93	93	91
1-2	95	88	100	92	92	90
2-3	93	87	100	91	90	90
3-4	94	87	97	91	88	86
4-5	99	91	96	92	90	85
5-6	100	100	96	94	92	88
6-7	100	99	93	95	96	92
7-8	96	97	92	95	98	100
8-9	91	94	92	100	96	97
9-10	83	92	93	93	90	95
10-11	73	87	87	88	80	90
11-12	63	81	72	80	70	85

Note: Wkdy-Weekday, Wknd-Weekend.

APPENDIX B. THE RTS LOAD DURATION CURVE DATA

Table B.1: The RTS load duration curve data

15- step		20- step		40- step	
Load level	Probability	Load level	Probability	Load level	Probability
1.00	0.00217	1.000	0.00023	1.000	0.00023
0.95	0.01096	0.990	0.00011	0.990	0.00011
0.90	0.03584	0.983	0.00057	0.983	0.00057
0.85	0.07511	0.966	0.00171	0.966	0.00171
0.80	0.08402	0.949	0.00171	0.949	0.00171
0.75	0.08219	0.932	0.00331	0.932	0.00331
0.70	0.11016	0.915	0.00616	0.915	0.00616
0.65	0.12146	0.898	0.00970	0.898	0.00970
0.60	0.09669	0.881	0.01153	0.881	0.01153
0.55	0.11884	0.864	0.01610	0.864	0.01610
0.50	0.12808	0.847	0.02363	0.847	0.02363
0.45	0.09795	0.830	0.02546	0.830	0.02546
0.40	0.03505	0.813	0.02386	0.813	0.02842
0.35	0.00148	0.800	0.03311	0.796	0.02911
0.30	0.00000	0.780	0.03459	0.779	0.02877
		0.760	0.01632	0.762	0.02683
		0.750	0.08219	0.745	0.02865
		0.700	0.23162	0.728	0.02877
		0.600	0.21553	0.711	0.02979
		0.500	0.26256	0.694	0.03584
				0.677	0.03938
				0.660	0.04030
				0.643	0.04372
				0.626	0.04235
				0.609	0.03733
				0.592	0.03116
				0.575	0.03071
				0.558	0.03482
				0.541	0.03893
				0.524	0.04441
				0.507	0.04772
				0.490	0.04737
				0.473	0.03881
				0.456	0.03493
				0.439	0.03527
				0.422	0.03231
				0.405	0.02066
				0.388	0.01084
				0.371	0.00902
				0.354	0.00354

APPENDIX C. MODEL DATA FOR DOUBLED ORIGINAL MEAN WIND SPEED (Swift Current)

Table C.1: The capacity outage levels and probabilities for a WTG with a 38.92 km/h mean wind speed

Capacity Outage (%)	Probability
0	0.5818
2.5	0.0238
7.5	0.0242
12.5	0.0245
17.5	0.0248
22.5	0.0249
27.5	0.0250
32.5	0.0249
37.5	0.0246
42.5	0.0242
47.5	0.0237
52.5	0.0229
57.5	0.0220
62.5	0.0209
67.5	0.0195
72.5	0.0180
77.5	0.0162
82.5	0.0142
87.5	0.0122
92.5	0.0101
97.5	0.0080
100	0.0098

Table C.2: SCOPTW models with the doubled wind speed (without FOR)

2-state (2SCOPTW)		3-state (3SCOPTW)		4-state (4SCOPTW)		5-state (5SCOPTW)	
Capacity Outage (%)	Prob.	Capacity Outage (%)	Prob.	Capacity Outage (%)	Prob.	Capacity Outage (%)	Prob.
0	0.81312	0	0.70403	0	0.63002	0	0.64232
100	0.18688	50	0.21817	20	0.12335	25	0.12342
		100	0.07780	50	0.16883	50	0.11468
				100	0.07780	75	0.08357
						100	0.03601

Cont--

6-state (6SCOPTW)		7-state (7SCOPTW)		8-state (8SCOPTW)		9-state (9SCOTPW)	
Capacity Outage (%)	Prob.	Capacity Outage (%)	Prob.	Capacity Outage (%)	Prob.	Capacity Outage (%)	Prob.
0	0.63003	0	0.63003	0	0.61780	0	0.61780
20	0.09881	20	0.09881	15	0.08619	15	0.07374
40	0.09689	40	0.07362	35	0.08633	30	0.07441
60	0.08471	50	0.06793	50	0.06957	45	0.07153
80	0.06014	70	0.07389	65	0.06013	60	0.05429
100	0.02942	90	0.03743	80	0.03943	70	0.03733
		100	0.01829	90	0.02226	80	0.03035
				100	0.01829	90	0.02226
						100	0.01829

Cont--

10-state (10SCOPTW)		11-state (11SCOPTW)	
Capacity Outage (%)	Probability	Capacity Outage (%)	Probability
0	0.61780	0	0.60568
15	0.07374	10	0.04870
30	0.06215	20	0.04960
40	0.04876	30	0.04972
50	0.04654	40	0.04876
60	0.04277	50	0.04654
70	0.03733	60	0.04277
80	0.03035	70	0.03733
90	0.02226	80	0.03035
100	0.01829	90	0.02226
		100	0.01829

DAFORW=0.18688

Table C.3: MSCOPTW models with the doubled mean wind speed

2-state (2MSCOPTW)		3-state (3MSCOPTW)		4-state (4MSCOPTW)		5-state (5MSCOPTW)	
Capacity Outage (MW)	Prob.	Capacity Outage (MW)	Prob.	Capacity Outage (MW)	Prob.	Capacity Outage (MW)	Prob.
0	0.78060	0	0.64771	0	0.50612	0	0.54047
20	0.21940	10	0.26576	4	0.23269	5	0.20956
		20	0.08653	10	0.17663	10	0.12121
				20	0.08456	15	0.08941
						20	0.03935

Cont--

6-state (6MSCOPTW)		7-state (7MSCOPTW)		8-state (8MSCOPTW)		9-state (9MSCOPTW)	
Capacity Outage (MW)	Prob.	Capacity Outage (MW)	Prob.	Capacity Outage (MW)	Prob.	Capacity Outage (MW)	Prob.
0	0.50613	0	0.50612	0	0.46778	0	0.46778
4	0.20495	4	0.20494	3	0.21075	3	0.19336
8	0.10289	8	0.07458	7	0.09668	6	0.09009
12	0.08969	10	0.07736	10	0.07523	9	0.07559
16	0.06452	14	0.07683	13	0.06395	12	0.05624
20	0.03183	18	0.04037	16	0.04190	14	0.04147
		20	0.01979	18	0.02453	16	0.03247
				20	0.01918	18	0.02380
						20	0.01918

Cont--

10-state (10MSCOPTW)		11-state (11MSCOPTW)	
Capacity Outage (MW)	Probability	Capacity Outage (MW)	Probability
0	0.46778	0	0.40267
3	0.19336	2	0.20151
6	0.07539	4	0.07983
8	0.05324	6	0.05482
10	0.04926	8	0.05119
12	0.04579	10	0.04903
14	0.03974	12	0.04578
16	0.03245	14	0.03974
18	0.02380	16	0.03245
20	0.01918	18	0.02380
		20	0.01918

MDAFORW=0.21940

APPENDIX D. THE ARMA TIME SERIES MODELS FOR THE FOUR SITES

Table D.1: Wind Speed Data at the Four Sites in Saskatchewan, Canada

Sites	Regina	Saskatoon	Swift Current	North Battleford
Mean wind speed μ (km/h)	19.52	16.78	19.46	14.63
Standard deviation σ (km/h)	10.99	9.23	9.70	9.75

Regina: ARMA (4, 3):

$$y_t = 0.9336y_{t-1} + 0.4506y_{t-2} - 0.5545y_{t-3} + 0.1110y_{t-4} + \alpha_t - 0.2033\alpha_{t-1} - 0.4684\alpha_{t-2} + 0.2301\alpha_{t-3} \quad (1)$$
$$\alpha_t \in NID(0, 0.409423^2)$$

Saskatoon: ARMA (3, 2):

$$y_t = 1.5047y_{t-1} - 0.6635y_{t-2} + 0.1150y_{t-3} + \alpha_t - 0.8263\alpha_{t-1} + 0.2250\alpha_{t-2} \quad (2)$$
$$\alpha_t \in NID(0, 0.447423^2)$$

Swift Current: ARMA (4, 3):

$$y_t = 1.1772y_{t-1} + 0.1001y_{t-2} - 0.3572y_{t-3} + 0.0379y_{t-4} + \alpha_t - 0.5030\alpha_{t-1} - 0.2924\alpha_{t-2} + 0.1317\alpha_{t-3} \quad (3)$$
$$\alpha_t \in NID(0, 0.524760^2)$$

North Battleford: ARMA (3, 2):

$$y_t = 1.7901y_{t-1} - 0.9087y_{t-2} + 0.0948y_{t-3} + \alpha_t - 1.0929\alpha_{t-1} + 0.2892\alpha_{t-2} \quad (4)$$
$$\alpha_t \in NID\left(0, 0.474762^2\right)$$

APPENDIX E. RELIABILITY INDICES OF THE RBTS OBTAINED USING THE SEQUENTICAL MONTE CARLO SIMULATION TECHNIQUE

These results were provided by Mr.Wijarn Wangdee using a program developed in his research.

Table E.1: HL-I annualized system reliability indices of the RBTS including 10×2 MW of WECS using Swift Current data.

WTG reliability parameters			System reliability indices				
λ (f/yr)	μ (occ/yr)	FOR	PLC (/yr)	EDLC (hrs/yr)	EFLC (occ/yr)	EENS (MWh/yr)	DPUI (sys·mins)
0	-	0.00	0.00613	53.541	5.958	574.813	186.425
2	198	0.01	0.00614	53.605	5.954	575.496	186.647
4	196	0.02	0.00616	53.793	5.943	577.529	187.307
8	192	0.04	0.00619	54.110	5.921	580.960	188.419
12	188	0.06	0.00622	54.379	5.899	583.757	189.327
16	184	0.08	0.00626	54.649	5.881	586.484	190.211
20	180	0.10	0.00628	54.902	5.859	589.422	191.164

Table E.2: HL-I annual system reliability indices of the RBTS including 10×2 MW of WECS using Swift Current data.

WTG reliability parameters			System reliability indices				
λ (f/yr)	μ (occ/yr)	FOR	PLC (/yr)	EDLC (hrs/yr)	EFLC (occ/yr)	EENS (MWh/yr)	DPUI (sys·mins)
0	-	0.00	0.00008	0.668	0.181	5.889	1.910
2	198	0.01	0.00008	0.670	0.181	5.905	1.915
4	196	0.02	0.00008	0.673	0.181	5.937	1.925
8	192	0.04	0.00008	0.678	0.182	5.986	1.941
12	188	0.06	0.00008	0.685	0.182	6.030	1.956
16	184	0.08	0.00008	0.689	0.183	6.074	1.970
20	180	0.10	0.00008	0.694	0.183	6.116	1.984

Table E.3: HL-II annual load point and system reliability indices of the RBTS including 10×2 MW of WECS (FOR=4%) using Swift Current data

Bus No.	System reliability indices				
	PLC (/yr)	EDLC (hrs/yr)	EENS (MWh/yr)	EFLC (occ/yr)	DPUI (sys·mins)
2	0.00000	0.003	0.007	0.001	0.002
3	0.00008	0.684	5.556	0.183	1.802
4	0.00000	0.018	0.092	0.005	0.030
5	0.00000	0.017	0.150	0.004	0.049
6	0.00113	9.890	120.303	0.942	39.017
Total	0.00120	10.451	126.110	1.092	40.900

Table E.4: The RBTS system results with the WECS added at different locations

Location	EDLC (hr/yr)	EENS (MWh/yr)
Bus 2	10.453	126.127
Bus 3	10.451	126.110
Bus 4	10.460	126.218
Bus 5	10.451	126.108

Note: number of simulation years = 40,000 years

APPENDIX F. INDEX VALUES FOR THE RBTS WITH WECS OR PVCS

Table F.1: The HL-I annual RBTS indices for different peak loads

Peak load (MW)	EDLC (hrs/yr)	EENS (MWH/yr)	PLC (/yr)	SI (sys.mins/yr)
165	0.16445	1.44289	0.00002	0.46796
175	0.61631	4.66647	0.00007	1.51345
185	1.15487	11.78207	0.00013	3.82121
195	2.86080	27.98933	0.00033	9.07762
205	7.06336	70.18954	0.00081	22.76417

Table F.2: The annual RBTS system indices for different peak loads

Peak Load (MW)	EDLC (hrs/yr)	EENS (MWH/yr)	PLC (/yr)	SI (sys.mins/yr)
165	10.66263	124.32520	0.00122	40.32169
185	11.69545	150.36530	0.00134	48.76712
205	18.03706	227.49820	0.00206	73.78320
215	25.02785	318.37160	0.00286	103.25570
225	44.29847	553.36790	0.00506	179.47060

Table F.3: The HL-I annual system EDLC (hrs/yr) of the RBTS including the WECS obtained using MECORE

State	Peak Load (MW)				
	165	175	185	195	205
2-state	0.12378	0.47289	0.89742	2.25540	5.64579
3-state	0.11799	0.43104	0.84050	2.14162	5.35593
4-state	0.12015	0.43368	0.84527	2.14015	5.33917
5-state	0.11558	0.38115	0.85129	2.18824	4.70956
6-state	0.11543	0.37648	0.85668	2.16987	4.60333
7-state	0.12099	0.38361	0.88136	2.07392	4.80394
8-state	0.11716	0.37546	0.85484	2.09623	4.70344
9-state	0.11722	0.37805	0.86697	2.11495	4.68741
10-state	0.11706	0.37526	0.86405	2.10346	4.69016
11-state	0.11942	0.37820	0.87275	2.11540	4.69078

Table F.4: The HL-I annual system LOLE (hrs/yr) of the RBTS including the PVCS obtained using the analytical approach

State	Peak Load (MW)				
	165	175	185	195	205
2-state	0.14087	0.47939	0.98427	2.45816	5.54218
3-state	0.13416	0.44786	0.93352	2.35028	5.34351
4-state	0.13400	0.44703	0.93330	2.34461	5.32868
5-state	0.13232	0.43556	0.93620	2.38508	5.15185
6-state	0.13179	0.43119	0.93830	2.35037	5.15540
7-state	0.13342	0.43429	0.95530	2.28160	5.20603
8-state	0.13283	0.43088	0.94627	2.30437	5.20308
9-state	0.13293	0.43280	0.94643	2.31942	5.15753
10-state	0.13286	0.43145	0.94649	2.31021	5.16992
11-state	0.13296	0.43132	0.94710	2.31032	5.16645

Table F.5: The HL-I annual system EDLC (hrs/yr) of the RBTS including the PVCS obtained using MECORE

State	Peak Load (MW)				
	165	175	185	195	205
2-state	0.13255	0.46334	0.95346	2.40087	5.46632
3-state	0.12483	0.43056	0.91031	2.31494	5.29648
4-state	0.12613	0.43218	0.91420	2.32318	5.29925
5-state	0.12709	0.42194	0.91616	2.33986	5.08766
6-state	0.12644	0.41645	0.92108	2.31205	5.01741
7-state	0.12961	0.42028	0.93577	2.24221	5.15506
8-state	0.13039	0.42223	0.93191	2.30176	5.12504
9-state	0.12849	0.42078	0.92812	2.28686	5.06350
10-state	0.12824	0.41746	0.92788	2.27101	5.08411
11-state	0.12875	0.41847	0.92957	2.27342	5.08095

The following data were obtained using MECORE and the number of samples is 2,000,000 if without special note. Tables F.6– F.7 show the RBTS EENS with WECS added at Buses 3 and 6 respectively.

Table F.6: The RBTS EENS (MWh/yr) with the WECS added at Bus3

Peak Load (MW)	Wind Penetration Level				
	7.7% (20 MW)	20% (60 MW)	30% (100 MW)	37% (140 MW)	43% (180 MW)
165	115.00435	114.77148	114.71102	114.69513	114.69128
185	136.41763	134.62141	134.17934	134.04571	134.00210
205	194.05012	182.96665	179.93334	179.00535	178.68622
215	269.21326	243.57583	236.61858	234.21311	233.38078
225	425.69903	368.47523	352.36576	346.88172	344.76966

Table F.7: The RBTS EENS (MWh/yr) with the WECS added at Bus6

Peak Load (MW)	Wind Penetration Level				
	7.7% (20 MW)	20% (60 MW)	30% (100 MW)	37% (140 MW)	43% (180 MW)
165	80.05931	62.97754	62.78092	62.76029	62.75643
185	99.72003	77.16817	75.98814	75.84003	75.79622
205	156.17907	120.68515	115.54001	114.56798	114.24682
215	230.89343	179.18569	169.15828	166.66542	165.82790
225	387.05611	302.08188	281.94270	276.25325	274.12978

Tables F.8 – F.9 show the RBTS EENS with PVCS added at Buses 3 and 6 respectively.

Table F.8: The RBTS EENS (MWh/yr) with the PVCS added at Bus 3

Peak Load (MW)	Solar Penetration Level				
	7.7% (20 MW)	20% (60 MW)	30% (100 MW)	37% (140 MW)	43% (180 MW)
165	115.10663	114.92368	114.88109	114.86893	114.86554
185	137.18790	135.81717	135.50171	135.41232	135.38206
205	198.29944	189.79378	187.59574	186.96173	186.74725
215	278.57339	258.98400	253.89749	252.22546	251.66151
225	446.17912	402.42031	390.58983	386.72498	385.26958

Table F.9: The RBTS EENS (MWh/yr) with the PVCS added at Bus 6

Peak Load (MW)	Solar Penetration Level				
	7.7% (20 MW)	20% (60 MW)	30% (100 MW)	37% (140 MW)	43% (180 MW)
165	88.23255	75.97566	75.81257	75.79567	75.79228
185	108.95993	92.75265	91.73253	91.62874	91.59827
205	169.21534	144.38333	139.18278	138.50632	138.29002
215	249.17577	214.23687	203.19289	201.44041	200.87180
225	416.56679	360.98367	337.67512	333.63464	332.16968

Tables F.10- F.13 show the system EENS of the RBTS associated with multiple independent wind farms/solar parks

Table F.10: The annual system EENS of the RBTS associated with the two wind farms located at Bus 3 and Bus 6

Peak Load (MW)	Wind Penetration Level				
	7.7% (20 MW)	20% (60 MW)	30% (100 MW)	37% (140 MW)	43% (180 MW)
165	96.20823	71.75792	62.83779	61.51252	61.49369
185	117.53748	87.48375	76.02411	72.36579	72.12851
205	173.57704	126.16491	107.62868	99.40150	97.46147
215	245.43235	174.43545	146.55313	133.55416	129.08573
225	395.23932	274.30481	226.85322	203.56448	193.79415

Table F.11: The annual system EENS of the RBTS associated with the two solar parks located at Bus 3 and Bus 6

Peak Load (MW)	Solar Penetration Level				
	7.7% (20 MW)	20% (60 MW)	30% (100 MW)	37% (140 MW)	43% (180 MW)
165	101.93973	83.37203	76.93722	75.98307	75.96600
185	124.10216	101.01733	92.63188	89.94007	89.72678
205	183.85921	146.54456	132.27624	125.92667	124.28272
215	261.38005	204.56728	182.37284	172.01407	168.22934
225	423.19414	325.13186	286.26624	267.09512	258.78584

Table F.12: The annual system EENS of the RBTS associated with the three wind farms located at Buses 3, 5 and 6

Peak Load (MW)	Wind Penetration Level				
	7.7% (20 MW)	20% (60 MW)	30% (100 MW)	37% (140 MW)	43% (180 MW)
165	101.26233	78.20239	67.81203	62.04156	59.60974
185	122.16908	94.17341	81.20956	73.75385	69.42462
205	176.87361	130.42375	108.88933	97.02094	89.61443
215	247.26331	174.35445	141.06454	123.23175	112.51752
225	394.33041	264.07215	206.30179	176.25318	157.99466

Table F.13: The annual system EENS of the RBTS associated with the three solar parks located at Buses 3, 5 and 6

Peak Load (MW)	Solar Penetration Level				
	7.7% (20 MW)	20% (60 MW)	30% (100 MW)	37% (140 MW)	43% (180 MW)
165	104.43393	85.89761	78.19853	73.99867	72.21399
185	126.16982	103.40223	93.46285	87.90424	84.66720
205	184.71926	146.42183	128.63919	119.00172	113.01885
215	260.97152	200.07998	171.57058	156.29029	147.09499
225	420.32617	310.57438	259.64513	232.72486	216.20913

Table F.14: The RBTS EENS with the addition of single and multiple wind/solar sites (Case 1) (5,000,000 iteration)

Peak Load (MW)	Location	Wind Penetration Level				
		7.7%	20%	30%	37%	43%
185	Bus 3	140.568	138.886	138.480	138.358	138.320
	Bus 3+5	140.666	137.776	136.839	136.445	136.257
	Bus 3+4+5	136.555	132.948	131.621	131.025	130.722
225	Bus 3	431.173	374.482	358.764	353.296	351.260
	Bus 3+5	418.477	329.580	296.068	279.799	271.428
	Bus 3+4+5	409.103	305.535	262.169	241.060	229.124
Peak Load (MW)	Location	Solar Penetration Level				
		7.7%	20%	30%	37%	43%
185	Bus 3	141.389	140.093	139.784	139.692	139.662
	Bus 3+5	141.570	139.199	138.391	138.050	137.884
	Bus 3+4+5	137.754	134.592	133.315	132.691	132.356
225	Bus 3	452.550	409.539	397.946	394.015	392.570
	Bus 3+5	441.222	367.884	339.217	325.136	317.865
	Bus 3+4+5	431.769	343.564	304.095	283.671	271.686

APPENDIX G. INDEX VALUES FOR THE RTS WITH WECS OR PVCS

Table G.1: The HL-I annual RTS indices for different peak loads

Peak load (MW)	EDLC (hrs/yr)	EENS (MWH/yr)	PLC (/yr)	SI (sys.mins/yr)
2450	0.85533	80.74802	0.00010	1.69996
2650	3.61345	408.23150	0.00041	8.59435
2850	13.00475	1673.53800	0.00148	35.23237
3050	39.59196	5805.77600	0.00452	122.22690
3250	109.00830	17521.40000	0.01244	368.87150

Table G.2: The annual RTS system indices for different peak loads

Peak Load (MW)	EDLC (hrs/yr)	EENS (MWH/yr)	PLC (/yr)	SI (sys.mins/yr)
2450	0.86231	81.21729	0.00010	1.70984
2650	3.62126	408.79170	0.00041	8.60614
2850	13.01818	1674.87700	0.00149	35.26057
3050	39.62077	5809.06200	0.00452	122.29600
3250	109.06590	17530.01000	0.01245	369.05280

Table G.3: The HL-I annual system EDLC (hrs/yr) of the RTS including the WECS obtained using MECORE

State	Peak Load (MW)				
	2450	2650	2850	3050	3250
2-state	0.65136	2.77611	10.10922	31.04889	86.44210
4-state	0.56877	2.46343	9.05711	28.21598	79.54903
5-state	0.51506	2.31173	8.66396	27.16471	77.03498
8-state	0.51871	2.29253	8.55468	27.06187	76.30411
11-state	0.51744	2.29102	8.55791	27.01367	76.11617

Table G.4: The HL-I annual system EENS (MWh/yr) of the RTS including the WECS obtained using MECORE

State	Peak Load (MW)				
	2450	2650	2850	3050	3250
2-state	61.87484	312.94600	1292.94200	4526.90400	13851.33860
4-state	53.79504	275.90160	1151.33837	4086.21252	12605.51512
5-state	48.46493	255.24029	1086.24451	3899.21904	12148.64478
8-state	48.64868	255.68485	1081.01919	3862.53625	12025.53287
11-state	48.30450	255.03114	1079.67995	3857.32472	12006.41766

Table G.5: The HL-I annual system EDLC (hrs/yr) of the RTS including the PVCS obtained using MECORE

State	Peak Load (MW)				
	2450	2650	2850	3050	3250
2-state	0.70460	2.97630	10.77854	33.01312	91.61562
4-state	0.63073	2.71476	9.92378	30.69662	86.06481
5-state	0.59778	2.61895	9.67361	29.97382	84.28195
8-state	0.59706	2.62548	9.70264	30.32156	84.83088
11-state	0.58712	2.58852	9.58553	29.93002	83.80857

Tables G.6 – G.7 show the RTS EENS with a 400 MW WECS/PVCS added at Bus 19.

Table G.6: The RTS EENS (MWh/yr) with the WECS added at Bus 19

Peak load (MW)	Wind Penetration Level					
	10.5% (400 MW)	15% (600 MW)	19% (800 MW)	23% (1000 MW)	29% (1400 MW)	35% (1800 MW)
2450	49.446	45.821	44.017	43.090	42.373	42.213
2650	256.721	235.504	224.177	217.795	211.885	209.965
2850	1088.538	994.895	942.594	911.654	880.640	868.726
3050	3905.444	3564.627	3365.537	3242.053	3111.397	3056.400
3250	12164.575	11090.843	10438.884	10022.629	9561.439	9349.324

Table G.7: The RTS EENS (MWh/yr) with the PVCS added at Bus 19

Peak load (MW)	Solar Penetration Level					
	10.5% (400 MW)	15% (600 MW)	19% (800 MW)	23% (1000 MW)	29% (1400 MW)	35% (1800 MW)
2450	57.558	54.918	53.607	52.931	52.414	52.299
2650	294.342	278.839	270.287	265.549	261.192	259.806
2850	1228.587	1158.479	1119.558	1096.515	1073.276	1064.402
3050	4349.608	4092.954	3944.461	3852.962	3755.880	3714.649
3250	13397.439	12582.572	12092.946	11785.081	11446.962	11290.302

Tables G.8- G.11 show the system EENS of the RTS associated with multiple independent wind farms/solar parks.

Table G.8: The annual system EENS of the RTS associated with the two wind farms located at Buses 15 and 19

Peak Load (MW)	Wind Penetration Level					
	10.5% (400 MW)	15% (600 MW)	19% (800 MW)	23% (1000 MW)	29% (1400 MW)	35% (1800 MW)
2450	42.532	36.013	32.165	29.684	26.846	25.419
2650	225.506	189.011	166.485	151.701	134.178	124.936
2850	973.608	817.770	718.219	650.515	568.195	523.294
3050	3542.515	2995.463	2630.089	2379.124	2063.199	1883.090
3250	11185.054	9522.887	8379.055	7568.799	6526.018	5911.683

Table G.9: The annual system EENS of the RTS associated with the two solar parks located at Buses 15 and 19

Peak Load (MW)	Solar Penetration Level					
	10.5% (400 MW)	15% (600 MW)	19% (800 MW)	23% (1000 MW)	29% (1400 MW)	35% (1800 MW)
2450	51.338	45.744	42.312	40.054	37.393	36.016
2650	265.201	234.646	215.177	202.117	186.268	177.644
2850	1119.663	989.952	905.091	846.520	774.096	733.800
3050	4010.772	3554.578	3244.333	3029.041	2755.450	2597.339
3250	12503.745	11124.414	10159.107	9466.259	8567.098	8033.046

Table G.10: The annual system EENS of the RTS associated with the three wind farms located at Buses 1, 15 and 19

Peak Load (MW)	Wind Penetration Level					
	10.5% (400 MW)	15% (600 MW)	19% (800 MW)	23% (1000 MW)	29% (1400 MW)	35% (1800 MW)
2450	31.418	27.741	22.743	19.510	15.811	13.861
2650	182.010	161.963	133.315	114.071	91.091	78.499
2850	814.736	730.672	605.630	519.245	412.252	352.004
3050	3032.634	2738.806	2292.108	1972.389	1566.250	1329.149
3250	9754.546	8867.027	7488.505	6480.367	5150.995	4355.096

Table G.11: The annual system EENS of the RTS associated with the three solar parks located at Buses 1, 15 and 19

Peak Load (MW)	Solar Penetration Level					
	10.5% (400 MW)	15% (600 MW)	19% (800 MW)	23% (1000 MW)	29% (1400 MW)	35% (1800 MW)
2450	41.687	38.294	33.365	29.996	25.898	33.365
2650	227.743	210.188	183.738	165.180	141.730	128.080
2850	984.255	911.336	799.163	718.866	614.403	551.986
3050	3576.666	3323.529	2928.598	2637.115	2249.906	2013.101
3250	11283.477	10523.942	9317.964	8409.355	7167.997	6395.851

APPENDIX H: DATA OF THE TWO 20-STEP IEEE-RTS LOAD DURATION CURVES

Table H.1: Data of the two 20-step IEEE-RTS load duration curves

Load Level	Probability	
	Original RTS-LDC	Modified RTS -LDC
1.000	0.00023	0.00028
0.990	0.00011	0.00015
0.983	0.00057	0.00059
0.966	0.00171	0.00127
0.949	0.00171	0.00196
0.932	0.00331	0.00328
0.915	0.00616	0.00536
0.898	0.00970	0.00774
0.881	0.01153	0.01052
0.864	0.01610	0.01449
0.847	0.02363	0.01824
0.830	0.02546	0.02152
0.813	0.02386	0.01862
0.800	0.03311	0.03032
0.780	0.03459	0.03175
0.760	0.01632	0.01645
0.750	0.08219	0.08643
0.700	0.23162	0.21375
0.600	0.21553	0.22331
0.500	0.26256	0.29397
Annual Peak Load	185 MW	181.5 MW

APPENDIX I. PARAMETERS DEFINING THE CURRENT-VOLTAGE RELATIONSHIP OF A CANROM30 SOLAR PANEL

Table I.1: Parameters defining the I-V relationship of a CANROM30 solar panel

DESCRIPTION	VALUE	UNIT
Number of series groups in parallel	2	
Number of modules in series	1	
Area per module	0.5	m^2
Tracking method	No	
Collector slope	60	degree
Collector azimuth	0	degree
Reference array operating temperature	25	$°C$
Reference radiation level	1000	W/m^2
Reference MPP voltage	16	V
Reference MPP current	2	A
Reference open circuit voltage	19.5	V
Reference short circuit current	2.6	A
Array resistance	0.06	Ω
Wind speed correction factor	1	
Alpha	0.0025	
Beta	0.5	
Gamma	0.0029	
Solar cell absorbance	0.9	
Front panel emmissivity	0.95	
Front panel transmittance	0.95	
Back panel emmissivity	0.9	
Back panel transmittance	0.9	